Molecular Clouds
and
Star Formation

Stars are formed in molecular cloud cores, whereas planets are condensed, contemporaneously, in young circumstellar disks.

http://www.astro.ncu.edu.tw/~wchen/Courses/Stars/Lada1995summerschool.pdf

wchen@astro.ncu.edu.tw

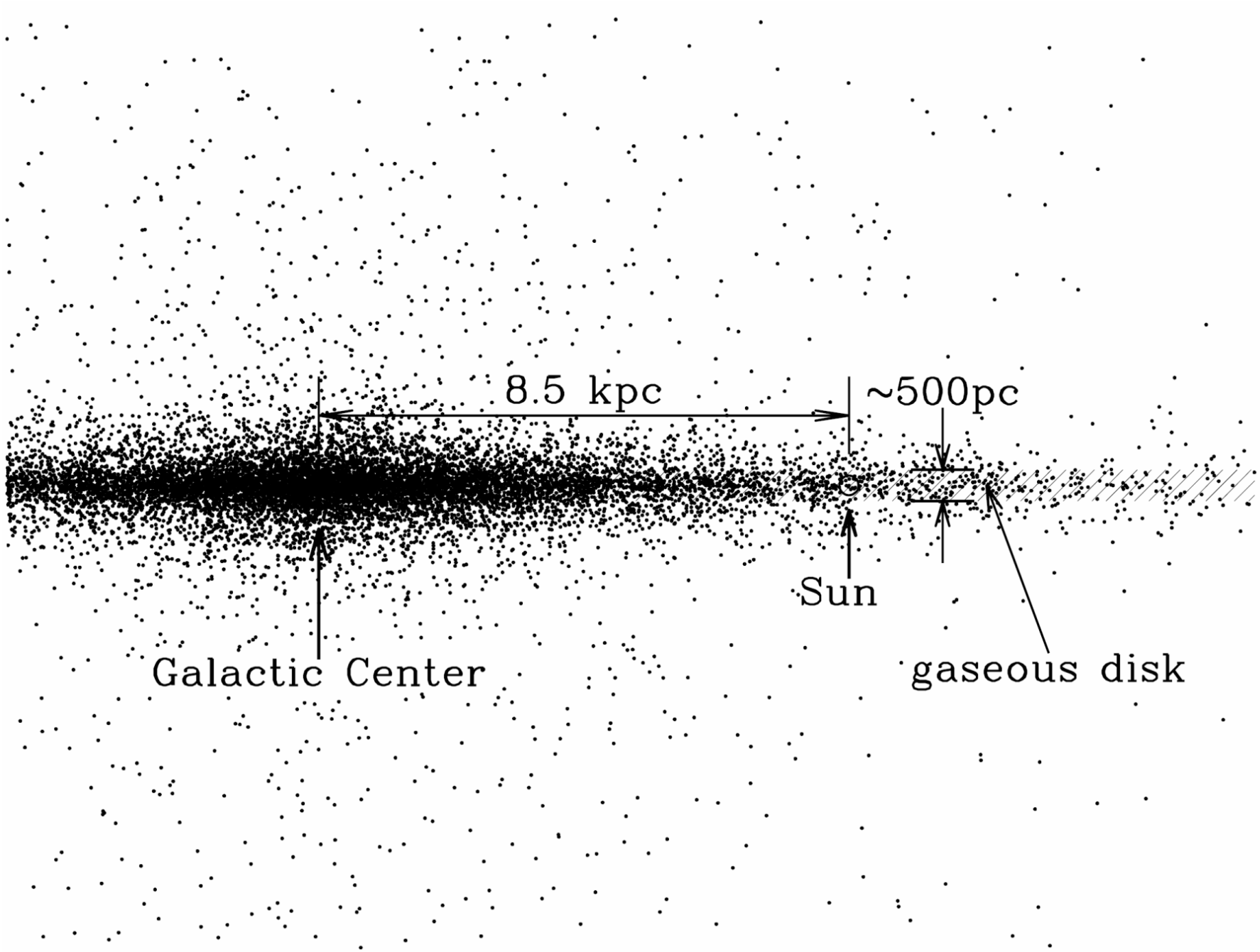
8.5 kpc
~500pc
Sun
Galactic Center
gaseous disk

THE ASTROPHYSICAL JOURNAL, 218:148–169, 1977 November 15

A THEORY OF THE INTERSTELLAR MEDIUM: THREE COMPONENTS REGULATED BY SUPERNOVA EXPLOSIONS IN AN INHOMOGENEOUS SUBSTRATE

CHRISTOPHER F. MCKEE
Departments of Physics and Astronomy, University of California, Berkeley
AND
JEREMIAH P. OSTRIKER
Princeton University Observatory
Received 1977 February 3; accepted 1977 May 2

ABSTRACT

Supernova explosions in a cloudy interstellar medium produce a three-component medium in which a large fraction of the volume is filled with hot, tenuous gas. In the disk of the galaxy the evolution of supernova remnants is altered by evaporation of cool clouds embedded in the hot medium. Radiative losses are enhanced by the resulting increase in density and by radiation from the conductive interfaces between clouds and hot gas. Mass balance (cloud evaporation rate = dense shell formation rate) and energy balance (supernova shock input = radiation loss) determine the density and temperature of the hot medium with $(n, T) = (10^{-2.5}, 10^{5.7})$ being representative values. Very small clouds will be rapidly evaporated or swept up. The outer edges of "standard" clouds ionized by the diffuse UV and soft X-ray backgrounds provide the warm ($\sim 10^4$ K) ionized and neutral components. A self-consistent model of the interstellar medium developed herein accounts for the observed pressure of interstellar clouds, the galactic soft X-ray background, the O VI absorption line observations, the ionization and heating of much of the interstellar medium, and the motions of the clouds. In the halo of the galaxy, where the clouds are relatively unimportant, we estimate $(n, T) = (10^{-3.3}, 10^{6.0})$ below one pressure scale height. Energy input from halo supernovae is probably adequate to drive a galactic wind.

Interstellar Medium (ISM)

- Gas, dust + radiation, magnetic fields, cosmic rays (i.e., charged particles)
- Very sparse ---

  [star-star distance] / [stellar diameter] ~ 1 pc/10^{11} cm ~ 3 x 10^{7} :1
  or ~1: 10^{22} in terms of volume (space)

- Mass: 99% mass in gas, 1% in dust ~ 15% of total MW visible matter
- Of the gas, 90%, H; 10% He

Typical gas-to-dust ratio ~ 100

- Hydrogen: mainly H I (atomic), H II (ionized), and H_2 (molecular)
- Studies of ISM ---
  - Beginning of evolution of baryonic matter "recombination"
  - Stars form out of ISM
  - Important ingredient of a galaxy

http://www.astro.ncu.edu.tw/~wchen/Courses/ISM/

Material Constituents of the ISM

Component	T (K)	n (cm^{-3})	Properties
Hot, intercloud and coronal gas	10^6	10^{-4}	
Warm intercloud gas	10^4	0.1	
Diffuse cloud (H I)	10^2	0.1	Mostly H I; $n_e/n_0=10^{-4}$
H II regions	10^4	>10	
Dark Molecular Clouds	10	$> 10^3$	Mostly H_2 mol. and dust
Supernova Remnants	$10^4 \sim 10^7$	>1	
Planetary Nebulae			

Energy Density in the Local ISM

Component	u (eV/cm^{-3})	Properties
Cosmic microwave background	0.265	
FIR radiation from dust	0.31	
Starlight	0.54	
Thermal kinetic energy	0.49	
Turbulent kinetic energy	0.22	
Magnetic field	0.89	
Cosmic rays	1.39	

There seems to be equipartition between these energies. Why?
Read Draine's book, page 10 link here

A "standard" HI cloud

$D \sim 5$ pc

$M \sim 50\ M_{\odot}$;

$d_{\text{intercloud}} \sim 100$ pc

$v_{\text{cloud}} \sim 10\ \text{kms}^{-1}$

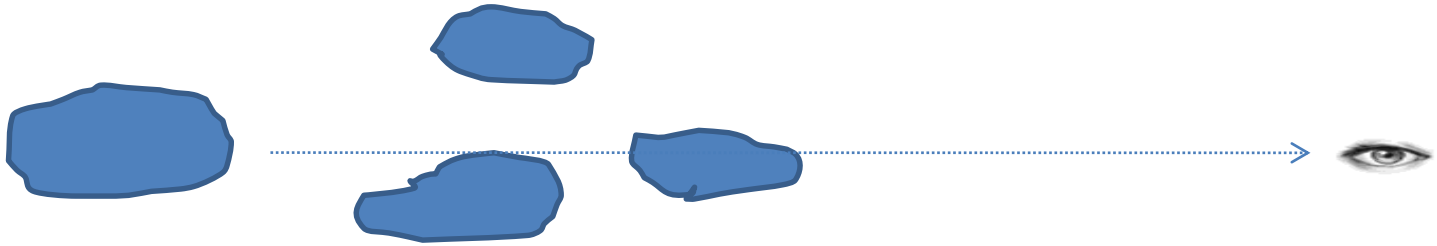

Clouds are patchy ➔ extinction depends greatly on the sightline

Extinction = absorption + scattering

A_V=30 toward the Galactic center

Extinction versus reddening

In the Galactic plane, $\boldsymbol{A_V \sim 0.7\text{-}1\ \text{mag kpc}^{-1}}$

Extinction ←→ amounts of dust grains along the line of sight

Reddening ←→ grain properties (size, shape, composition, structure)

Different clouds along the line of sight …

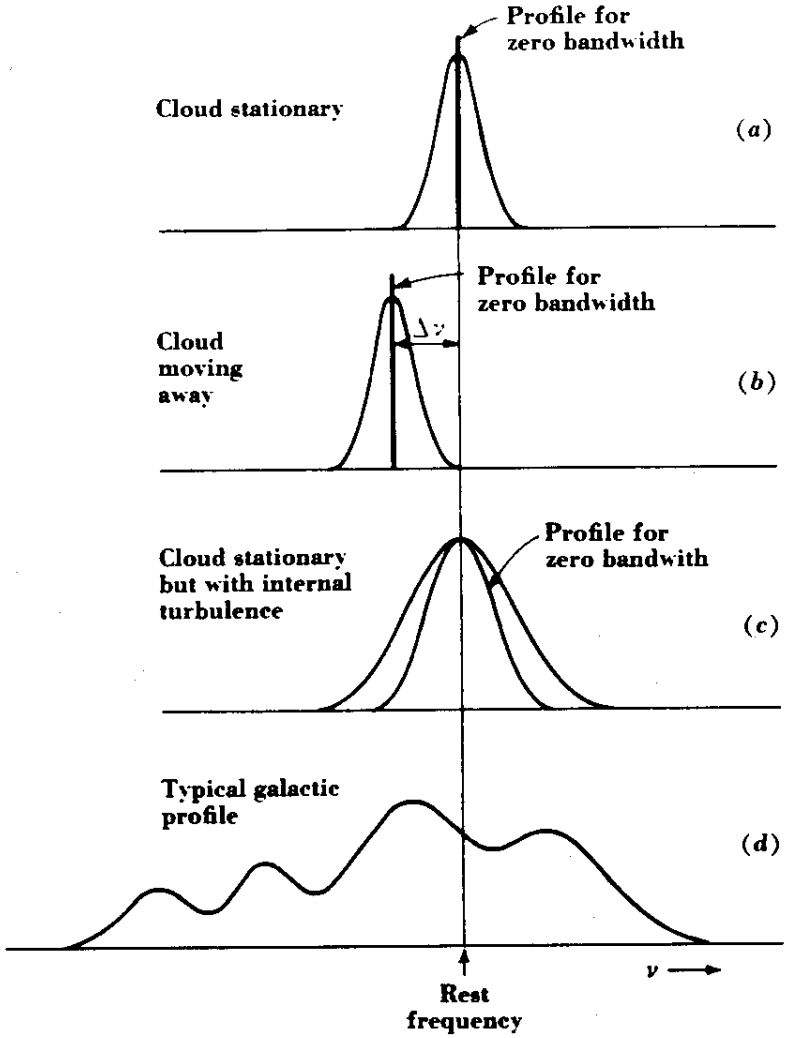

Fig. 8-59. Idealized hydrogen-line profiles.

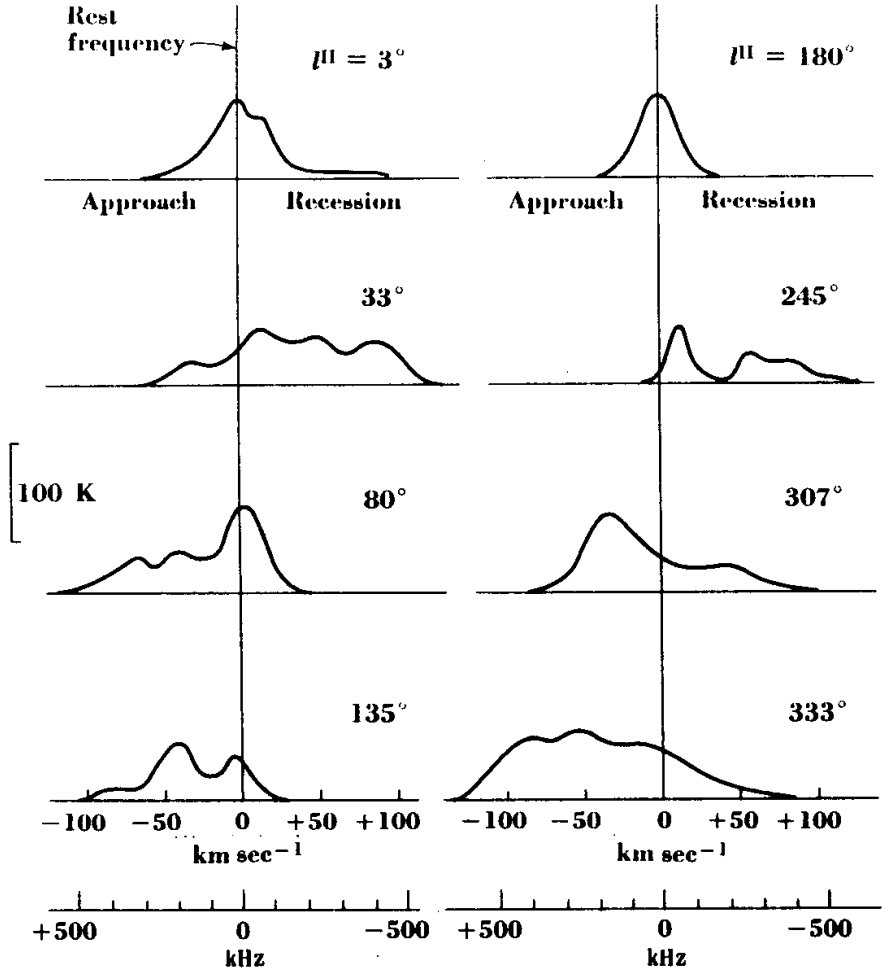

Fig. 8-60. Hydrogen-line profiles at different longitudes in the plane of our galaxy. (*After Kerr and Westerhout*, 1964).

John Kraus "Radio Astronomy"

The ‘normalized’ extinction (extinction law)

$$F(\lambda) = \frac{A_\lambda - A_V}{A_B - A_V} = \frac{E_{\lambda-V}}{E_{B-V}}$$

The UV ‘bump’
1/λ~4.6 → λ~2200Å

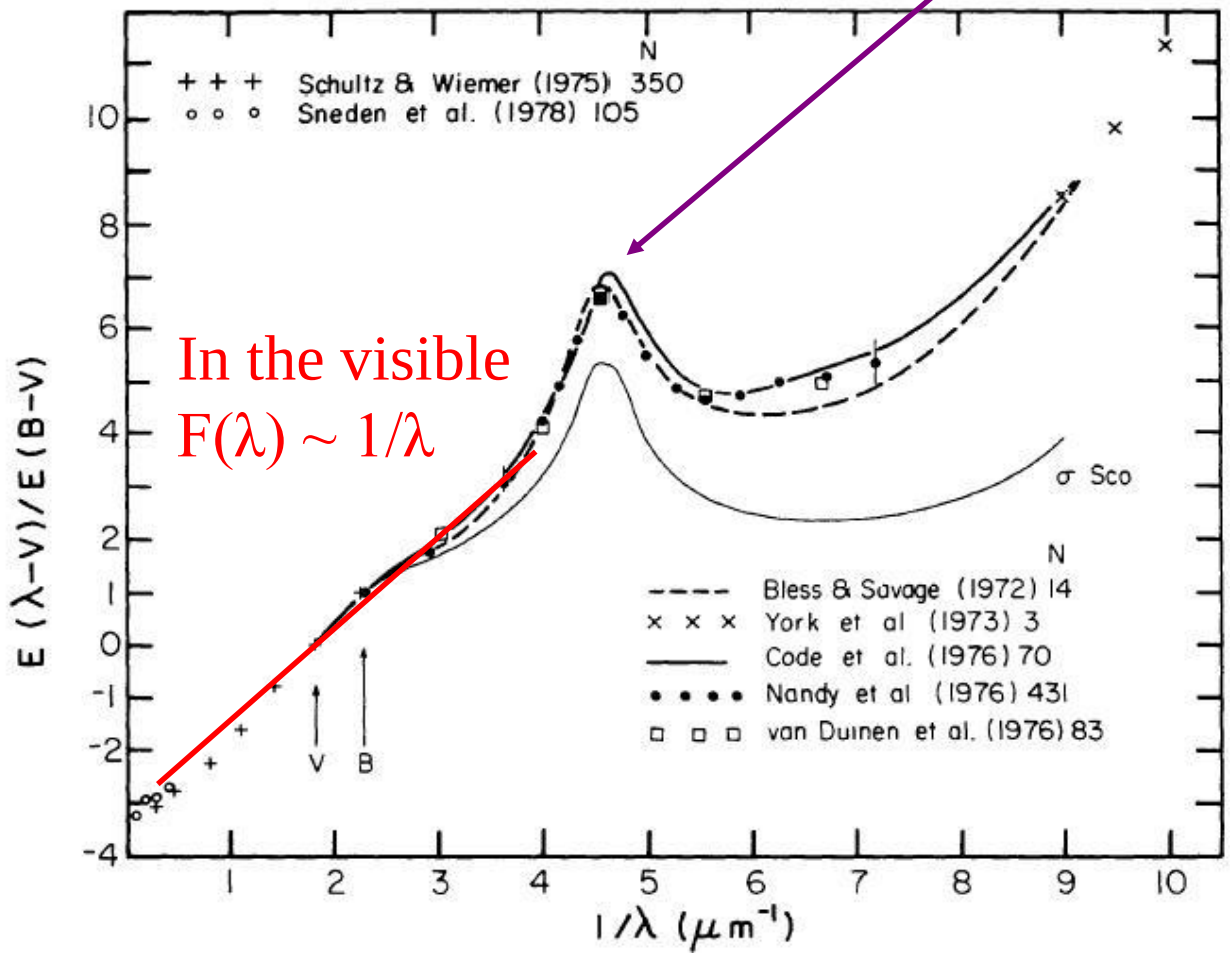

F(V) = 0

F(B) = +1

Find
A_B/A_V=?

The 'normalized' extinction (extinction law)

$$F(\lambda) = \frac{A_\lambda - A_V}{A_B - A_V} = \frac{E_{\lambda-V}}{E_{B-V}}$$

F(V) = 0

F(B) = +1

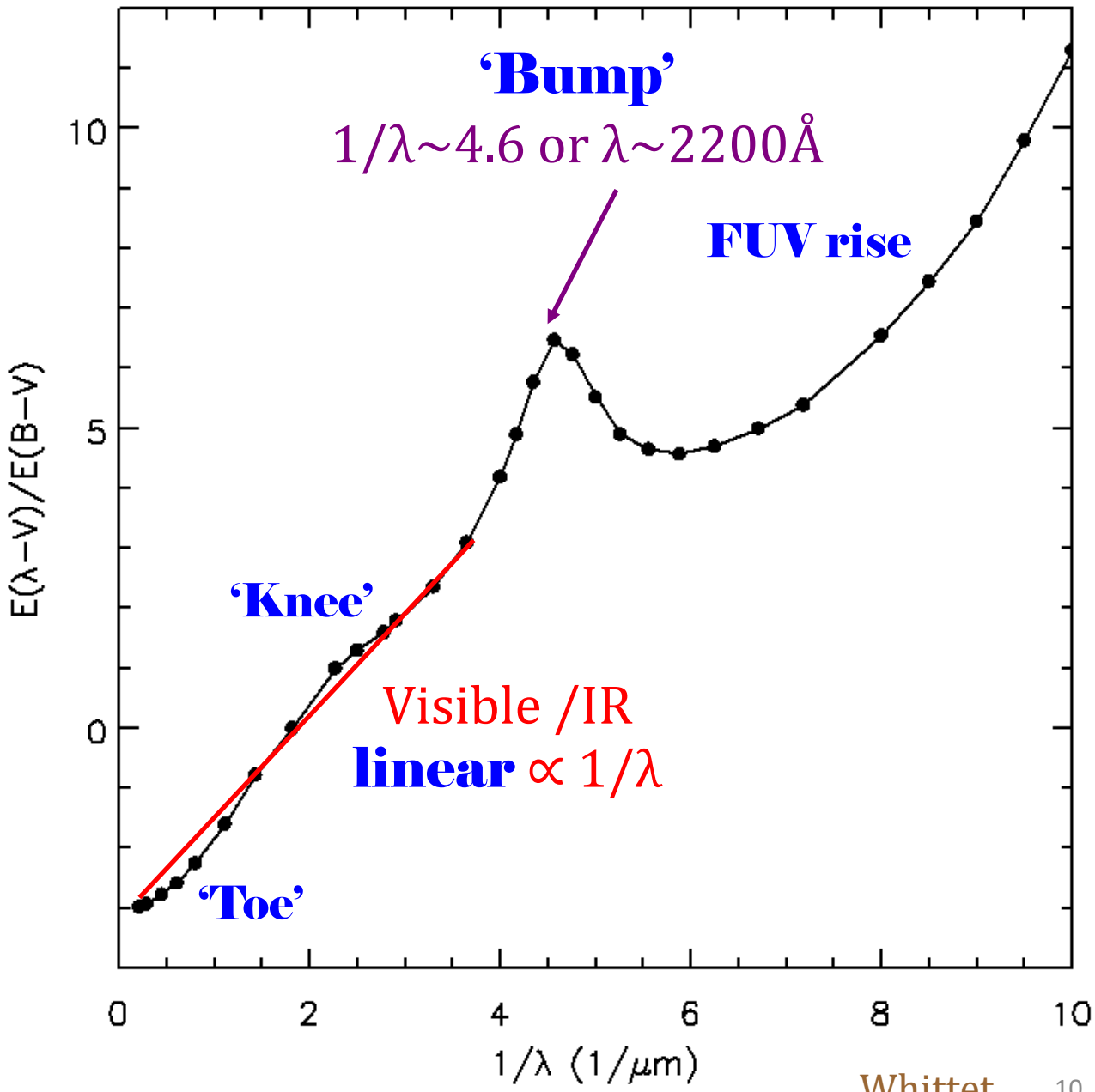

$$A_\lambda = -2.5 \log(e^{-\tau_\lambda}) \equiv 1.086 \tau_\lambda \equiv 1.086 N_d \sigma_\lambda Q_{ext}$$

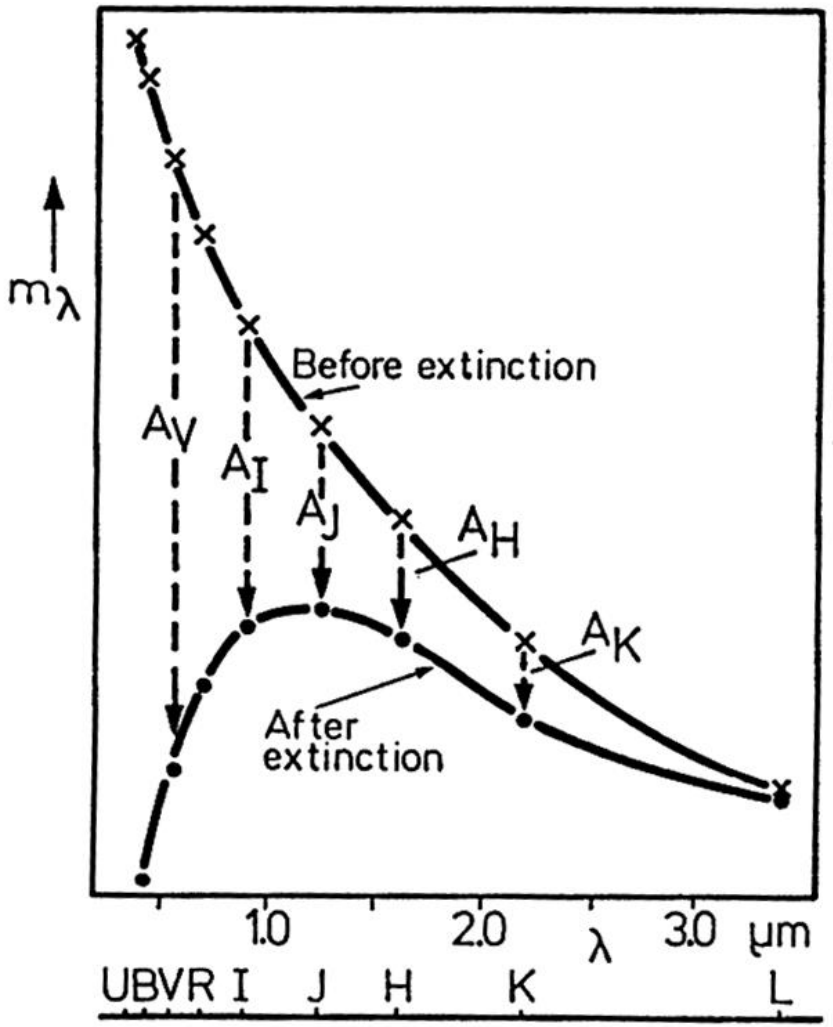

Filter	A_λ / A_V
U	1.531
B	1.324
V	1.000
R	0.748
I	0.482
J	0.282
H	0.175
K	0.112
L	0.058
M	0.023
N	0.052

$A_K \approx 0.1\, A_V$

Rieke & Lebofsky (1985)

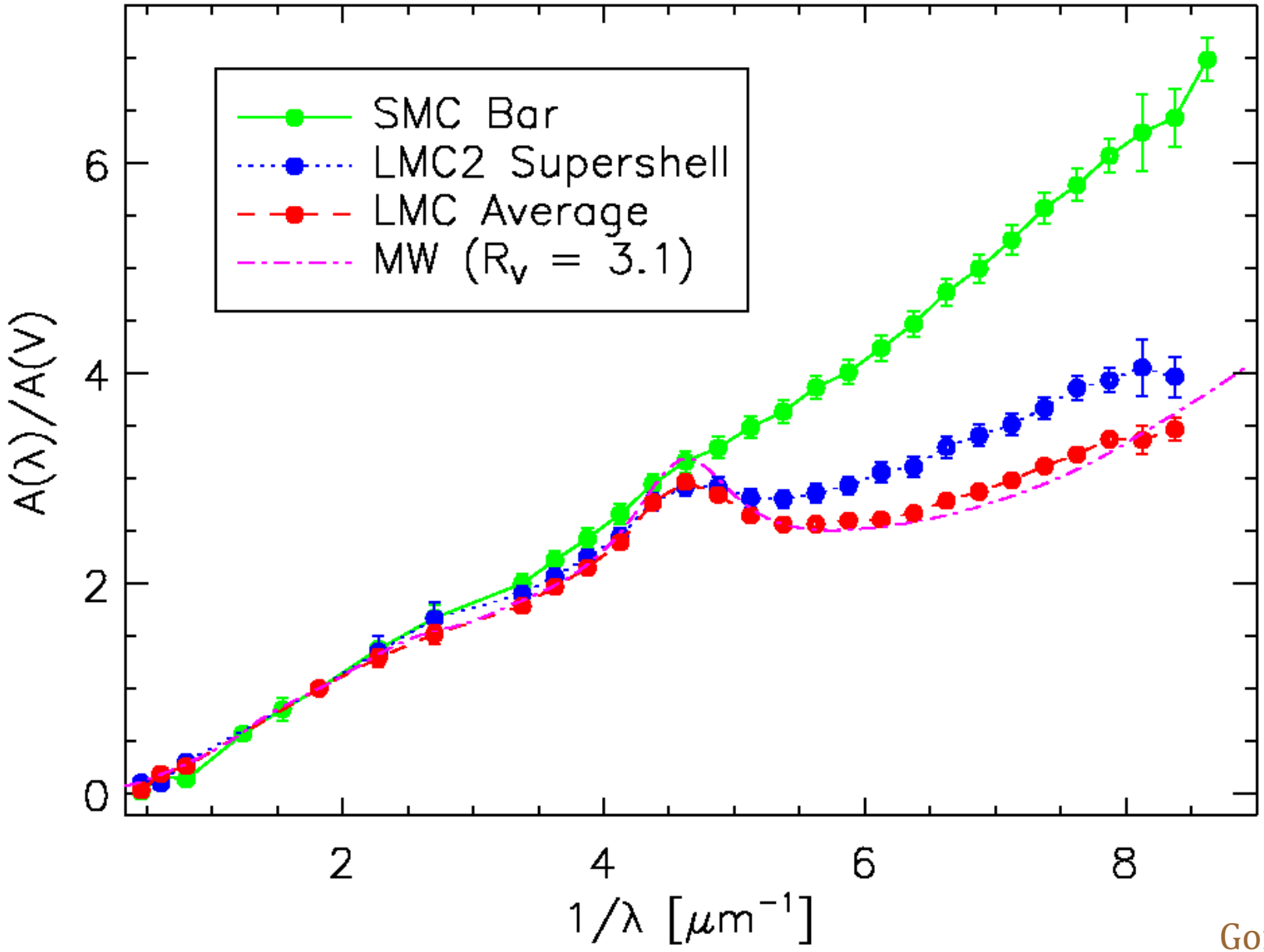

Gordon et al (2003)

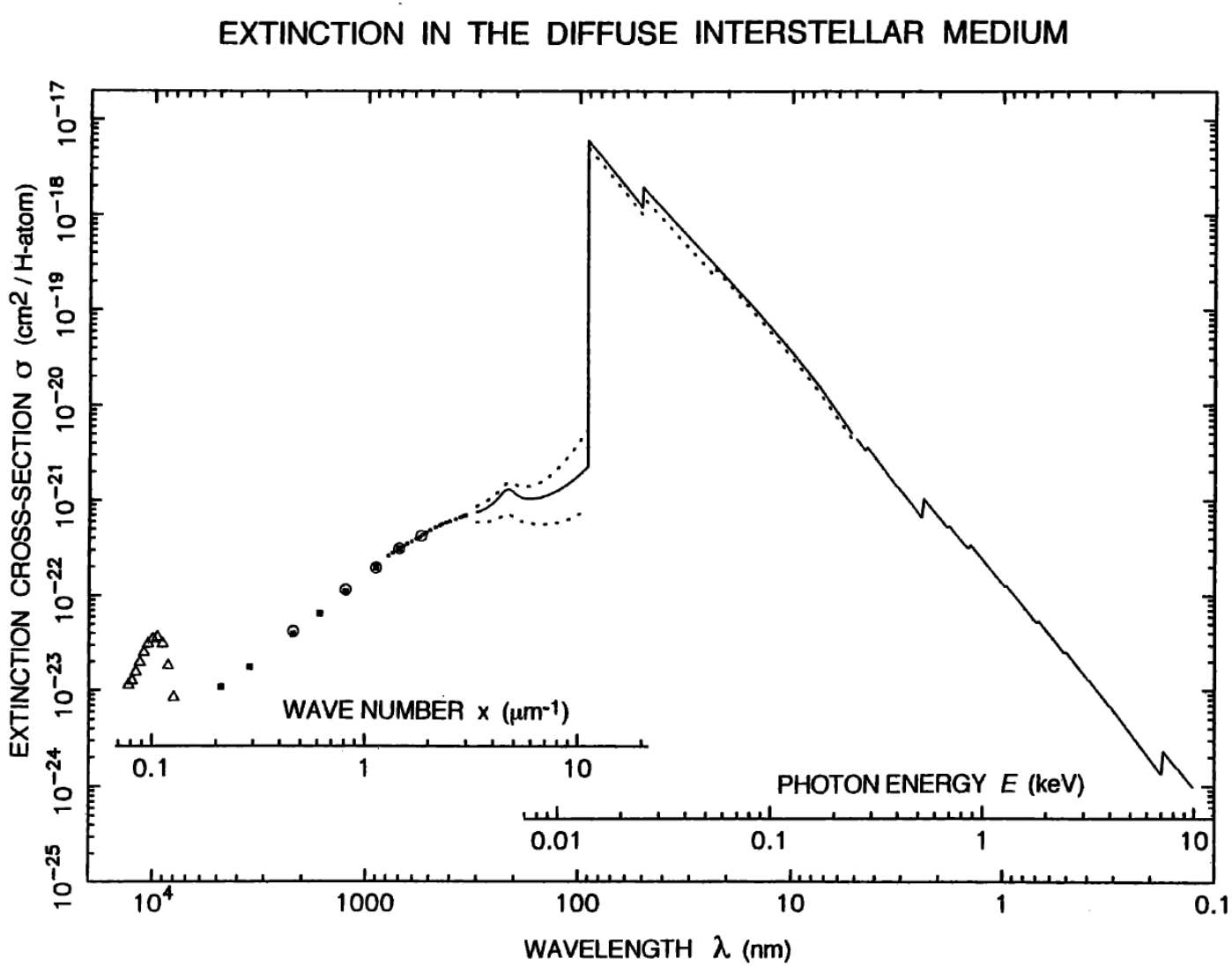

Figure 1. Solid line: The extinction cross-section normalized per H-atom of the diffuse neutral (95% HI, 5% HII, 10% HeI) interstellar medium from the far-infrared to the X-rays. Dotted lines: The UV extinction on the lines of sight in two extreme cases, HD 204827 (upper curve) and HD 37023 (θ_1-Orionis D, lower curve). Shortward of the Lyman limit, the dotted line corresponds to the ionization state of the solar neighbourhood (80% HI, 20% HII, 5% HeI, 5% HeII). The sources of the data are given in the text.

Ryter (1996)

Gas and dust coexist.

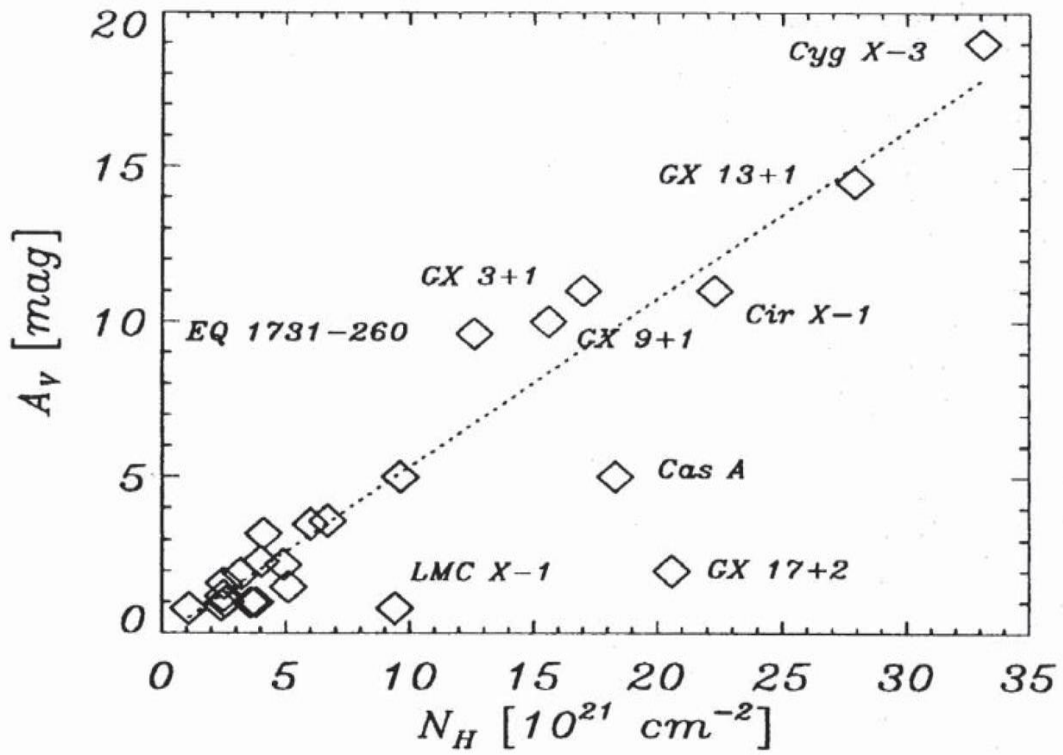

Fig. 3. Visual extinction vs. equivalent hydrogen column density. The fit (dotted line) does not contain GX 17+2 and LMC X-1. It yields $N_H = 1.79 \pm 0.03\ A_V[mag] \times 10^{21}[cm^{-2}]$

A gas-to-dust ratio ~100 (by mass) seems universal.

$$\frac{N_H}{A_V} \approx 1.8 \times 10^{21} \text{atoms cm}^{-2}\ \text{mag}^{-1}$$

Predehl & Schmitt (1995)

Exercise

1. The star Vega is used to define the zeroth magnitude in all the classical (Vega) photometric systems, e.g., Johnson.
2. Plot its spectral energy distribution (SED) from UV to IR.
3. What is the spectral type of Vega? What is its effective temperature?
4. Compare this in a plot with a blackbody curve of the temperature.
5. It was surprising hence when *IRAS* data revealed IR excess of Vega. What are the flux densities observed by *IRAS*? Given the age of Vega, why is this discovery significant?

http://www.astro.utoronto.ca/~patton/astro/mags.html#conversions

Band	lambda_c	dlambda/lambda	Flux at m=0	Reference
	um		Jy	
U	0.36	0.15	1810	Bessel (1979)
B	0.44	0.22	4260	Bessel (1979)
V	0.55	0.16	3640	Bessel (1979)
R	0.64	0.23	3080	Bessel (1979)
I	0.79	0.19	2550	Bessel (1979)
J	1.26	0.16	1600	Campins, Reike, & Lebovsky (1985)
H	1.60	0.23	1080	Campins, Reike, & Lebovsky (1985)
K	2.22	0.23	670	Campins, Reike, & Lebovsky (1985)

Astronomical Magnitude Systems.pdf

Stars are formed in groups → seen as star clusters if gravitationally bound

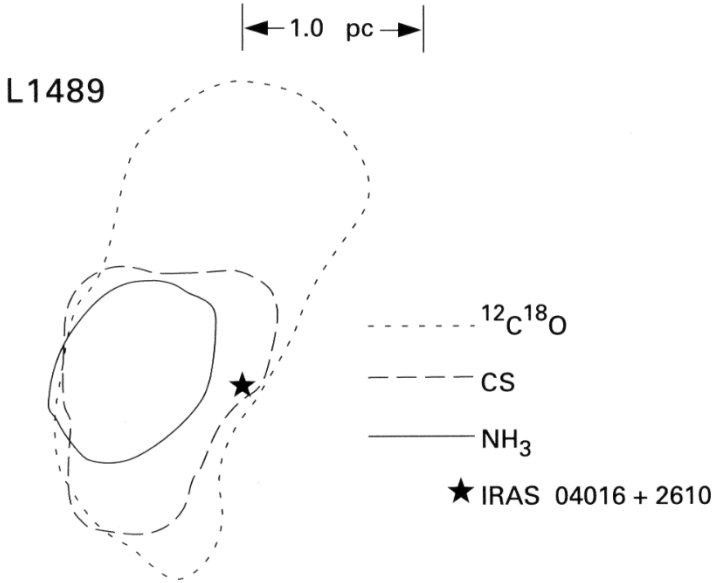

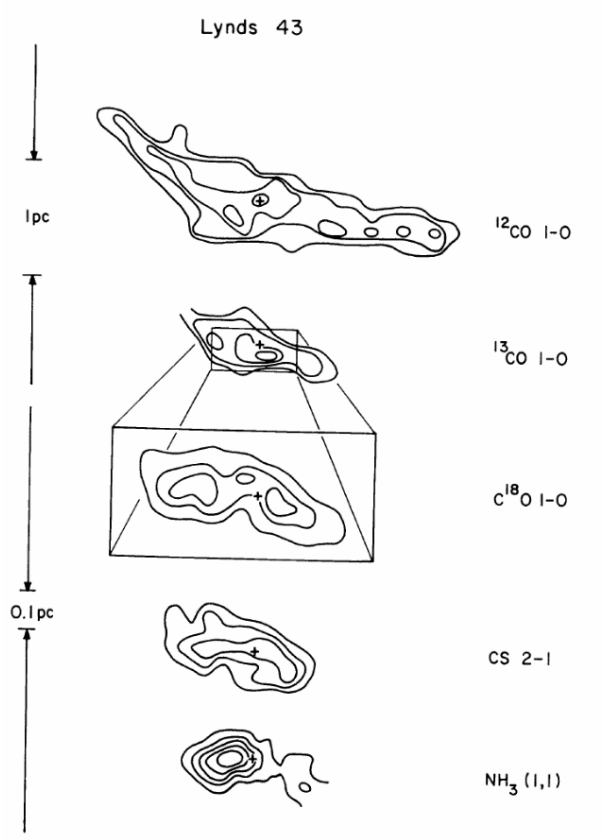

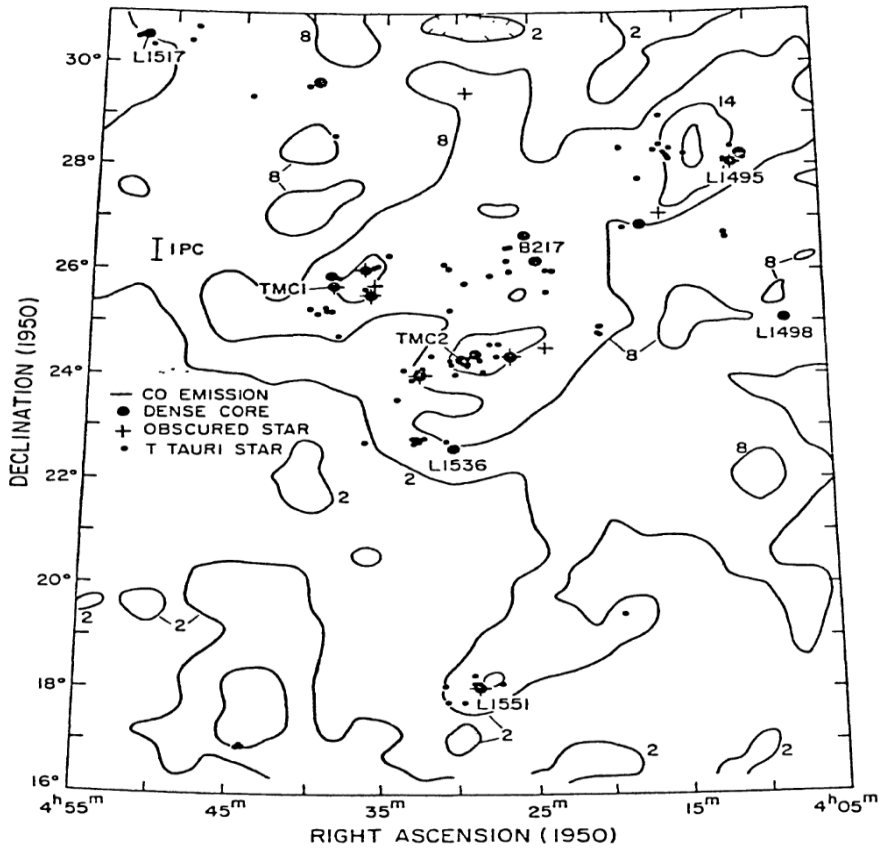

Figure 2 CO contour map of the Taurus molecular cloud with positions of dense NH_3 cores, embedded infrared sources, and visible T Tauri stars (from Myers 1986).

Molecular clouds observed by different tracers …

Taurus molecular cloud

Filamentary Molecular Clouds

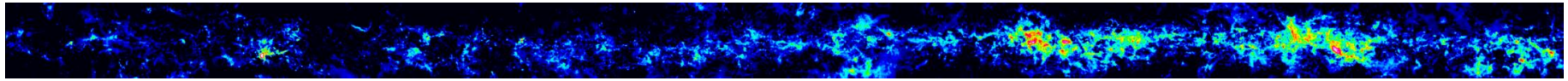

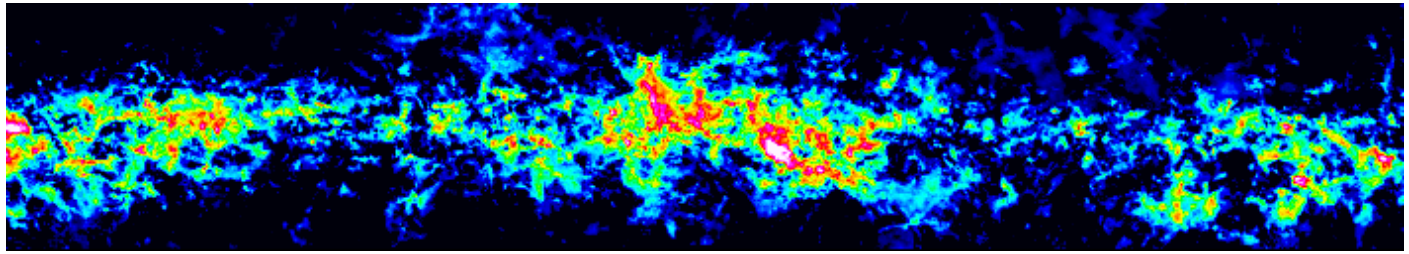

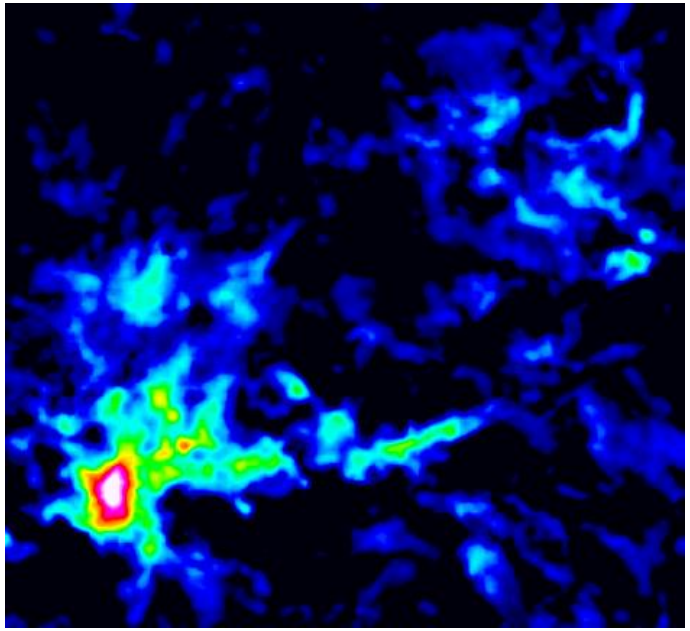

Molecular clumps/ clouds/condensations

- $n \sim 10^3$ cm^{-3}, $D \sim 5$ pc,
- $M \sim 10^3\,M_\odot$

Dense molecular cores

- $n \geq 10^4$ cm^{-3}, D ~ 0.1 pc,
- $M \sim$ 1-2 $M_\odot$

Giant Molecular Clouds

- D=20~100 pc
- $\mathcal{M} = 10^5 \sim 10^6\ \mathcal{M}_\odot$
- $\rho \approx 10 \sim 300\ \mathrm{cm}^{-3}$
- $T \approx 10 \sim 30$ K
- $\Delta v \approx 5 \sim 15\ \mathrm{km}^{-1}$

http://www.bu.edu/galacticring/outgoing/PressRelease/

Nearby Examples

Massive Star-Forming Regions

- *Per OB2* (350 pc)
- *Orion OB Association* (350--400 pc) … rich

Low-Mass Star-Forming Regions

- *Taurus Molecular Cloud (TMC-1)* (140 pc)
- *Rho Ophiuchi cloud* (130 pc)
- *Lupus* (140 pc)
- *Chamaeleon* (160 pc)
- *Corona Australis* (130 pc)

} 4/5 in the southern sky … why?

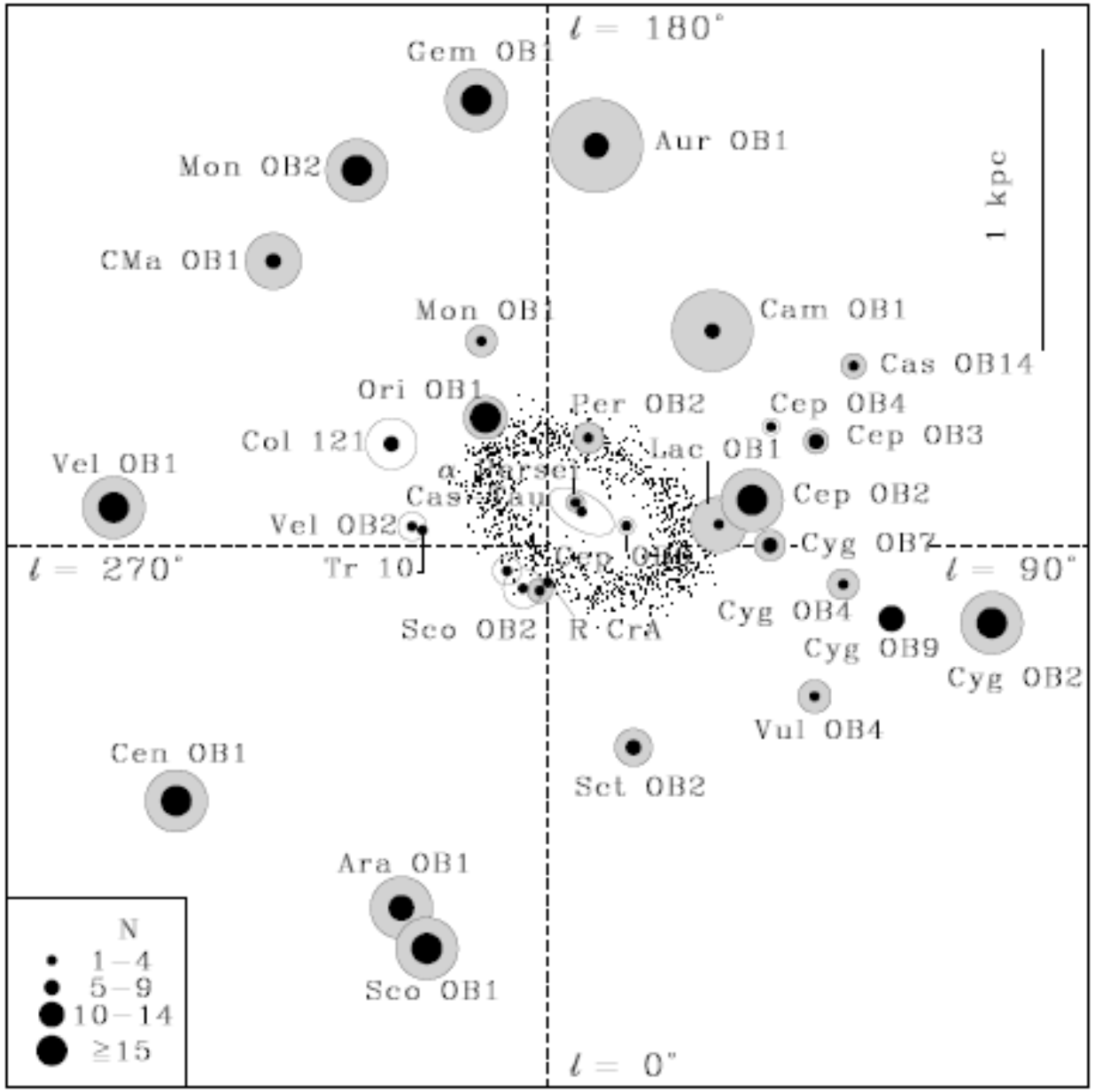

http://hera.ph1.uni-koeln.de/~heintzma/All/OB_stars.htm

The **Gould Belt**, a (partial) ring in the sky, ~1 kpc across, centered on a point 100 pc from the Sun and tilted about 20 deg to the Galactic plane, containing star-forming molecular clouds and OB stars
= local spiral arm

Origin unknown (dark matter induced star formation?)

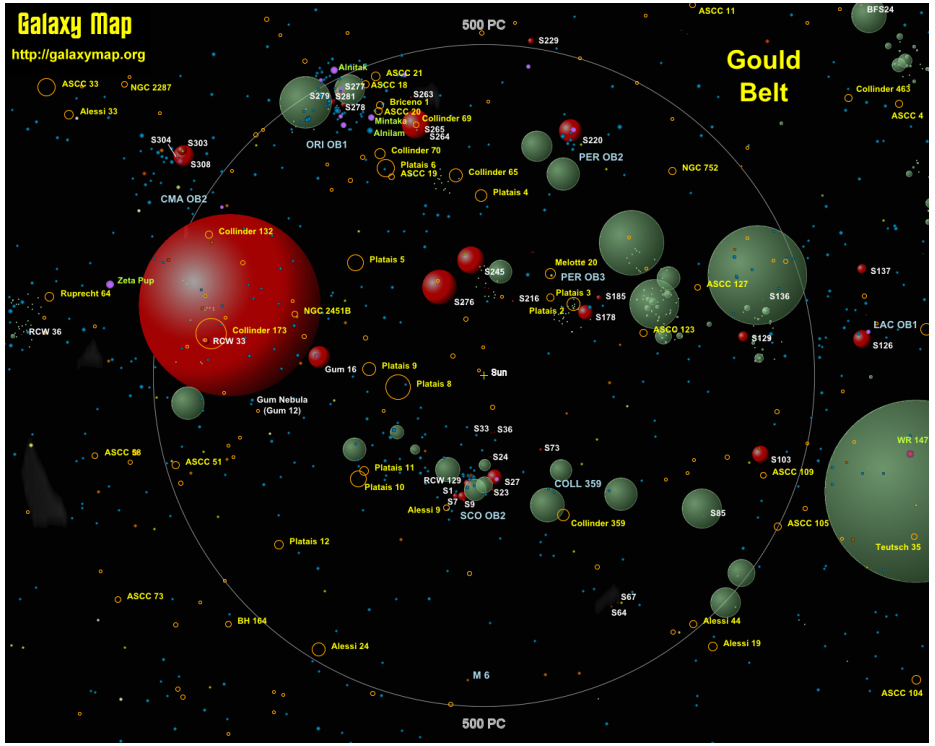

http://galaxymap.org/detail_maps/download_maps/gould.png

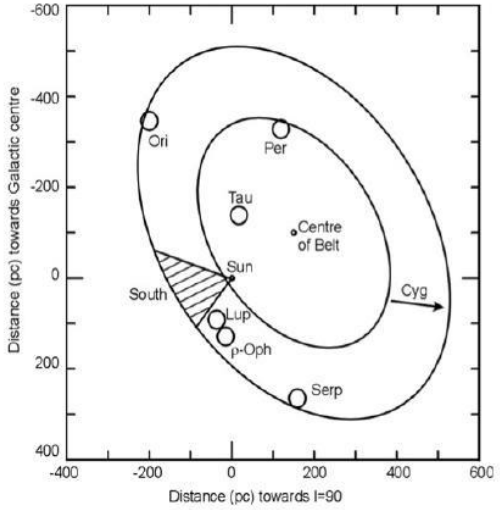

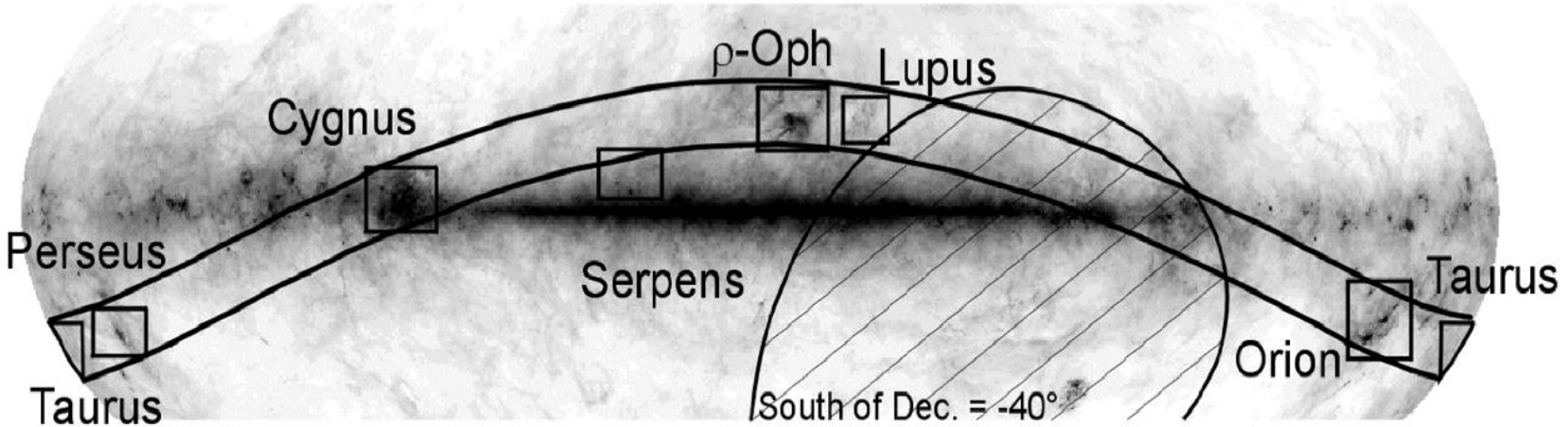

http://www.jach.hawaii.edu/JCMT/surveys/gb/ *Gould's Belt superimposed on to an IRAS 100 micron emission map*

The **Local Bubble** = a cavity of sparse, hot gas, ~100 pc across, in the interstellar medium, with H density of 0.05 cm^{-3}, an order less than typical in the Milky Way.

Likely caused by a (or multiple) supernova explosion (10--30 Myr ago).

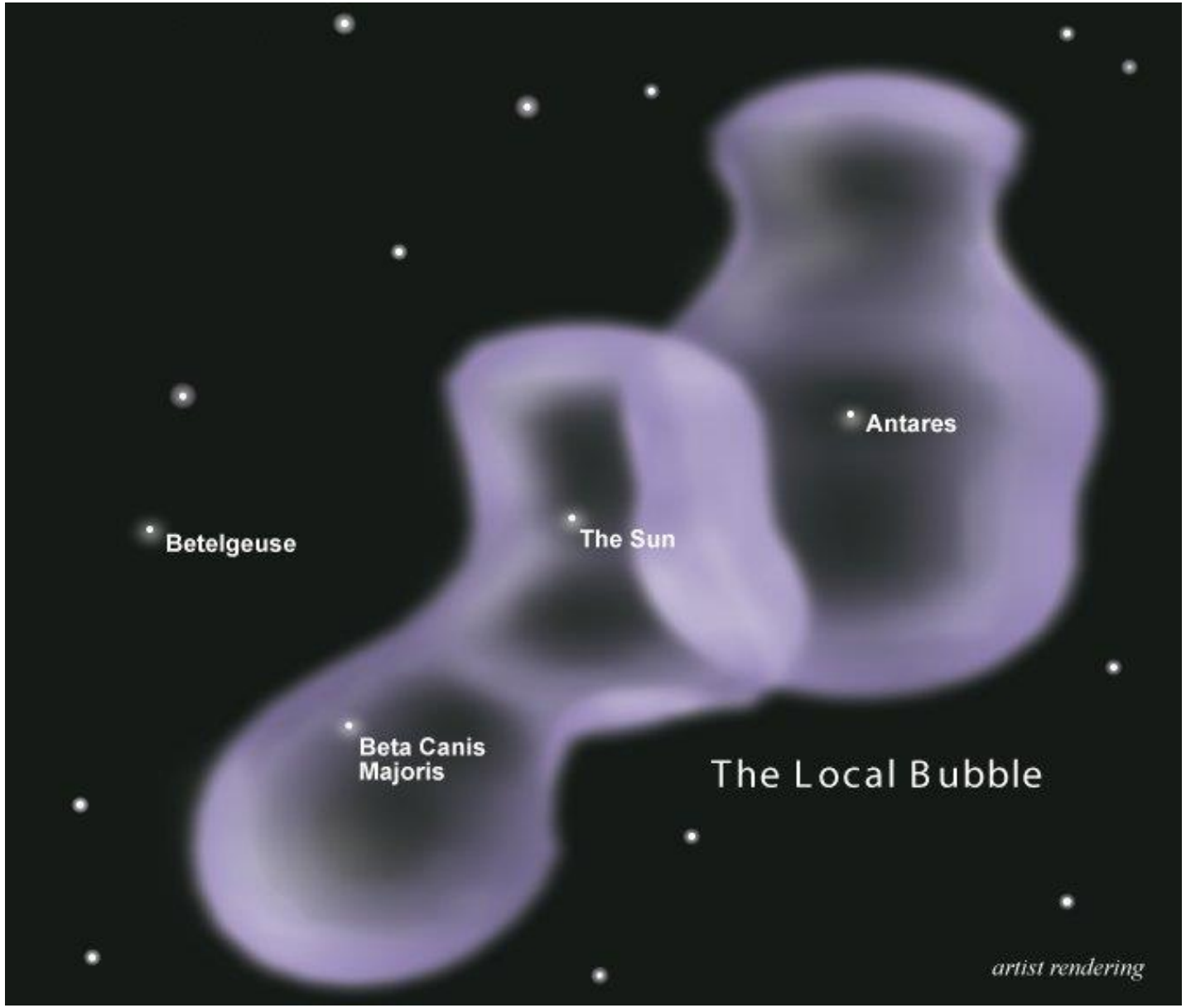

Where is the supernova (remnant)?
Check out the Orion-Eridanus Superbubble

https://en.wikipedia.org/wiki/Local_Bubble

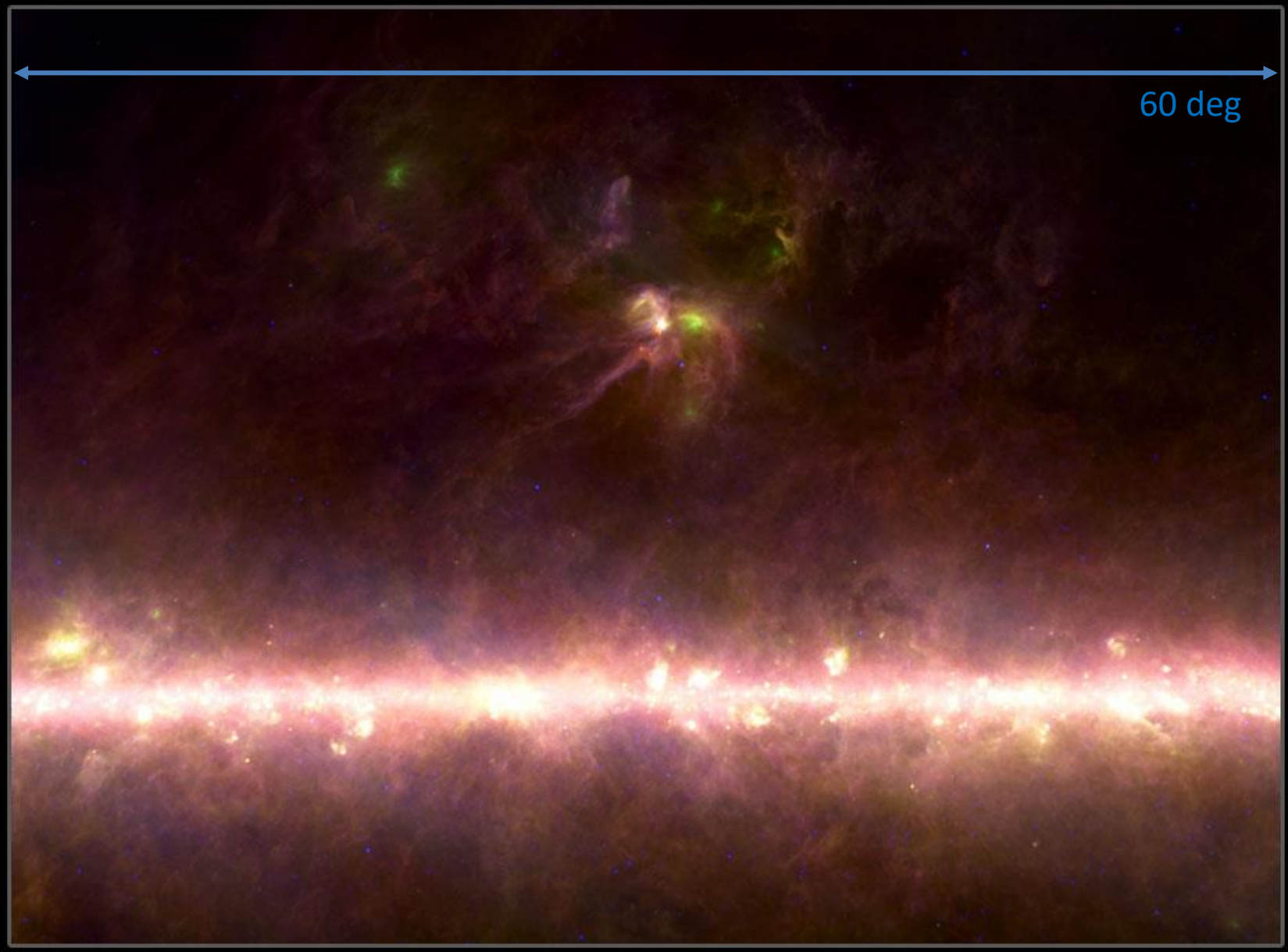

Rho Oph & The Galactic Center

IRAS

InfraRed Legacy

Blue , green and red = 12, 60, and 100 micron

Barnard 72 in Ophiuchus

http://www.robgendlerastropics.com/B72JMM.jpg

Massive Star-Forming Regions ---- OB associations

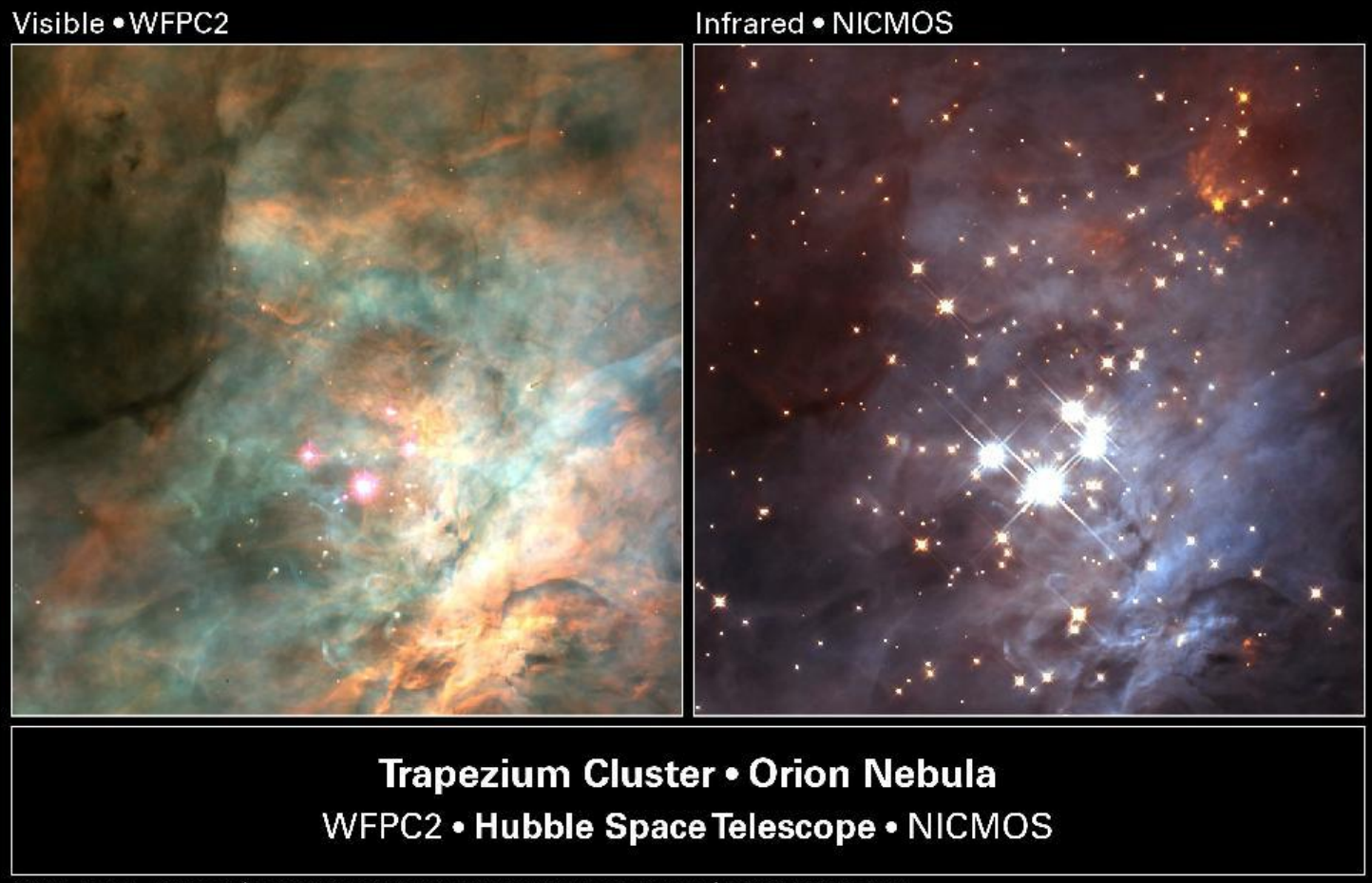

(Bok) Globules silhouetted against emission nebulosity

A dark cloud core seen against a star field

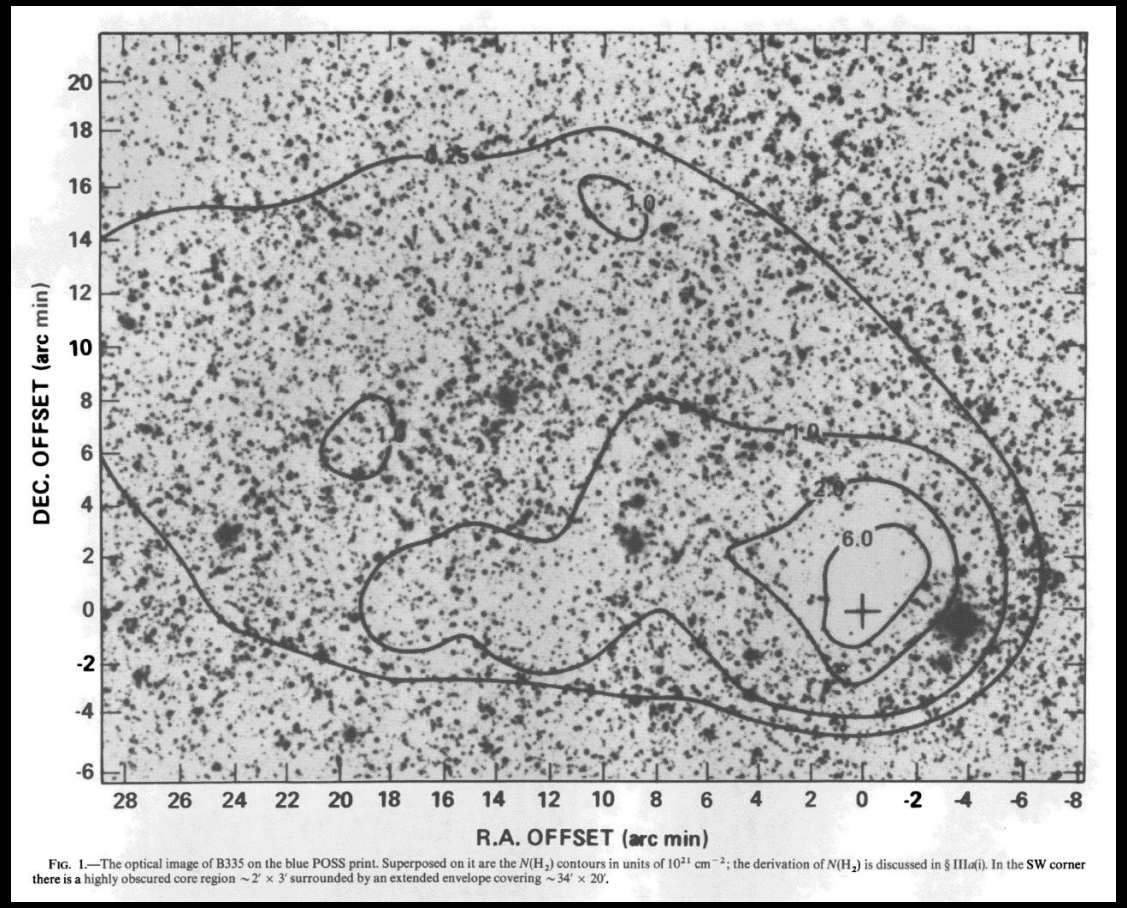

FIG. 1.—The optical image of B335 on the blue POSS print. Superposed on it are the $N(H_2)$ contours in units of 10^{21} cm^{-2}; the derivation of $N(H_2)$ is discussed in § IIIa(i). In the SW corner there is a highly obscured core region ~2′ × 3′ surrounded by an extended envelope covering ~34′ × 20′.

Frerking et al. (1987)

Exercise

1. The interstellar extinction at visual wavelengths toward the Galactic center is about A_V=30 mag. The brightest star in the region in the infrared is IRS 7, an M2 supergiant, and has been measured J=14.2 mag, K=6.50 mag. What is its absolute J magnitude?
2. What is the expected extinction at infrared K band, A_K?

Molecules in space

H_2 molecules

- the main constituent of cold clouds, but lacking a permanent electric dipole moment, so very difficult to detect. A rotationally excited molecule would radiate through a relatively slow electric quadrupole transition.
- Only in a hot medium, where stellar radiation or stellar wind excites vibrational and electronic states which then decay relatively quickly.

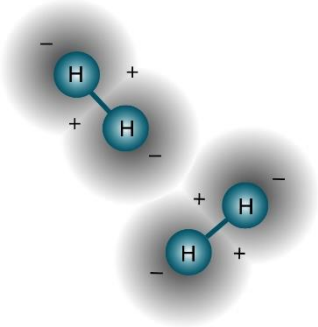

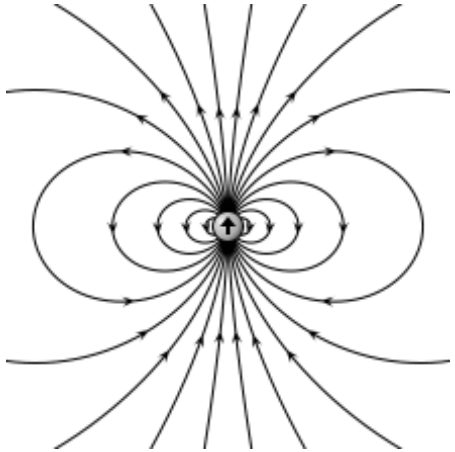

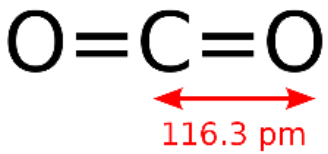

Zero electric dipole moment

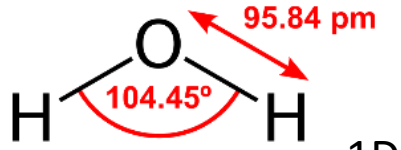

Dipole moment = 1.85 Debyes

1D = 10^{-18} statC·cm

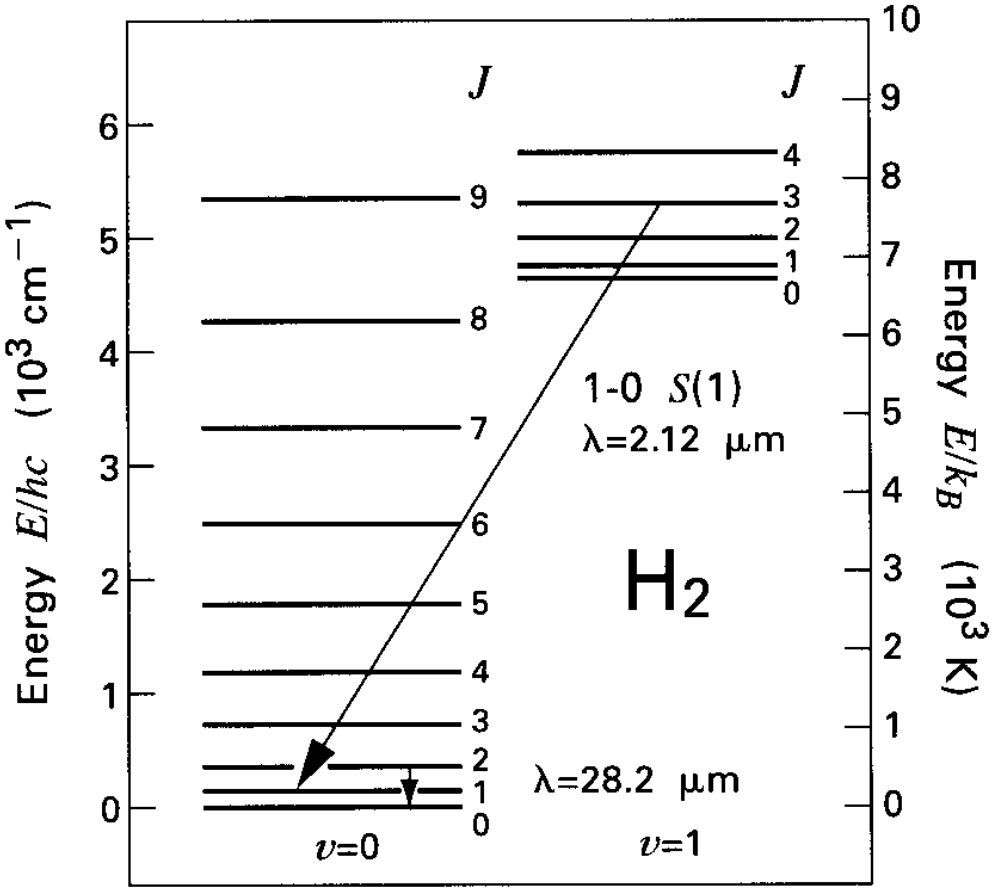

Figure 5.4 Rotational levels of H_2 for the first two vibrational states. Within the $v = 0$ state, the $J = 2 \rightarrow 0$ transition at 28.2 μm is displayed. Also shown is the transition giving the 1-0 S(1) rovibrational line at 2.12 μm. Note that two different energy scales are used.

Stahler & Palla

Monthly Notices
of the
ROYAL ASTRONOMICAL SOCIETY

MNRAS **477,** 4577–4595 (2018) doi:10.1093/mnras/sty853

YSO jets in the Galactic plane from UWISH2 – V. Jets and outflows in M17

M. R. Samal,[1★] W. P. Chen,[1★] M. Takami,[2] J. Jose[3,4] and D. Froebrich[5]

[1]*Graduate Institute of Astronomy, National Central University 300, Jhongli City, Taoyuan County 32001, Taiwan*
[2]*Institute of Astronomy and Astrophysics, Academia Sinica, PO Box 23-141, Taipei 10617, Taiwan*
[3]*Indian Institute of Science Education and Research, Rami Reddy Nagar, Karakambadi Road, Mangalam (PO) Tirupati 517507, India*
[4]*Kavli Institute for Astronomy and Astrophysics, Peking University, Yi He Yuan Lu 5, Haidian Qu, Beijing 100871, China*
[5]*Centre for Astrophysics, and Planetary Science, The University of Kent, Canterbury, Kent CT2 7NH*

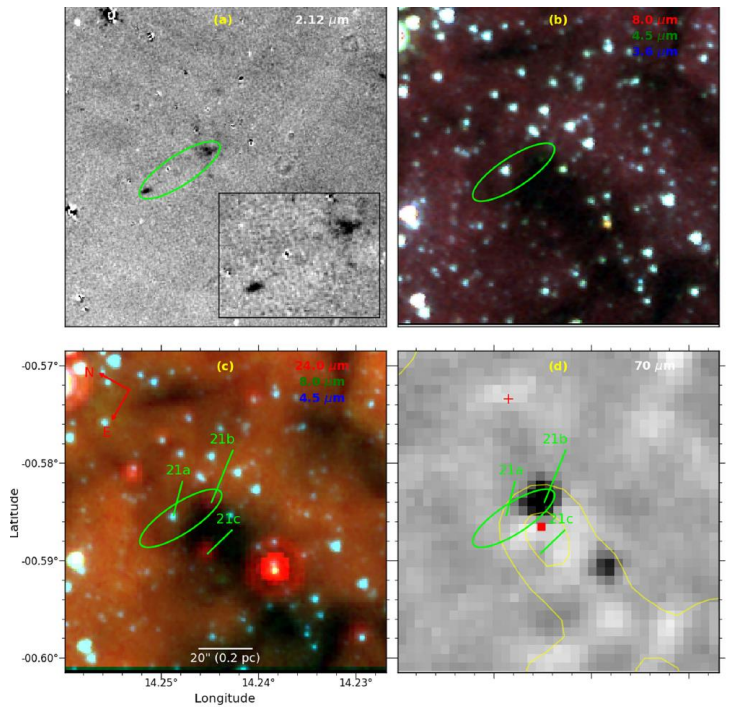

ABSTRACT

Jets and outflows are the first signposts of stellar birth. Emission in the H_2 1–0 S(1) line at 2.122-μm is a powerful tracer of shock excitation in these objects. Here we present the analysis of 2.0×0.8 deg^2 data from the UK Wide-field Infrared Survey for H_2 (UWISH2) in the 1–0 S(1) line to identify and characterize the outflows of the M17 complex. We uncover 48 probable outflows, of which 93 per cent are new discoveries. We identified driving source candidates for 60 per cent of outflows. Among the driving source candidate young stellar objects (YSOs), 90 per cent are protostars and the remaining 10 per cent are Class II YSOs. In comparison with results from other surveys, we suggest that H_2 emission fades very quickly as the objects evolve from protostars to pre-main-sequence stars. We fit spectral energy distribution (SED) models to 14 candidate outflow-driving sources and conclude that the outflows of our sample are mostly driven by moderate-mass YSOs that are still actively accreting from their protoplanetary disc. We examined the spatial distribution of the outflows with the gas and dust distribution of the complex and observed that the filamentary dark cloud M17SWex, located on the south-western side of the complex, is associated with a greater number of outflows. We find that our results corroborate previous suggestions that, in the M17 complex, M17SWex is the most active site of star formation. Several of our newly identified outflow candidates are excellent targets for follow-up studies to understand better the very early phase of protostellar evolution.

CO molecules

- simple and abundant. Strong binding energy E=11.1 eV self-shielding against UV field
- with a permanent electric dipole moment; radiating strongly at radio frequencies.
- $^{12}C^{16}O$ easiest to detect; isotopes $^{13}C^{16}O$, $^{12}C^{18}O$, $^{12}C^{17}O$, $^{13}C^{18}O$ also useful
- Excitation of CO to the J=1 level mainly through collisions with ambient H_2 $X_{CO} = 2 \times 10^{20}\ \mathrm{cm^{-2}}\ [\mathrm{K\ km/s}]^{-1}$ (Bolatto et al. 2013, ARAA)
- At low densities, each excitation is followed by emission of a photon. At high densities, the excited CO transfers the energy by collision to another H_2 molecule; $n_{\mathrm{crit}} \approx 3 \times 10^3\ \mathrm{cm^{-3}}$. Low critical density → CO to study large-scale distribution of clouds, as a tracer of H_2
- $^{12}C^{16}O$ almost always optically thick; same line from other rare isotopes usually not → estimate of column density (total mass) of molecular gas $N_H = 10^6\ N_{13_{CO}}$

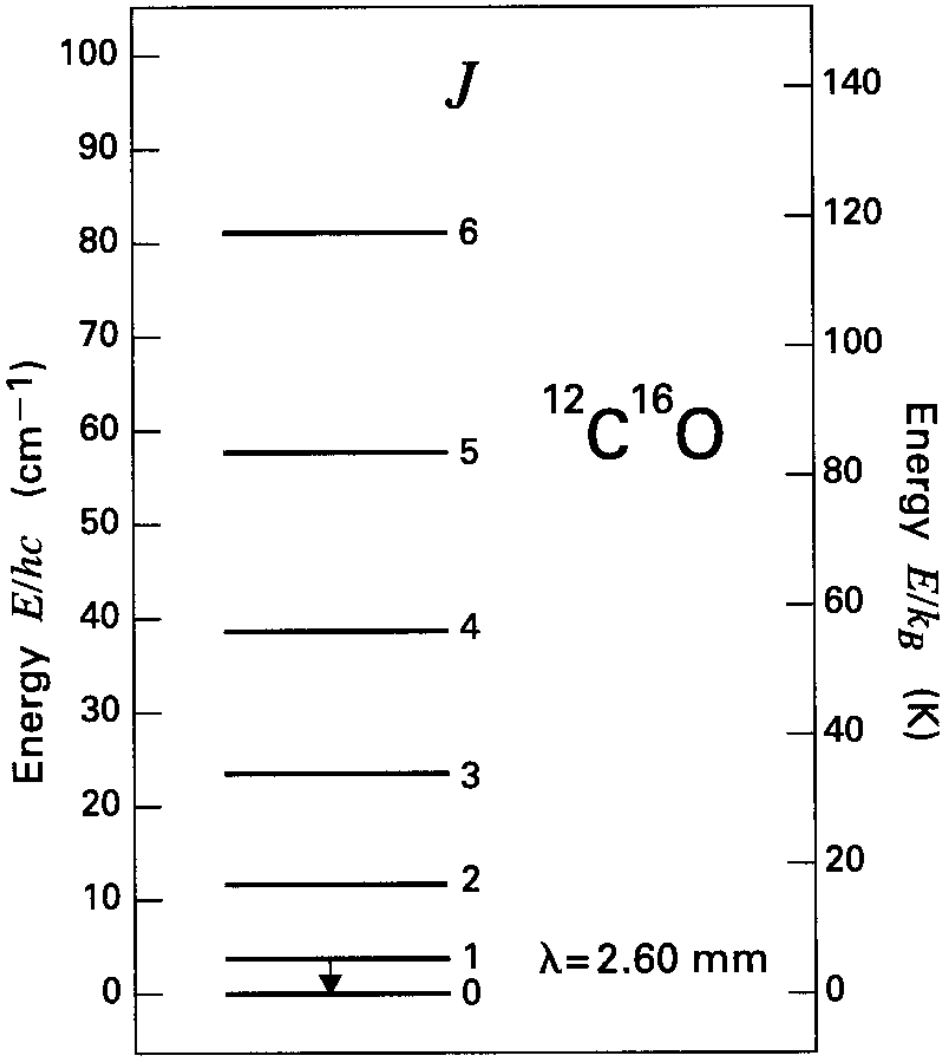

2.6 mm = 115 GHz

Only 5 K above the ground level … can be excited by collisions with ambient molecules or CMB photons

Figure 5.6 Rotational levels of $^{12}C^{16}O$ within the ground ($v = 0$) vibrational state. The astrophysically important $J = 1 \rightarrow 0$ transition at 2.60 mm is shown.

Stahler & Palla

CO band heads in the Becklin-Neugebauer (BN) object --- an infrared-emitting, embedded, massive protostar

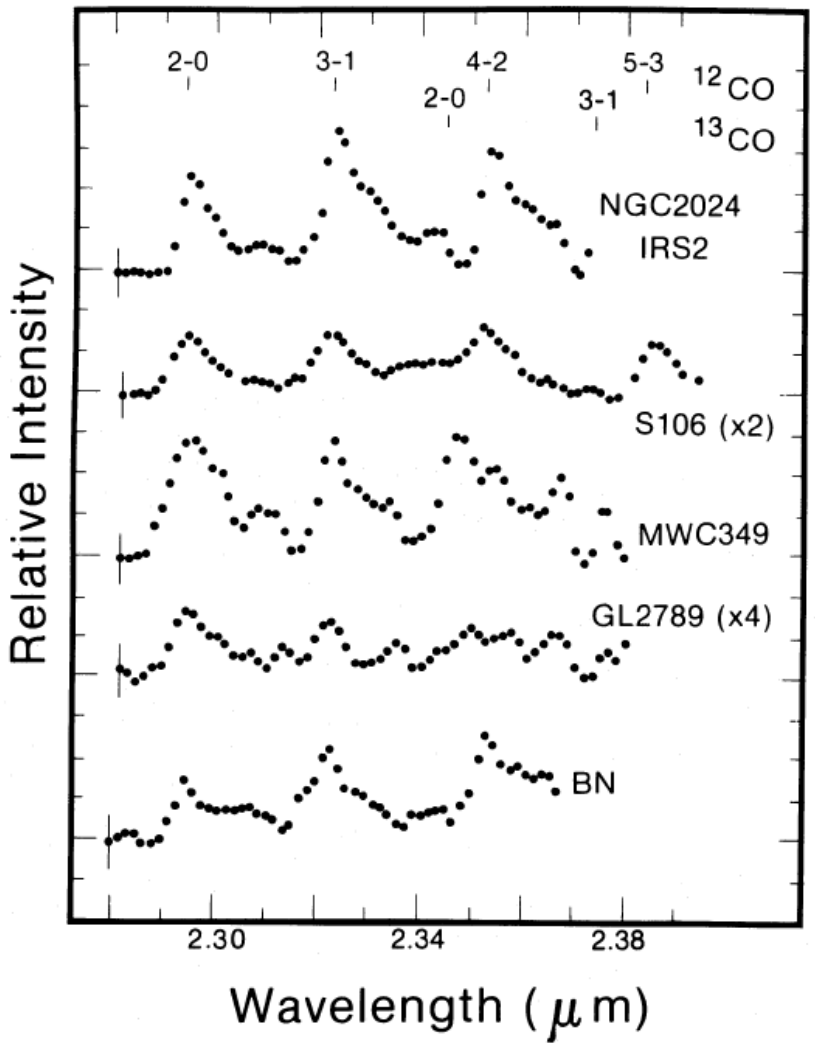

FIG. 2.—Spectra of those sources in which CO band head emission was detected. Linear baselines have been subtracted from each spectrum. The positions of the band heads are indicated at the top of the figure. Vertical scale marks are separated by 2×10^{-17} W cm^{-2} μm^{-1}. Noise levels are indicated on the short wavelength data points.

Gaballe & Persson (1987)

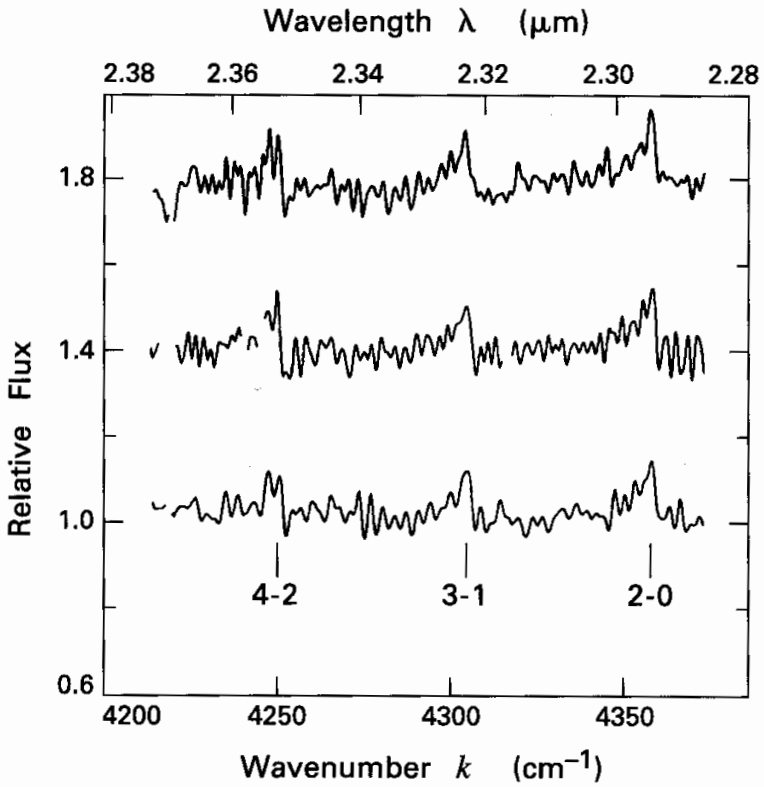

Figure 5.8 Near-infrared spectrum of the BN object in Orion, shown at three different observing times. The relative flux is plotted against the wave number k, defined here as $1/\lambda$.

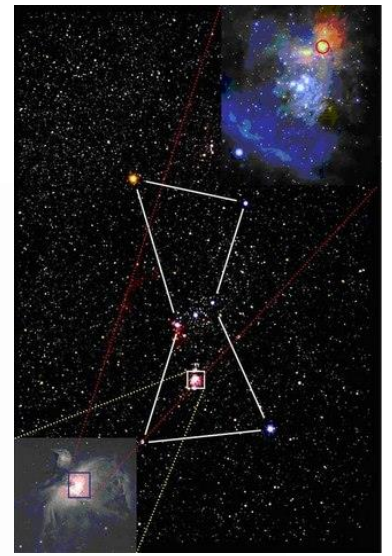

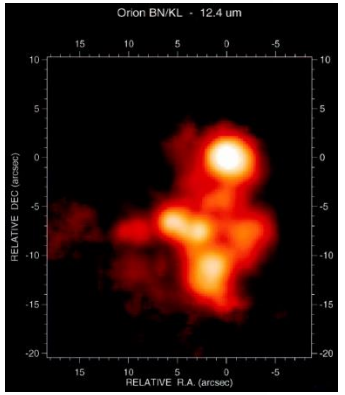

Stahler & Palla

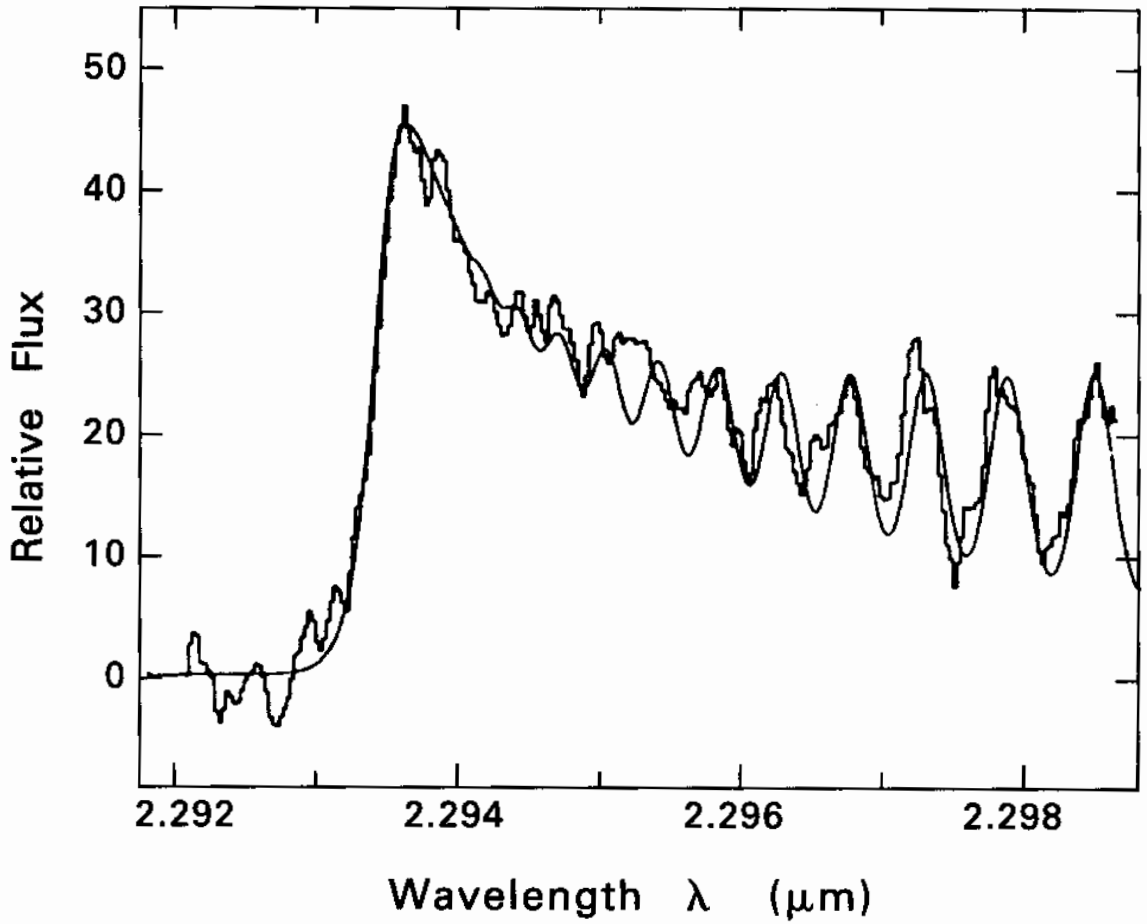

Figure 5.9 High-resolution near-infrared spectrum of the embedded stellar source SSV 13. The structure of the $v = 2 \rightarrow 0$ band head in $^{12}C^{16}O$ is evident. The smooth curve is from a theoretical model that employs an isothermal slab at 3500 K. Note that the spectrum here represents only a portion of the R-branch.

Stahler & Palla

Each species has a different set of excitation conditions (density, temperature; cf. Boltzmann equation)

➔ Different molecules/isotopes serve as <u>tracers</u> of these conditions, e.g., C18O traces denser parts of a cloud than 12CO does; NH3 maps the dense cores where protostars are located.

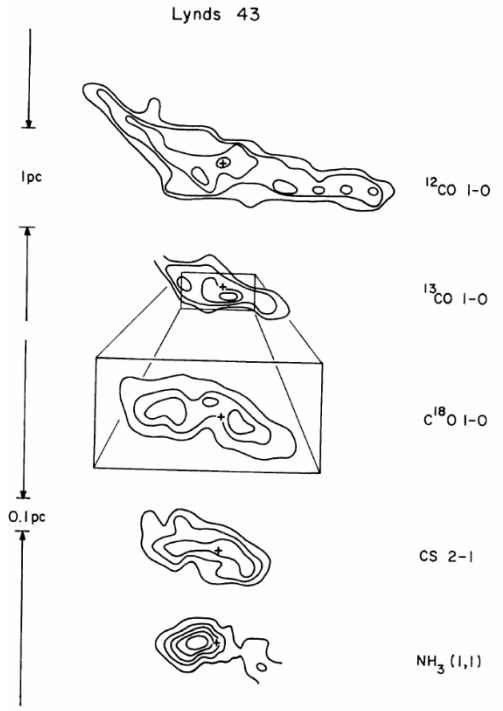

Myers et al. 1991

^{12}CO

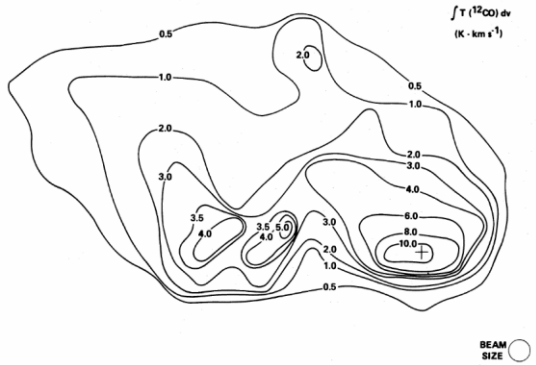

^{13}CO

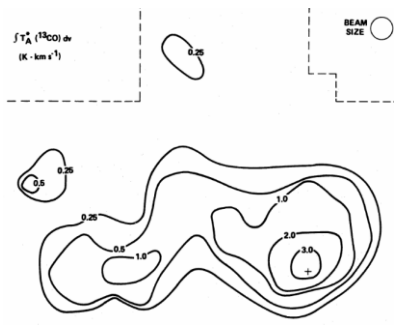

C^{18}O

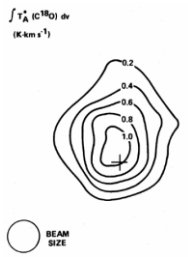

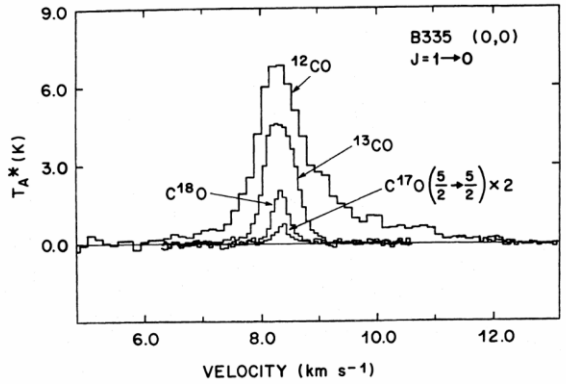

Frerking et al. (1987)

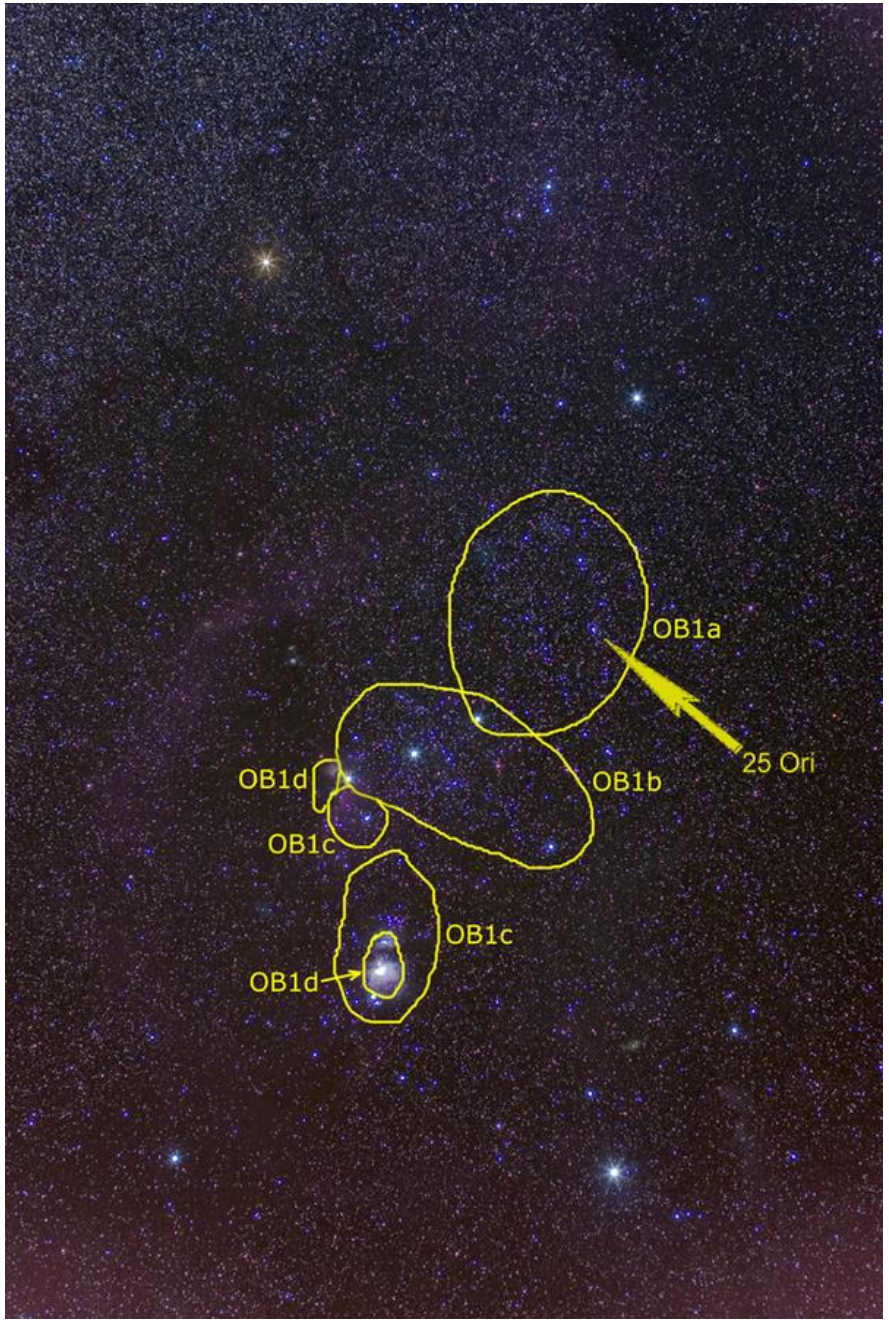

http://en.wikipedia.org/wiki/File:Orion_OB1_%26_25_Ori_Group.png

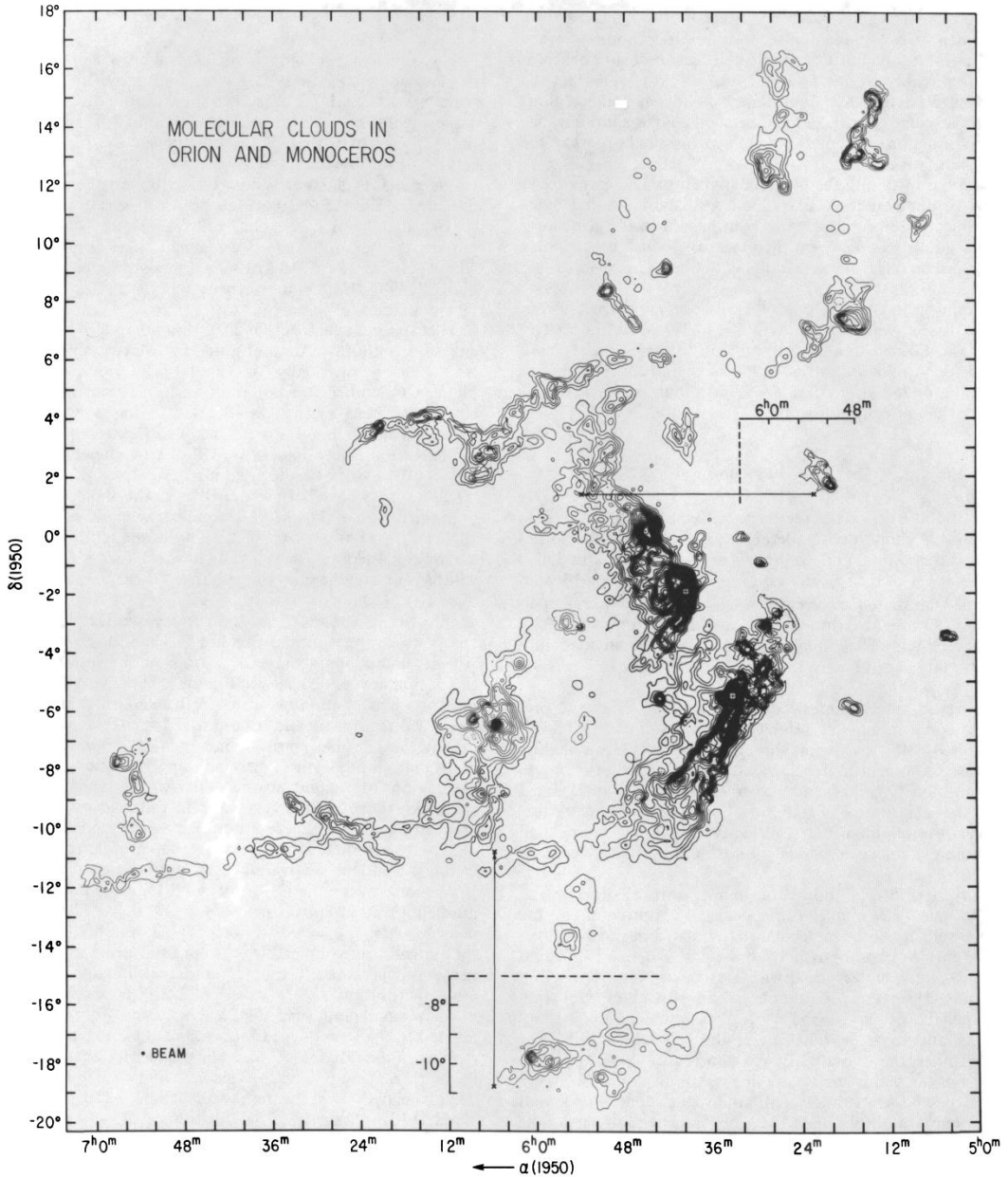

FIG. 2.—Contour map of integrated intensity of CO emission (W_{CO}) in the velocity range of −10 to 20 km s^{-1}. (Along the Galactic plane, CO emission was found at higher velocities, presumably from unrelated clouds more distant than the Orion clouds. These clouds are discussed elsewhere.) The lowest contour level is at 1.28 K km s^{-1} with subsequent levels at 3, 5, 7, ... times this value. The peaks of emission from the Orion Nebula and from NGC 2023 and 2024 (see Fig. 3) are designated by crosses. Two clouds, shown here in insets (see § III and also Figs. 3–5), that overlap other clouds in the survey lie at the positions indicated by arrows.

Maddalena+86

HCN (hydrogen cyanide) the poisonous gas? HCO^+? What is going on?

Layers of circumstellar envelope of IRC+10216 (Leão+06)

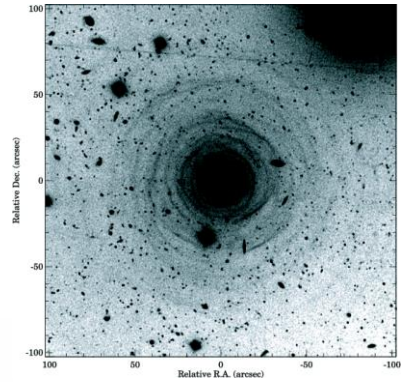

Kleinmann-Low (KL) object

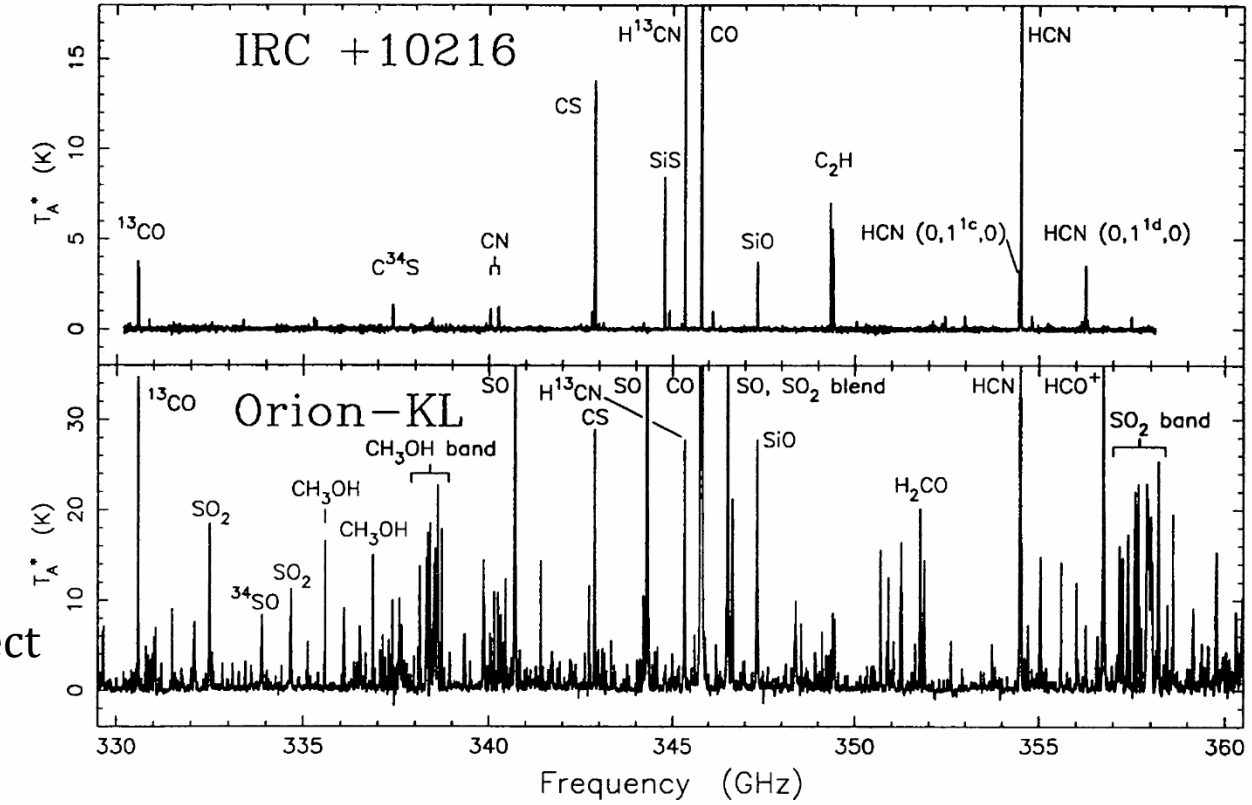

= CW Leo, a carbon (i.e., evolved) star, puffing off its dusty atmosphere

A protostar in Orion

FIG. 4.—Comparison of the CSO spectral line surveys of IRC +10216 and Orion-KL. The data have been corrected by the main beam (0.6) and extended efficiencies (0.76) for IRC +10216 and Orion-KL, respectively. Note the difference in vertical scale between the two panels.

Groesbeck+94

Star formation is not an isolated event.

Massive stars in particular may trigger the birth of next-generation stars → **triggered star formation**

… also possible by stellar jets, Galactic density waves, cloud-cloud collisions …

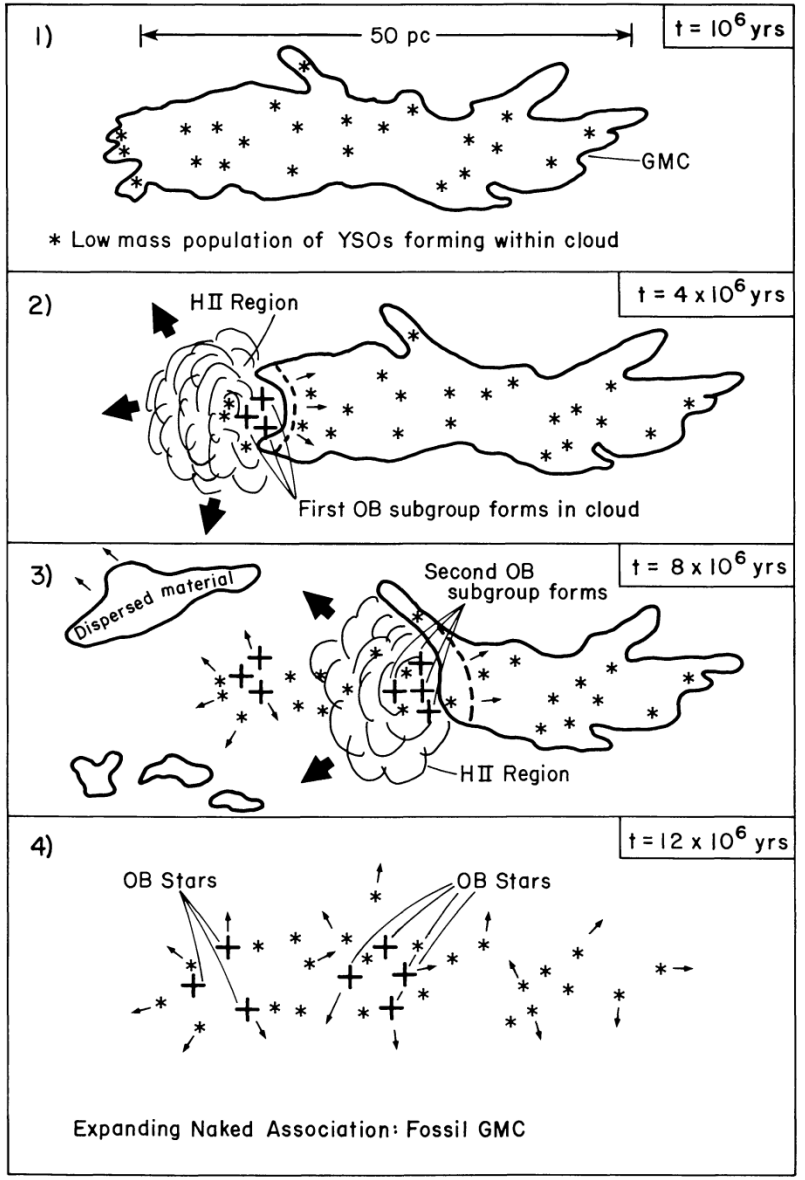

Figure 1. Probable stages in the formation of an expanding OB association from a giant molecular cloud. Low star formation efficiency in conjunction with efficient dispersal of residual, unprocessed molecular gas by OB stars result in a stellar system with positive total energy.

Lada 1987

Luminous stars → photoionization of a nearby cloud
→ Radiative driven implosion

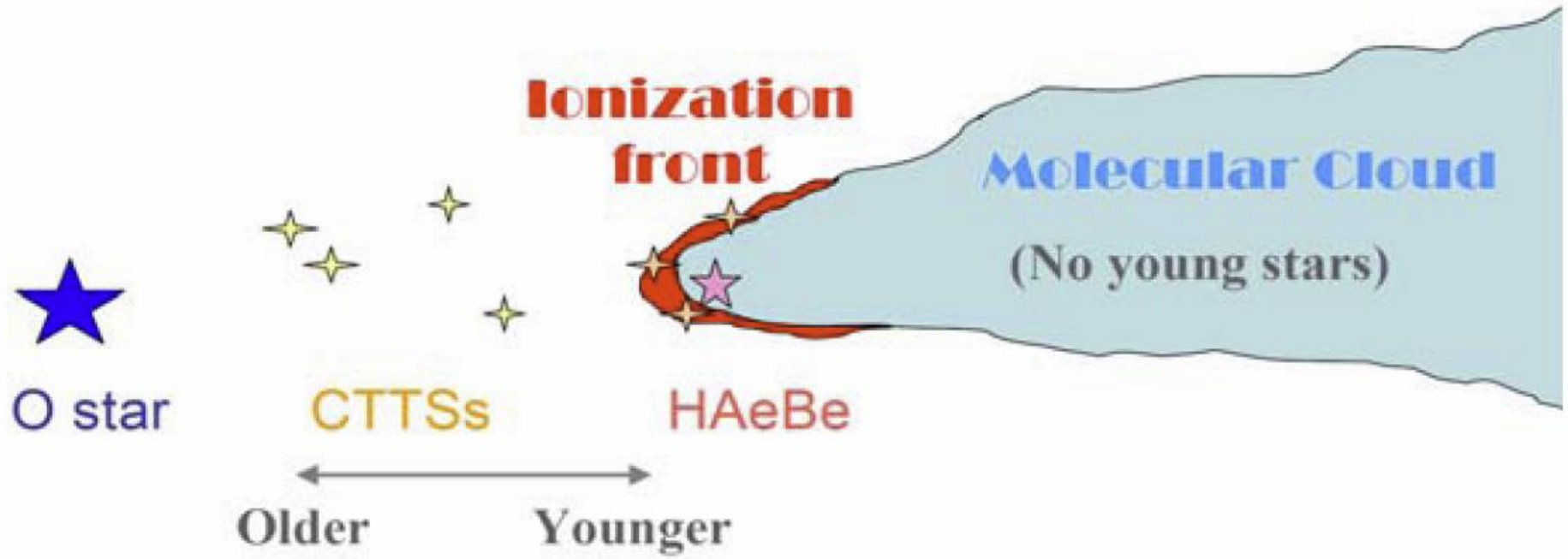

Figure 2. An illustration of a massive star to trigger star formation in a nearby molecular cloud.

Chen+06

Luminous stars → photoionization/winds on surrounding clouds → Collect and collapse

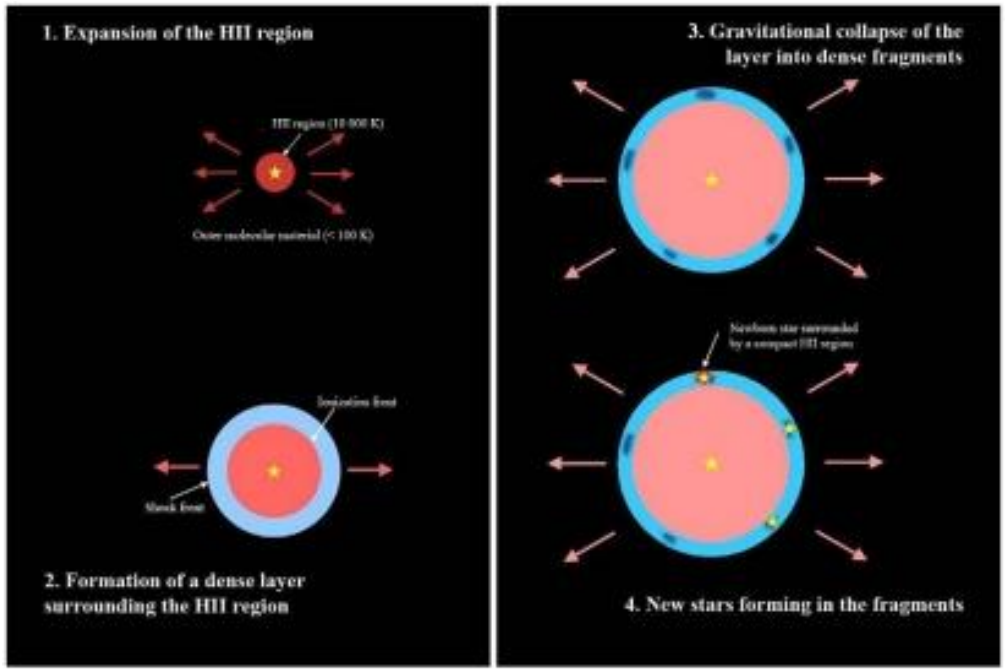

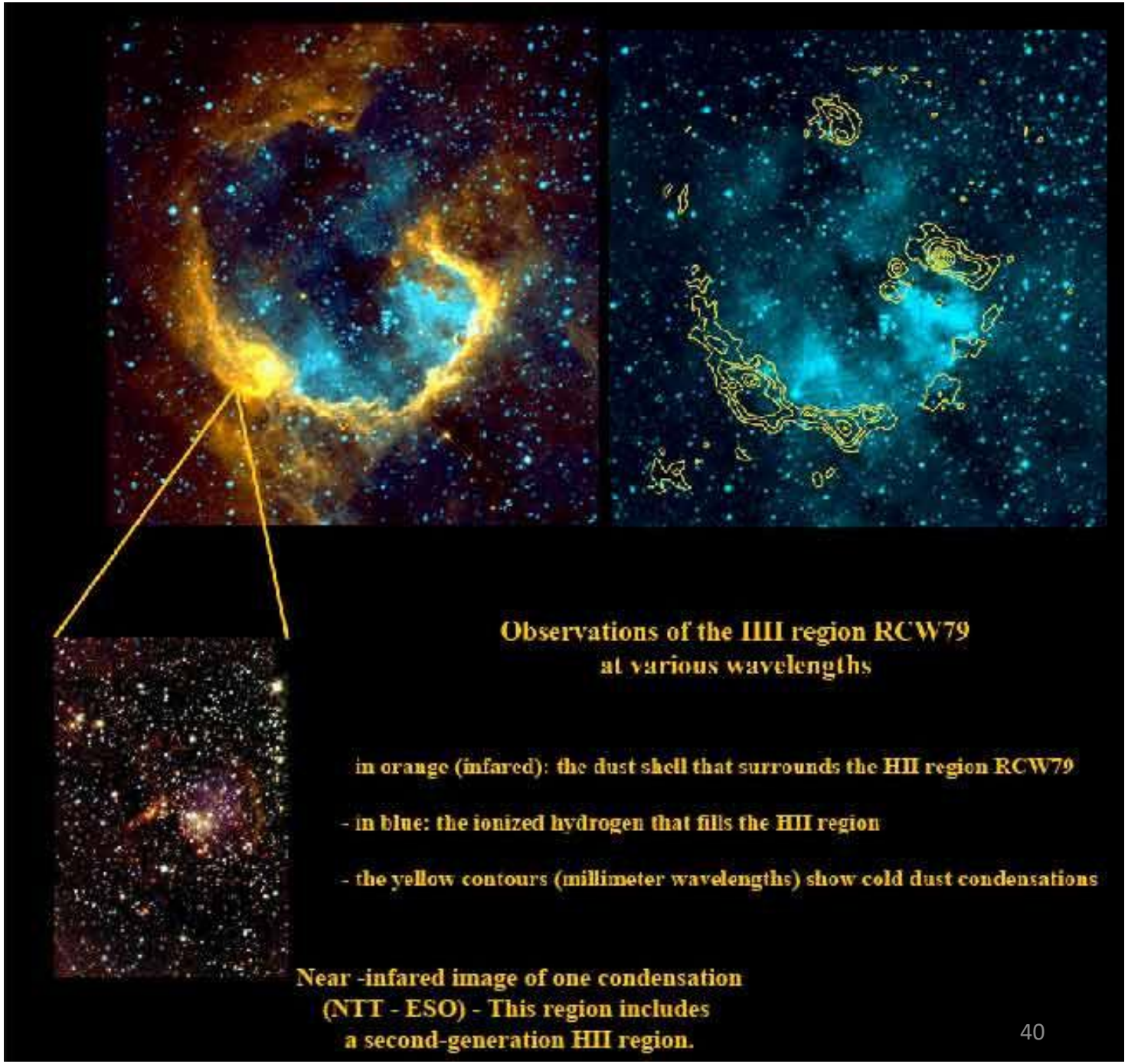

Size Scales for Star Formation

Object	log size scale [cm]
Galactic spiral arm	22
Giant molecular cloud	20
Molecular dense core	17
Protostellar accretion disk	15
Protostar	11

Myers in You & Yuan (1995), p. 47

Mass Inventory in a Star-Forming Galaxy

Component	log M [$M_\odot$]
Molecular clouds	9
H_2	9
He	8
CO	7
Young stars	5

Myers in You & Yuan (1995), p. 47

Properties of Giant Molecular Clouds

Diameter [pc]	Mass [$M_\odot$]	Density [cm^{-3}]	T [K]	Velocity Width [km/s]
20-100	$10^5 - 10^6$	10-300	10-30	5-15

Myers in You & Yuan (1995), p. 47

Exercise

1. What is the BN object (why is it called an “object”)? What is its brightness, distance, luminosity, and mass (how are these known)?
2. Answer the same for the KL object. What is the relation between the two?
3. There is a class of objects called the “Herbig-Haro objects”. What are they?

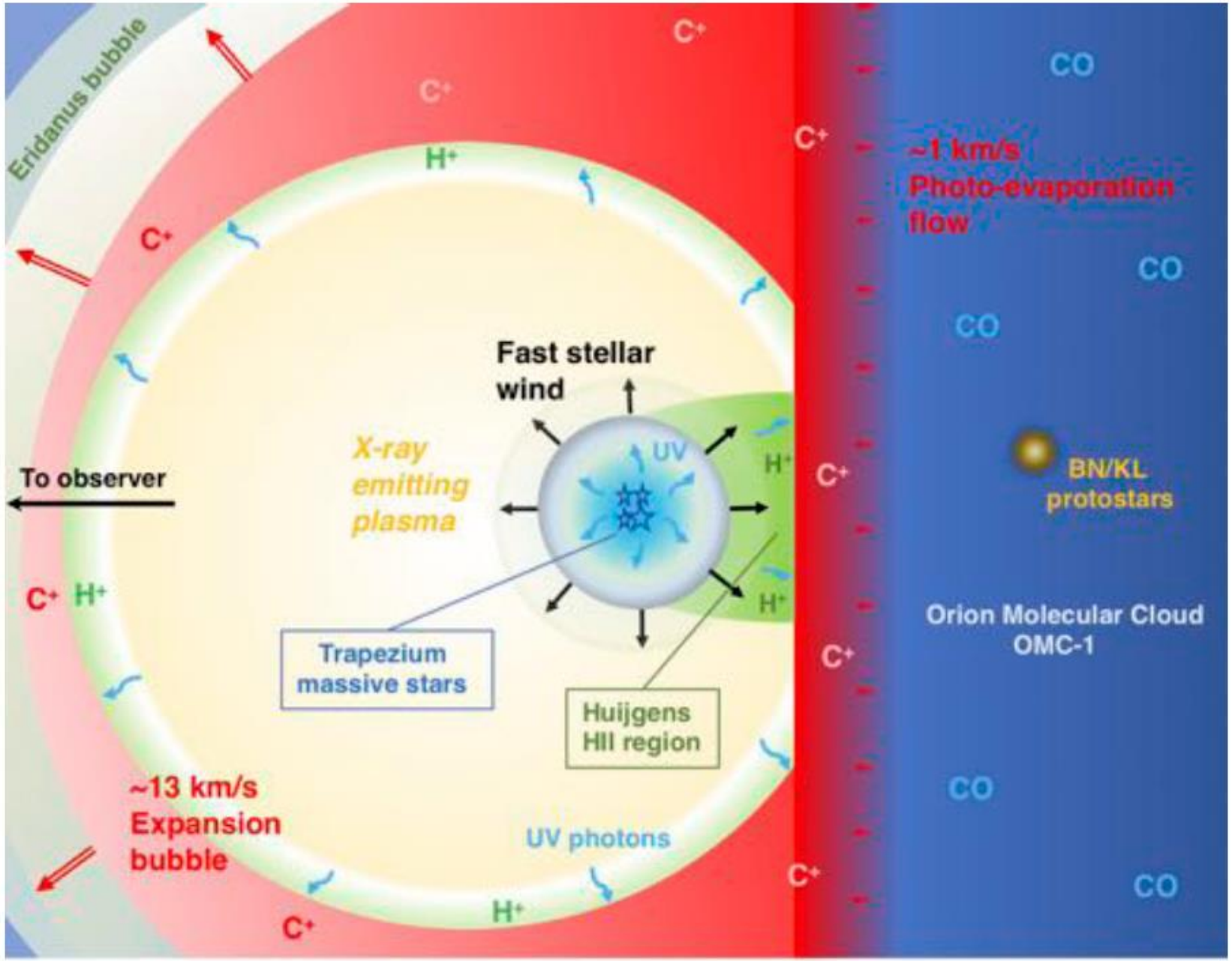
Eridanus bubble
C+
H+
CO
~1 km/s
Photo-evaporation
flow
Fast stellar
wind
X-ray
emitting
plasma
To observer
UV
BN/KL
protostars
Trapezium
massive stars
Huijgens
HII region
Orion Molecular Cloud
OMC-1
~13 km/s
Expansion
bubble
UV photons

Pabst+19

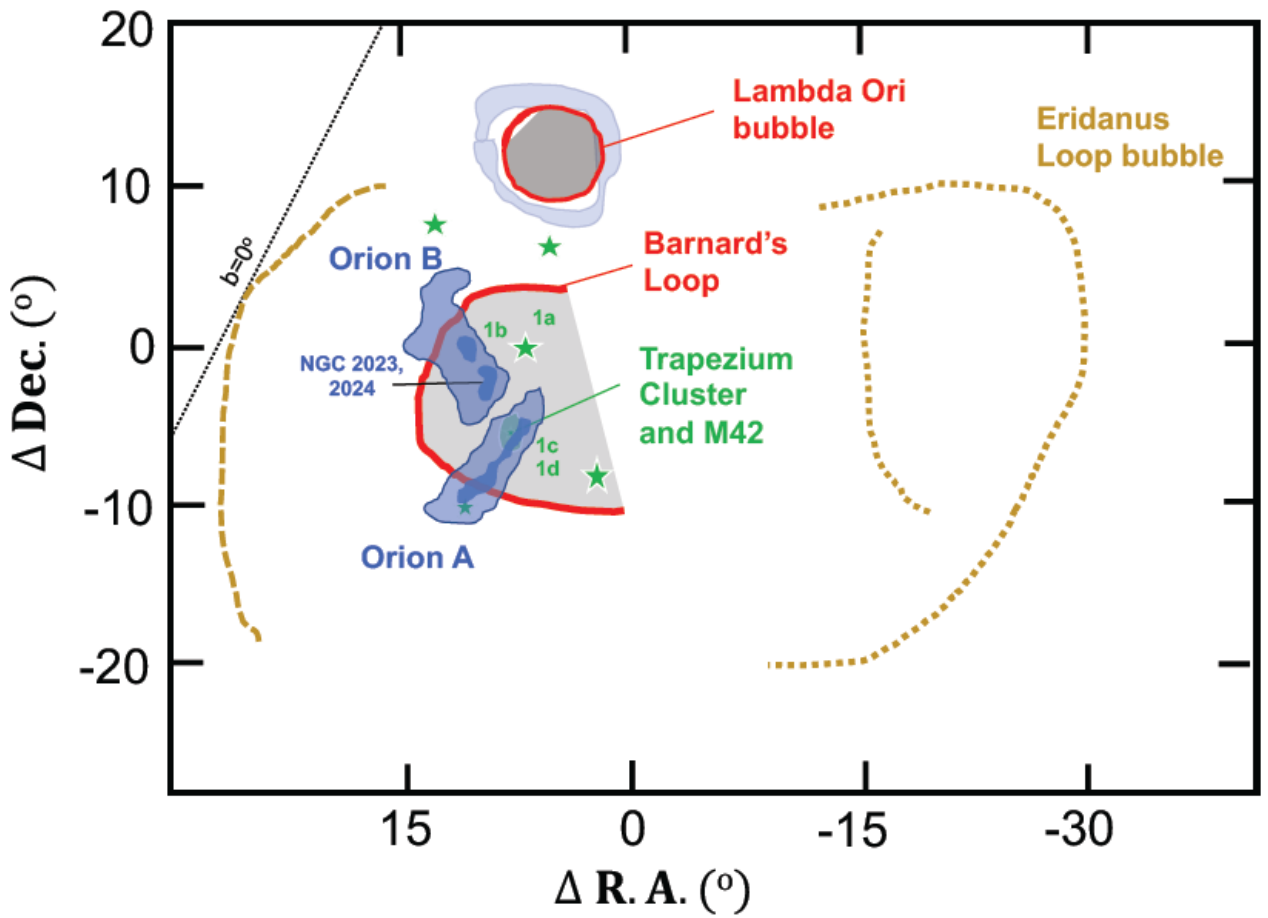

Extended Data Figure 3: **Schematic overview of the large scale (~350 pc) structure of Orion.** We mark with green stars the locations of the massive stars spanning up the Orion constellation (shoulders and knees, but the belt is indicated by a single star; M42 is at the tip of the sword), in blue outline the two giant molecular clouds A & B, in green filled trace the prominent HII regions including M42 powered by the trapezium cluster, in red Barnard's loop, which is very prominent in Hα. The bubble surrounding λ Ori is also indicated (red=ionized gas, blue swept up molecular shell, and the boundaries of the superbubble (yellow). The locations of the Orion OB subassociations are marked in green.

Pabst+19

https://en.wikipedia.org/wiki/File:Orion_Head_to_Toe.jpg

Cloud Stability --- The Virial Theorem

Moment of Inertia $$I = \int r^2 dm = \sum_i m_i r_i^2$$

$$\frac{d^2 I}{dt^2} = \frac{d^2}{dt^2}(mr^2) \cdots (\text{if } \dot{m} = 0) \cdots$$

$$= 2m\frac{d}{dt}(r\dot{r}) = 2m(\dot{r}^2 + r\ddot{r})$$

$$\boxed{\frac{1}{2}\frac{d^2 I}{dt^2} = 2E_K + E_P}$$

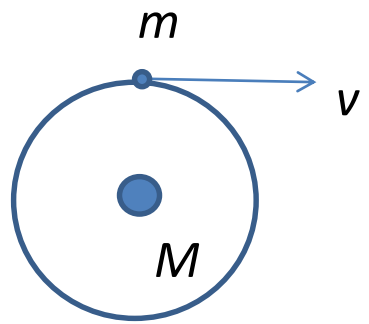

$$\frac{GmM}{r^2} = m\frac{v^2}{r}$$

To be stable, LHS = 0

$$2\left({}^{1}/_{2}\right) mv^2 = GmM/r$$

$$\boxed{2E_K + E_P = 0}$$

Virial Mass

MASS, LUMINOSITY, AND LINE WIDTH RELATIONS OF GALACTIC MOLECULAR CLOUDS

P. M. SOLOMON, A. R. RIVOLO, J. BARRETT, AND A. YAHIL
Astronomy Program, State University of New York–Stony Brook
Received 1986 October 2; accepted 1987 February 2

THE ASTROPHYSICAL JOURNAL, **319**:730–741, 1987 August 15

ABSTRACT

We present measurements of the velocity line width, size, virial mass, and CO luminosity for 273 molecular clouds in the Galactic disk between longitudes of 8° and 90°. These are obtained from three-dimensional data in the Massachusetts–Stony Brook CO Galactic Plane Survey. From an analysis of these measurements we show that the molecular clouds are in or near virial equilibrium and are not confined by pressure equilibrium with a warm or hot phase of interstellar matter. The velocity line width is shown to be proportional to the 0.5 power of the size, $\sigma_v \propto S^{0.5}$. Combined with virial equilibrium, this shows that the clouds are characterized by a constant mean surface density of 170 $M_\odot$ pc^{-2} and have a mass $M \propto \sigma_v^4$. A tight relationship, over four orders of magnitude, is found between the cloud dynamical mass, as measured by the virial theorem, and the CO luminosity $M \propto (L_{CO})^{0.81}$. This relationship establishes a calibration for measuring the total molecular cloud mass from CO luminosity for individual clouds and for the Galactic disk. The cloud CO luminosity is $L_{CO} \propto \sigma_v^5$, which is the molecular cloud analog of the Tully-Fisher or Faber-Jackson law for galaxies.

The mass-luminosity law is accounted for by a cloud model consisting of a large number of optically thick clumps in virial equilibrium, each with a thermal internal velocity dispersion, but with the clouds effectively optically thin at a fixed velocity along the line of sight. The typical clump mass is of order a stellar mass and approximately equal to the Jeans mass at the clump density and thermal velocity dispersion.

TABLE 1

GALACTIC FIRST QUADRANT MOLECULAR CLOUD CATALOG

(1)	(2)	(3)	(4)	(5)	(6)	(7)	(8)	(9)	(10)	(11)	(12)	(13)	(14)	(15)
No.	$T_{min}-I$	ℓ_p	b_p	v_p	T_p	R	D	z	σ_ℓ	σ_b	σ_v	$L_{CO}/10^4$	$M_{VT}/10^4$	Flag
	(K)	(Deg.)	(Deg.)	(km·s^{-1})	(K)	(kpc)	(kpc)	(pc)	(Deg.)	(Deg.)	(km·s^{-1})	(K·km·s^{-1}·pc^2)	($M_\odot$)	
1	4–3	8.00	−0.50	128.	5.7	1.4	10.1	−89.	0.06	0.07	4.4	7.27	44.4	T
2	5–3	8.20	0.20	20.	10.2	6.2	15.9	56.	0.17	0.21	4.1	140.2	176.3	F,V
3	4–4	8.30	0.00	3.	5.7	4.0	6.2	0.	0.40	0.11	3.8	22.6	65.4	X
4	4–5	8.30	−0.10	48.	8.2	3.6	13.2	−23.	0.05	0.05	2.2	5.02	11.1	F,U
5	5–6	8.40	−0.30	37.	17.0	4.4	5.7	−30.	0.32	0.15	3.9	23.3	66.5	N,H

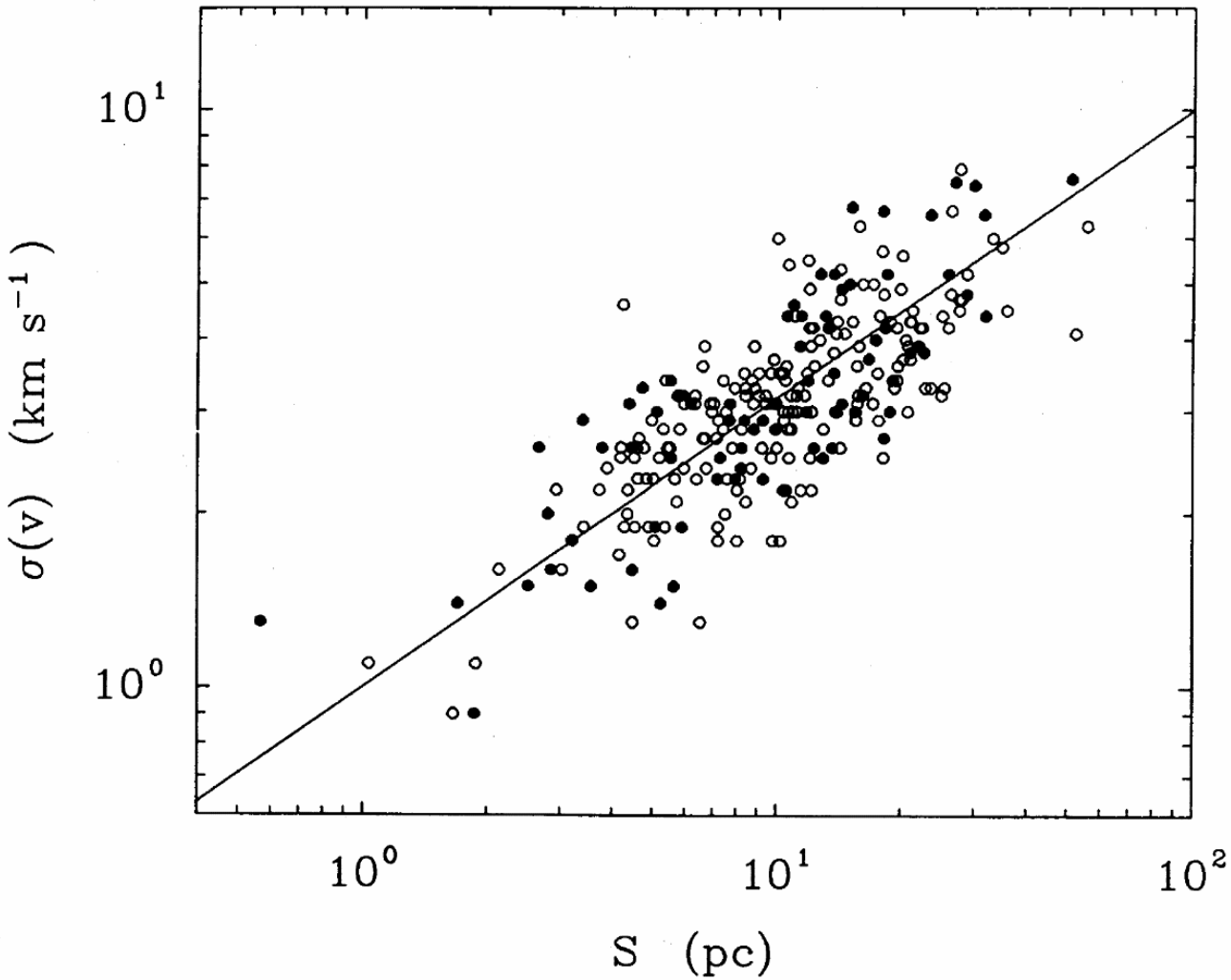

FIG. 1.—Molecular cloud velocity dispersion $\sigma(v)$ as a function of size S (defined in text) for 273 clouds in the Galaxy. The solid circles are calibrator clouds with known distances and the open circles are for clouds with the near-far distance ambiguity resolved by the method discussed in the text. The fitted line is $\sigma(v) = S^{0.5}$ km s^{-1}. For virial equilibrium the 0.5 power law requires clouds of constant average surface density.

LHS $= 0$ → stable

LHS < 0 → collapsing

LHS > 0 → expanding

E_K a variety of kinetic energies

- ✓ Kinetic energy of molecules
- ✓ Bulk motion of clouds
- ✓ Rotation
- ✓ …

E_P a variety of potential energies

- ✓ Gravitation
- ✓ Magnetic field
- ✓ Electrical field
- ✓ …

$$E_{\text{total}} = E_K + E_P$$
$$= E_K + \Omega \text{ (mostly)}$$

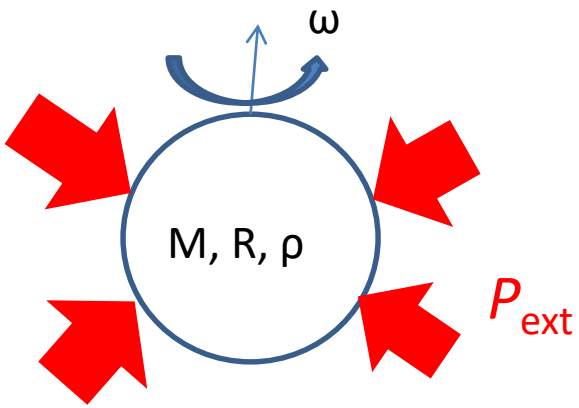

Cloud of mass M, radius R, rotating at ω

$$E_{rot} = \frac{1}{2} I \omega^2 \qquad I = \frac{2}{5} M R^2 \qquad \Omega = -\frac{3}{5}\frac{GM^2}{R}$$

Generalized virial theorem

$$\frac{1}{2}\frac{d^2 I}{dt^2} = 2 < E_K > + \int \vec{r} \cdot \vec{F} dm \quad + 3 \int P dV - \oint P \vec{r} \cdot d\vec{s}$$

If $\omega = 0$, and $P_{\text{ext}} = 0$

$$2 \cdot \frac{3}{2}\frac{M}{\mu m_H} kT - \frac{3}{5}\frac{GM^2}{R} = 0$$

$$R_J = \frac{1}{5}\frac{GM\mu m_H}{kT}$$

This is the **Jeans length**.

$\mu \approx 2.37$ for solar abundance with H_2

Jeans length = critical spatial wavelength

If perturbation length scale is longer
→ Medium is decoupled from self-gravity ➔ stable

$$M_J = \frac{4}{3}\pi R_J^3 \rho$$

$$R_J = \left(\frac{15}{4\pi}\frac{kT}{\mu m_H G \rho}\right)^{1/2} \sim \sqrt{\frac{T}{\rho}}$$

$$M_J = \left(\frac{\pi kT}{4\mu m_H G}\right)^{3/2} \sqrt{\frac{1}{\rho}} \sim \frac{T^{3/2}}{\rho^{1/2}}$$

This is the **Jeans mass** … the **critical** mass for onset of gravitational collapse

If cloud mass M > M_{Jeans} ➔ cloud collapse

Note the above does not consider external pressure, or other internal supporting mechanisms.

A non-magnetic, isothermal cloud in equilibrium with external pressure
→ a **Bonnor-Ebert sphere** (Bonnor 1956, Ebert 1955)

$$2E_K + E_P - 3P_{\text{ext}}V = 0$$

The potential term can include, other than the gravitational force, also rotation, magnetic field, etc.

At first, the cloud is optically **thin**.

Contraction → density ↑ → collisions more frequent
→ molecules excited and radiated → radiation escapes
→ cooling → less resistance to the contraction
➔ collapse (free fall)

$R_J \approx c_s \, \tau_{\text{ff}}$ = [isothermal sound speed] * [free fall time]

To maintain $2E_K + E_P = 0$, the total energy $E_t = E_K + E_P$ must change.
The gravitational energy

$$\Omega \sim -\frac{GM^2}{r} \rightarrow d\Omega \sim \frac{dr}{r^2}$$

For contraction, $dr < 0$, so $d\Omega < 0$, then $\mathrm{d}E_t = \mathrm{d}E_K + \mathrm{d}\Omega = ½\,\Omega = L\,\Delta t$

This means to maintain quasistatic contraction, **half** of the gravitation energy from the contraction is radiated away.

Eventually the cloud becomes dense enough (i.e., optically **thick**) and contraction leads to temperature increase.

The cloud's temperature increases while energy is taken away
→ negative heat capacity

Numerically, $M_J = 1.0 \left(\frac{T}{10\ \mathrm{K}}\right)^{3/2} \left(\frac{n_{\mathrm{H_2}}}{10^4\ \mathrm{cm^{-3}}}\right)^{-1/2} [\mathcal{M}_\odot]$

- <u>H I clouds</u>

  $T \approx 100$ K, $n_H \approx 100$, $R_{\mathrm{J}} \approx 25$ pc; $M_{\mathrm{J}} \approx 300\ \mathcal{M}_\odot > M_{\mathrm{obs}}$

  So H I clouds are not collapsing.

- <u>Dark molecular clouds</u>

  $T \approx 15$ K, $n_H \approx 10^5$, $M_{\mathrm{J}} \approx 20\ \mathcal{M}_\odot < M_{\mathrm{obs}} \approx 100\text{–}1000\ \mathcal{M}_\odot$

  So H_2 clouds (dense cores and Bok globules) should be collapsing. But observations show that most are not.

  → There is additional support other than the thermal pressure, e.g., rotation, magnetic field, turbulence, etc.

Roughly, the requirement for a cloud to be gravitational stable is

$$\left|E_{\text{grav}}\right| > E_{\text{th}} + E_{\text{rot}} + E_{\text{turb}} + E_{\text{mag}} + \ \ldots$$

For a spherical cloud, $E_{\text{grav}} = -C_{\text{grav}} {}^{GM^2}/_{R}$, where C_{grav} is a constant depending on the mass distribution (=3/5 for uniform density).

The thermal energy, $E_{\text{th}} = \frac{3}{2} \frac{m}{\mu m_H} k_B T$, where μ is the mean molecular weight of the gas in atomic mass units.

The rotational energy $E_{\rm rot} = C_{\rm rot}\, M\, R^2 \omega^2$, where $C_{\rm rot}$ depends on the mass distribution and is $2/5$ for uniform density; ω is the (assumed) uniform angular velocity.

The turbulent kinetic energy $E_{\rm turb} = \frac{1}{2}\, M\sigma^2$, where σ is the mean turbulent velocity.

The magnetic energy $E_{\rm mag} = \frac{1}{8\pi}\int B^2\, {\rm d}V \approx \frac{1}{6} B^2 R^3$, where B is the uniform magnetic field.

In MKS, $E_{\rm mag} = \frac{\rm B^2}{2\mu_0}$, where μ_0 is permeability of free space

For **rotational support** to be important,

$$\frac{3}{5}\frac{GM^2}{R} = \frac{1}{2}I\omega^2 = \frac{1}{2}\left(\frac{2}{5}MR^2\right)\left(\frac{v_{\rm crit}}{R}\right)^2 = \frac{1}{5}Mv_{\rm crit}^2$$

So $v_{\rm crit} = (3GM/R)^{1/2}$, where $v_{\rm crit}$ is the critical rotation velocity at the equator.

Fluid bodies (stars, clouds, galaxies) do not spin like solid bodies. Instead, they rotate differentially, i.e., faster (shorter period) at low latitudes.

Numerically, $v_{\rm crit} = 0.11\left[\frac{M}{\mathcal{M}_\odot}\frac{\rm pc}{R}\right]^{1/2}$ [km/s]

For HI clouds, $v_{\rm crit} = 0.11\left[\frac{50}{2.5}\right]^{1/2} \approx 0.5$ [km/s]

Typically, $\omega \approx 10^{-16}$ s^{-1}, so $v \approx 0.01$ to 0.1 [km/s]

➔ Clouds are generally **not** rotationally supported.

Rotation of Molecular Cloud Cores

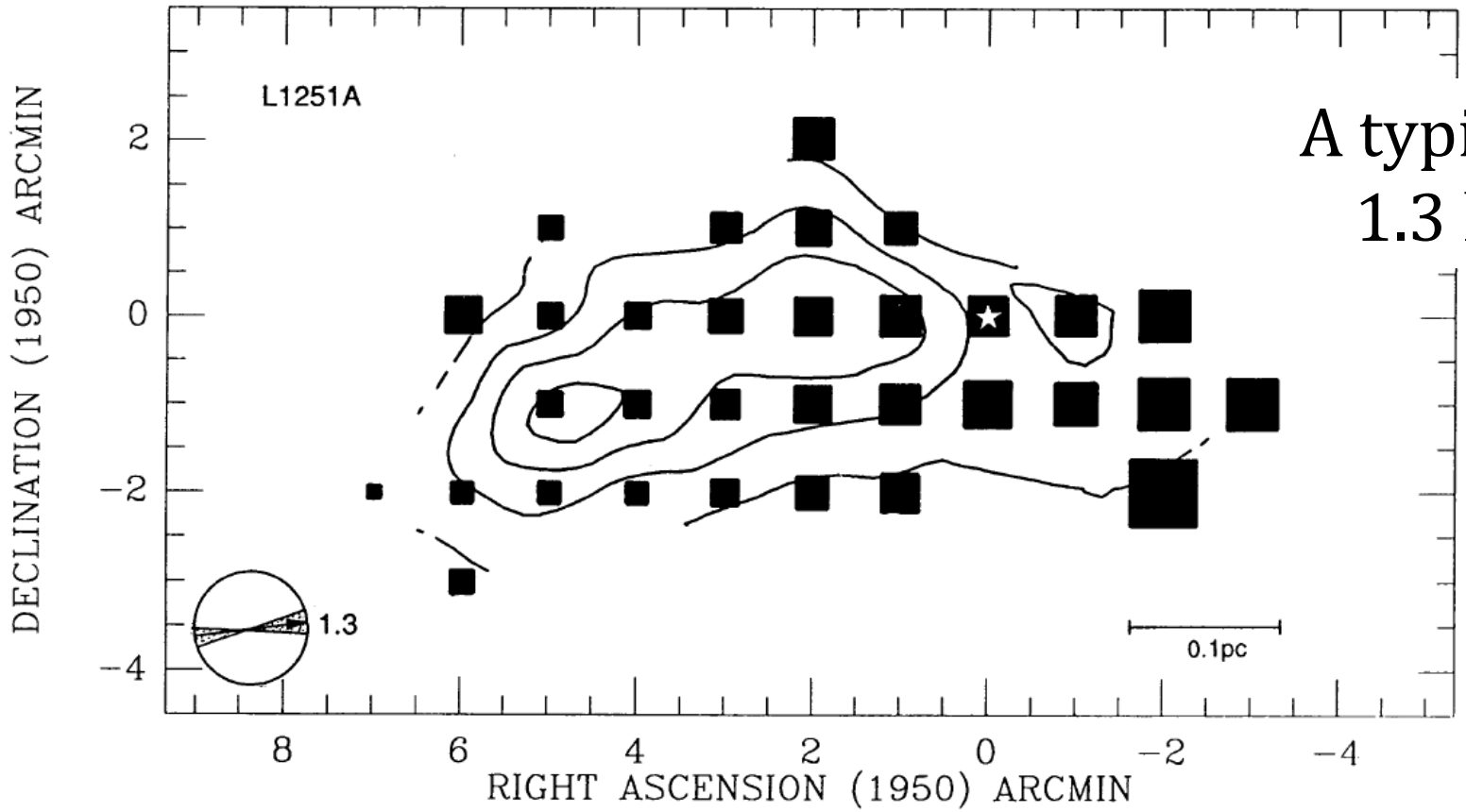

A typical gradient of $1.3\ \mathrm{km\ s^{-1}\ pc^{-1}}$

1.3 cm NH3 line with the line center velocity increasing with the size of the square at each map point. The progression of the line velocity, (−3.46,-4.65) km/s, from east to west indicates core rotation (Goodman+1993).

Measuring the ISM Magnetic Fields

Method	Medium	Info
Polarization of starlight	Dust	$B_{\perp}$
Zeeman effect	Neutral hydrogen; a few mol. lines	$B_{\parallel}$
Synchrotron radiation	Relativistic electrons	$B_{\perp}$
Faraday rotation	Thermal electrons	$B_{\parallel}$

The Zeeman effect is the only technique for **direct** measurements of the magnetic field **strengths**.

Unsöld, Crutcher (2012) ARAA

Polarization of Starlight

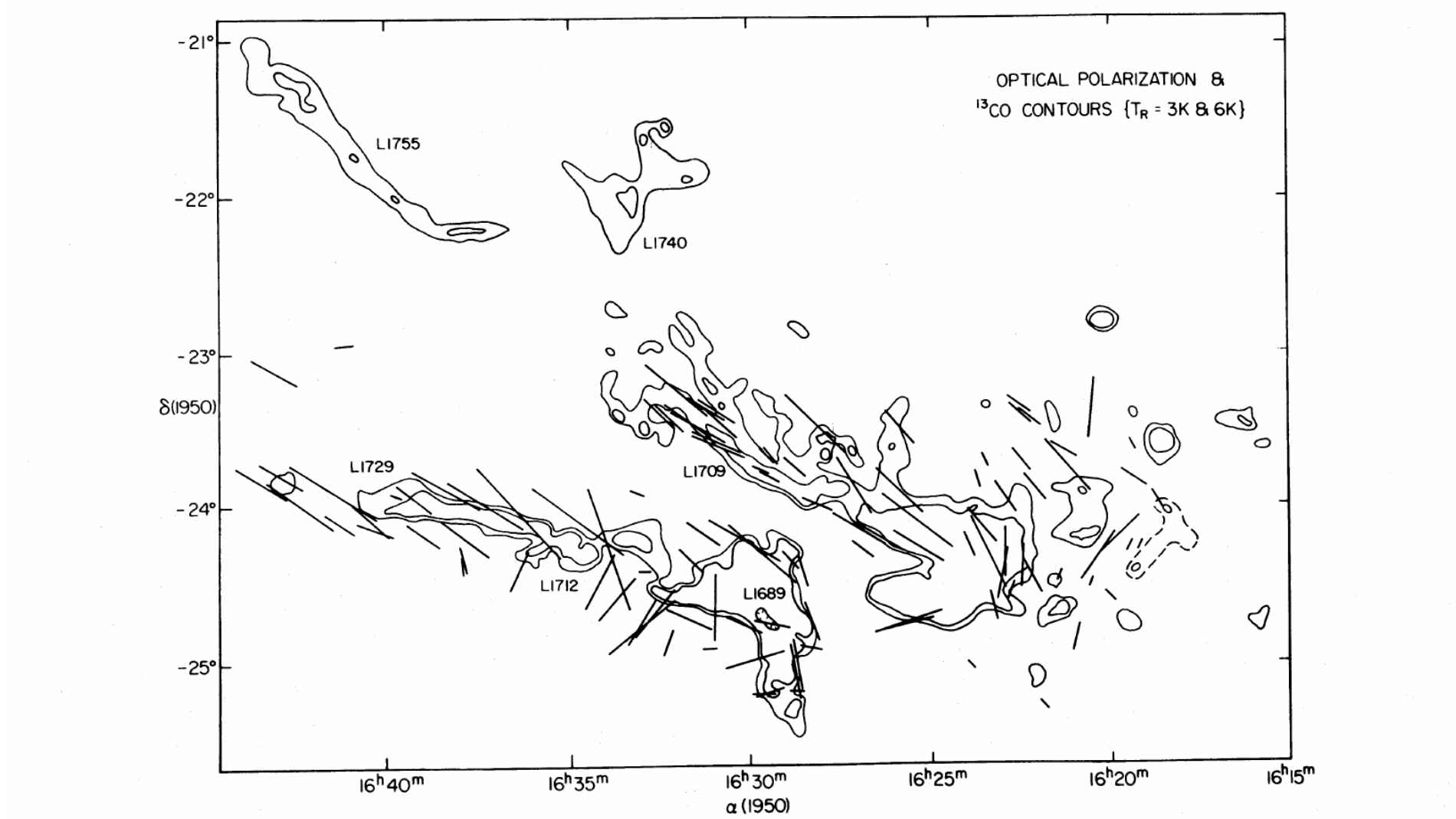

FIG. 7.—Orientation and relative magnitude of optical polarization vectors toward field stars at the cloud edges (Vrba, Strom, and Strom 1976). Solid contours of $T_R^*(^{13}CO)$ are at 3 and 6 K, with a dotted 1 K contour added around R5–R6 and R8–R9.

Loren (1989)

A thermalized ISM elongated grain tends to spin along its minor axis: $\vec{\omega} \longrightarrow \vec{B}$

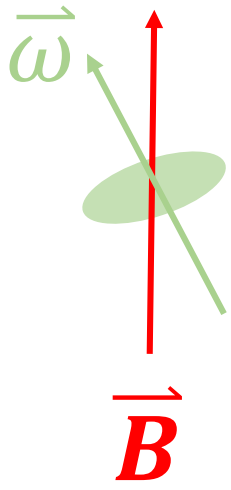

[Davis-Greenstein](#) alignment mechanism --- paramagnetic dissipation

http://bgandersson.net/grain-alignment

Observations in OIR

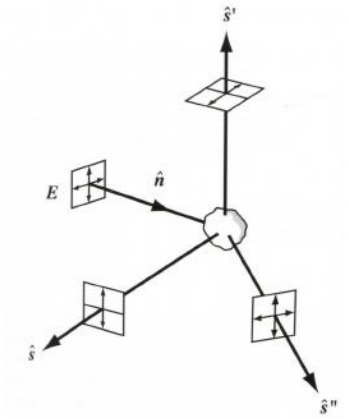

Stahler & Pallo 2004

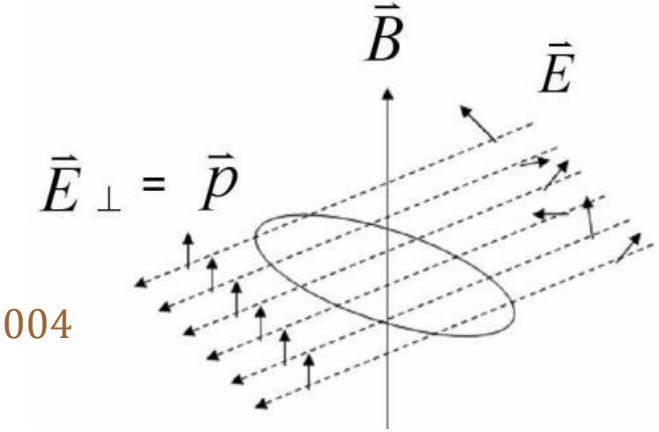

Scattering by dust

Dichroic extinction by aligned dust

Observations in FIR to mm

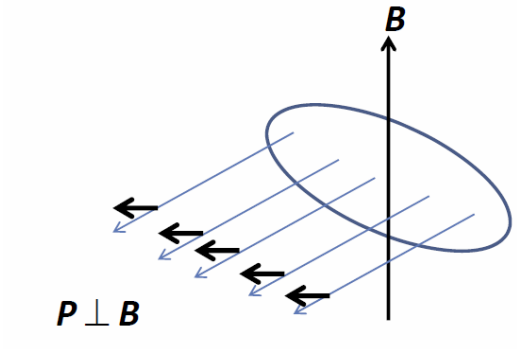

*Polarized thermal emission by dust aligned by **B***

Courtesy: Tamura

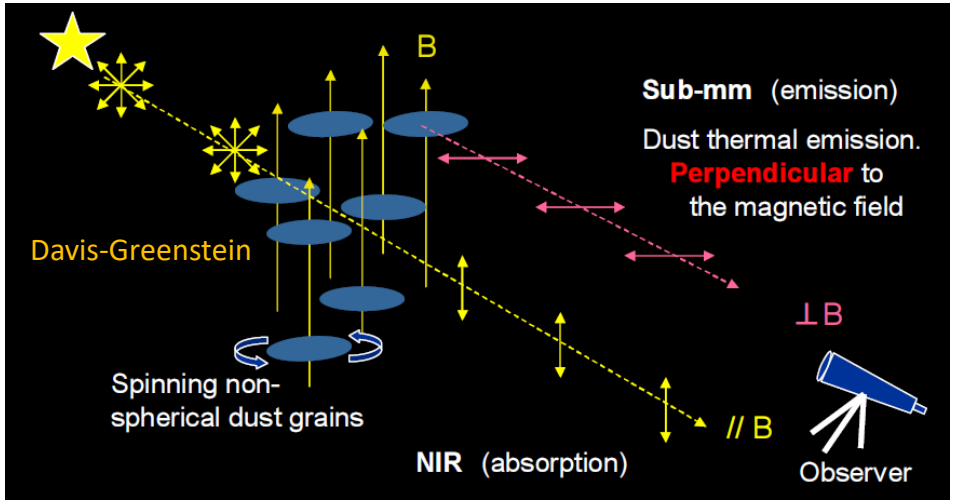

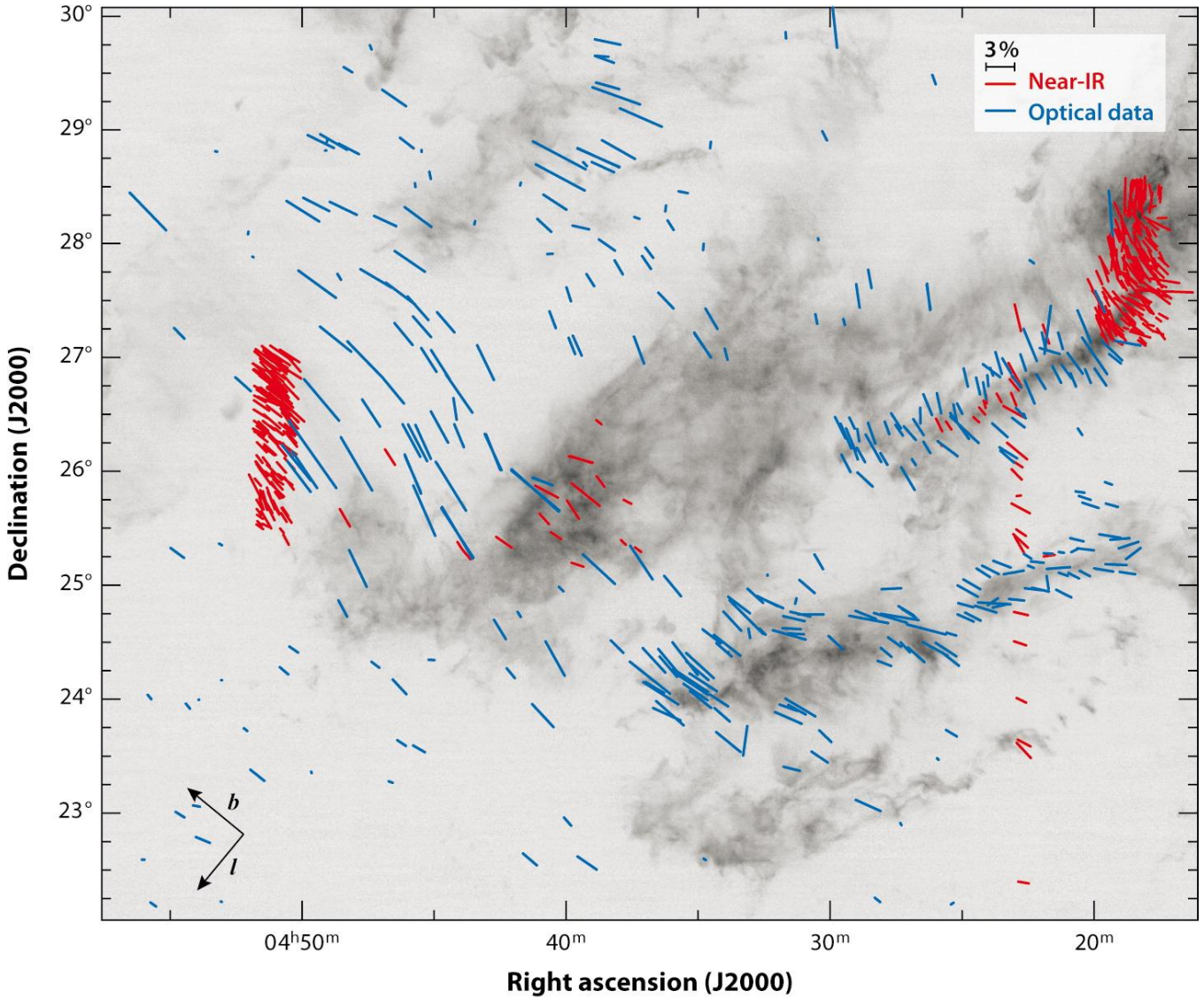

Crutcher RM. 2012.
Annu. Rev. Astron. Astrophys. 50:29–63

Organized magnetic field morphology in the Taurus dark-cloud complex superposed on a ^{13}CO map (Chapman et al. 2011). Blue lines show polarization measured at optical wavelengths and red lines show near-IR (*H*-band and *I*-band) polarization.

Dichroic extinction by dust (optical and near-IR)

$$\vec{P} \parallel \vec{B}$$

Interstellar Polarization of the Milky Way

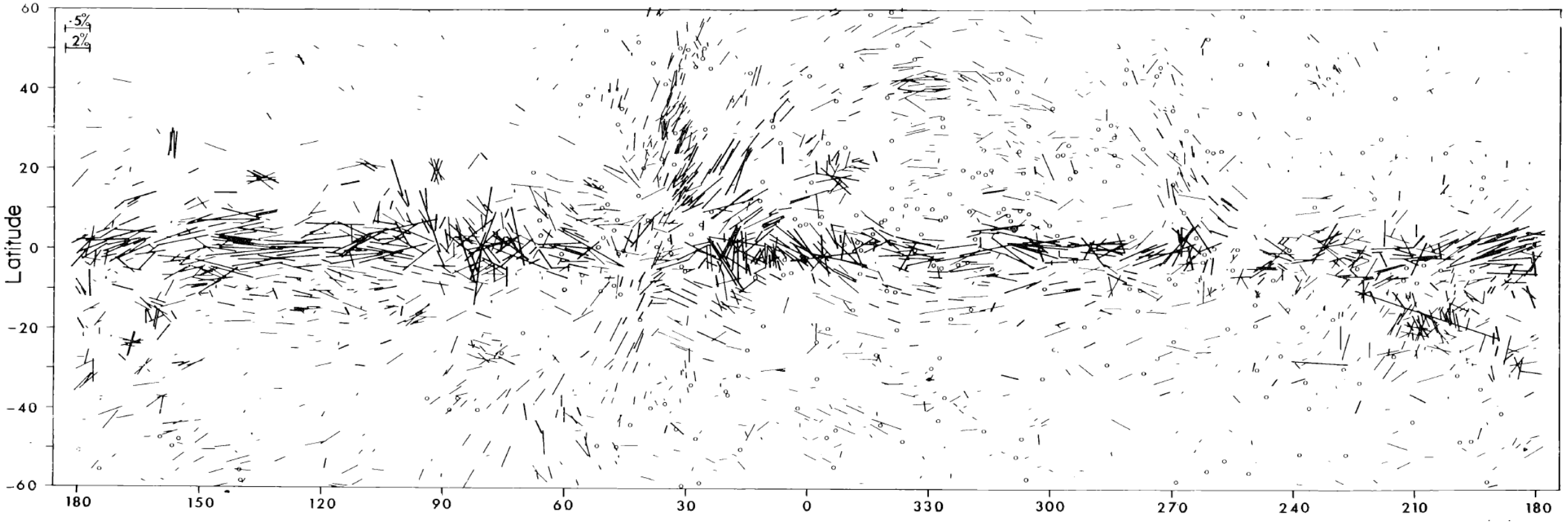

Mathewson & Ford (1970)

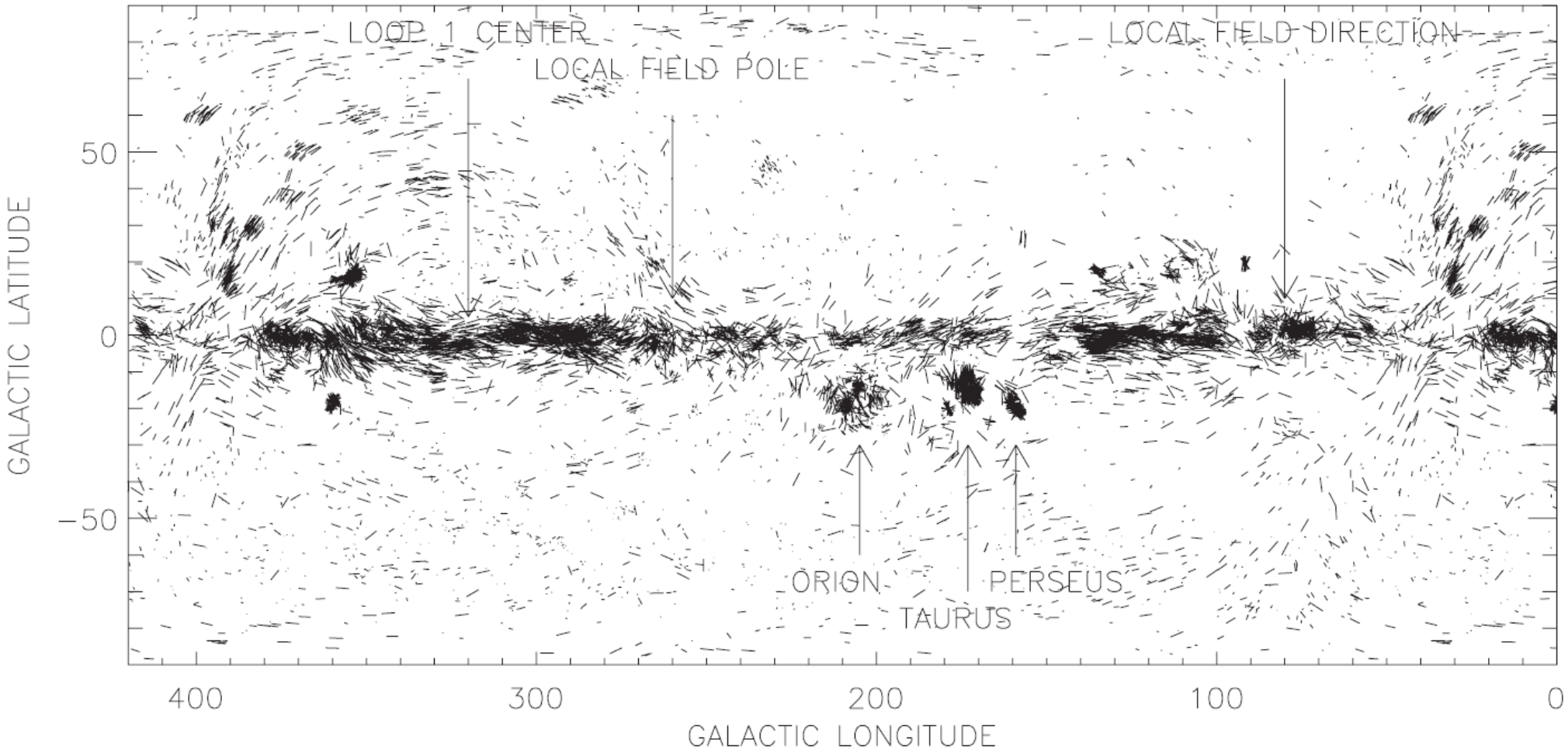

Fig. 1. Starlight polarization of 8662 stars. The orientation of each star's polarization is indicated by a short line whose length L in great-circle degrees is $L = [4 < 2P]^\circ$, where P is the percentage polarization; for L, we plot whichever of the two quantities is smaller

Heiles & Crutcher (2005)

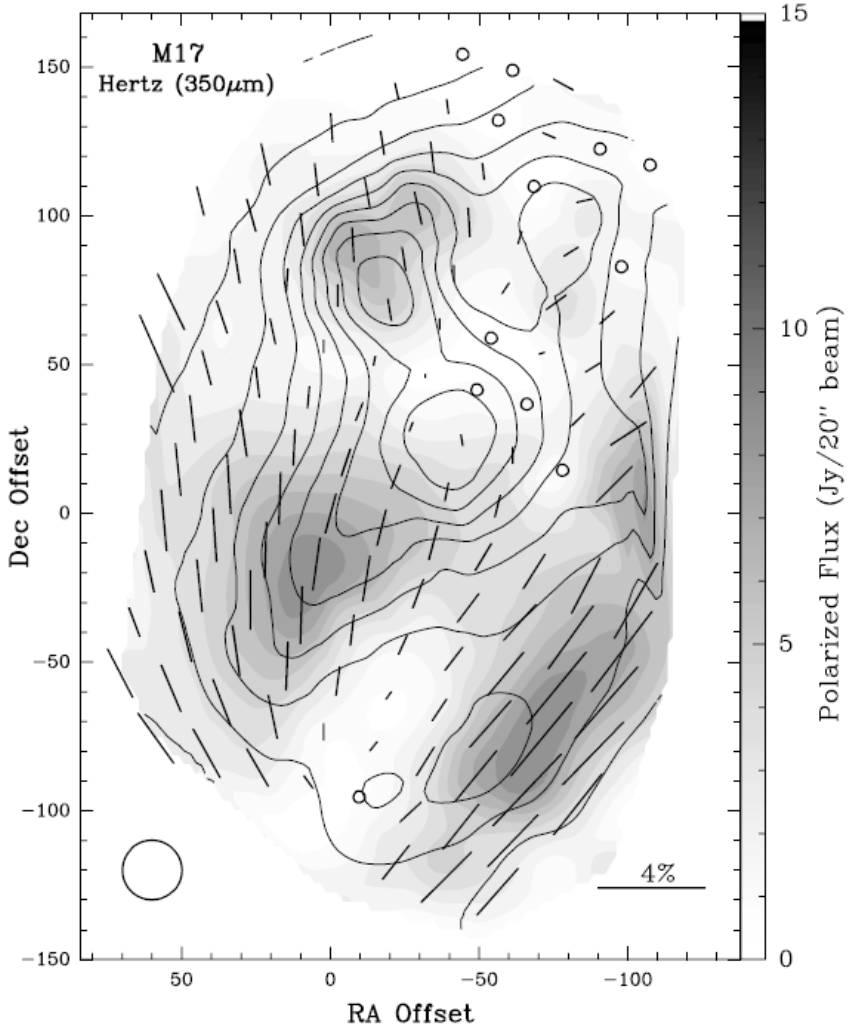

FIG. 6.—HERTZ polarization map of M17 at 350 μm. All of the polarization vectors shown have a polarization level and error such that $P > 3\sigma_P$. Circles indicate cases where $P + 2\sigma_P < 1\%$. The contours delineate the total continuum flux (from 10% to 90% with a maximum flux of ≈700 Jy), whereas the underlying gray scale gives the polarized flux according to the scale on the right. The beam width (≃20″) is shown in the lower left corner and the origin of the map is at R.A. = $18^h17^m31^s.4$, decl. = −16°14′25″.0 (B1950.0).

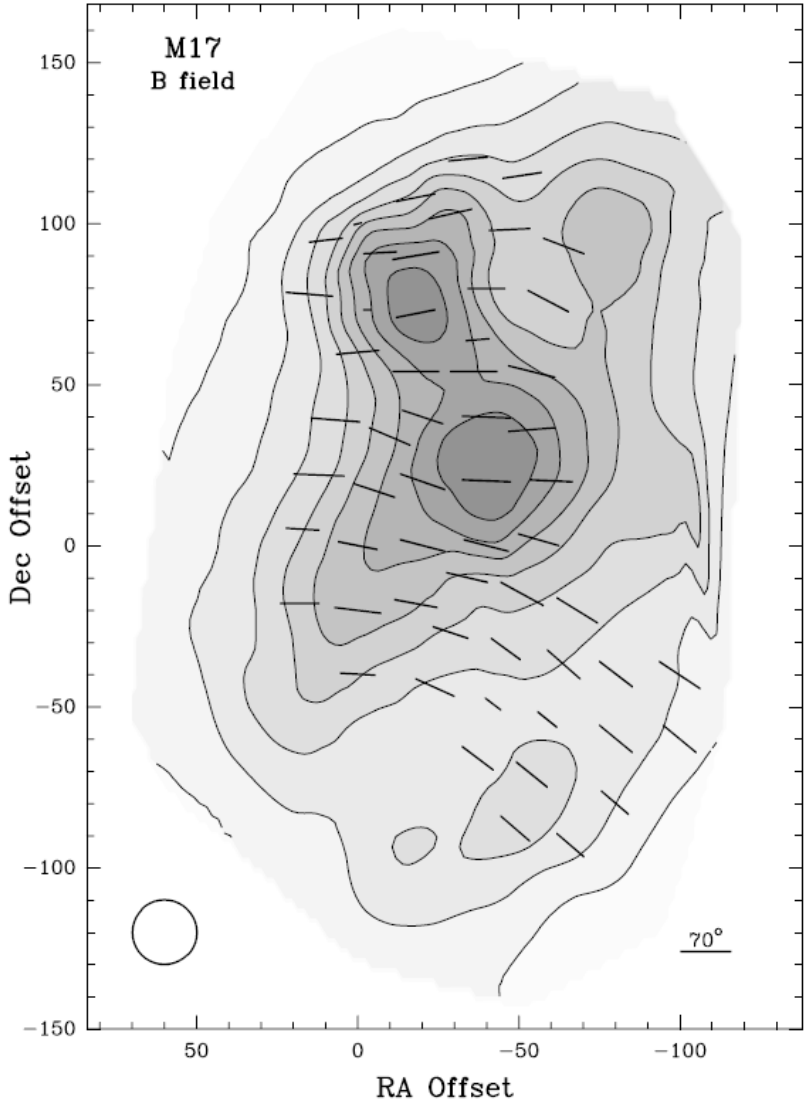

FIG. 11.—Orientation of the magnetic field in M17. The orientation of the projection of the magnetic field in the plane of the sky is shown by the vectors and the viewing angle is given by the length of the vectors (using the scale shown in the bottom right corner). The contours and the gray scale delineate the total continuum flux. The beam width (≃20″) is shown in the lower left corner, and the origin of the map is at R.A. = $18^h17^m31^s.4$, decl. = −16°14′25″.0 (B1950.0).

Thermal emission by dust (far-IR, and smm)

$\overrightarrow{P} \perp \overrightarrow{B}$

Houde et al. (2002)

Zeeman effect

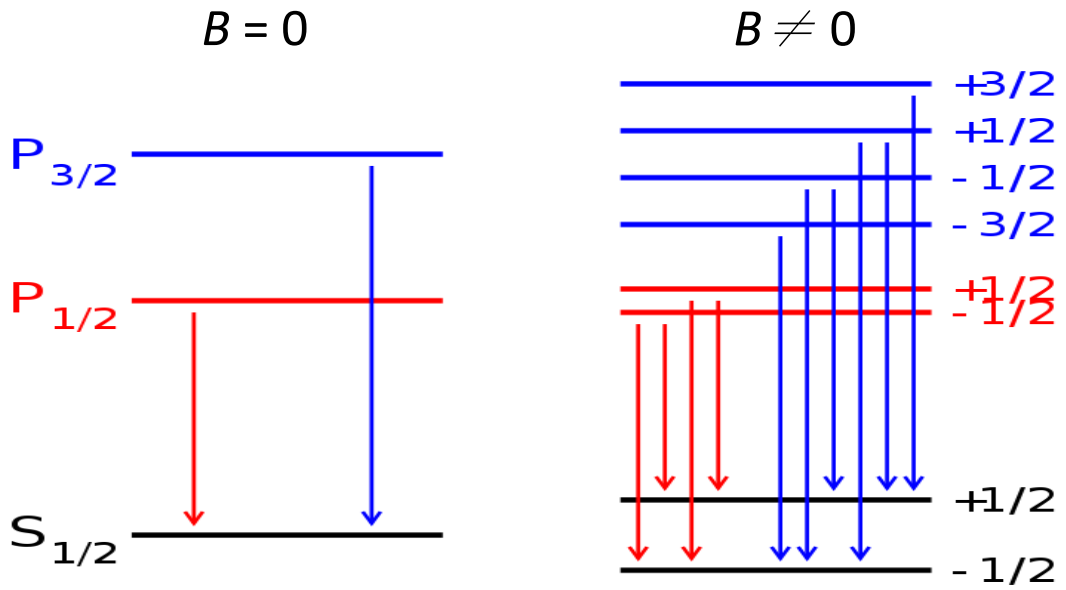

$\Delta \nu_B$ [Hz] = 1.40 x 10^{10} g B[T]

$\Delta \lambda_B$ [nm] = 4.67 x 10^{-8} g (λ_0 [nm])^2 B[T]

g: Landé or g factor (L, S, J) ~ 1

Ex: B = 0.1 T (1 kG) for a typical sunspot, at 500 nm, g=1

→ wavelength shift 0.001 nm ≈ natural line width

→ difficult to measure

Astron. Astrophys. 125, L 23–L 26 (1983)

Letter to the Editor

The magnetic field of the NGC 2024 molecular cloud: detection of OH line Zeeman splitting

Richard M. Crutcher[1,2] and Ilya Kazès[1]

[1] Department de Radioastronomie, Observatoire de Paris-Meudon, F-92195 Meudon, France
[2] Department of Astronomy, University of Illinois, Urbana, IL 61801, USA

Summary

Zeeman splitting of the main lines of OH in absorption has been detected for the first time. The derived magnetic field for a clump in the NGC 2024 molecular cloud is −38 ± 1 microgauss.

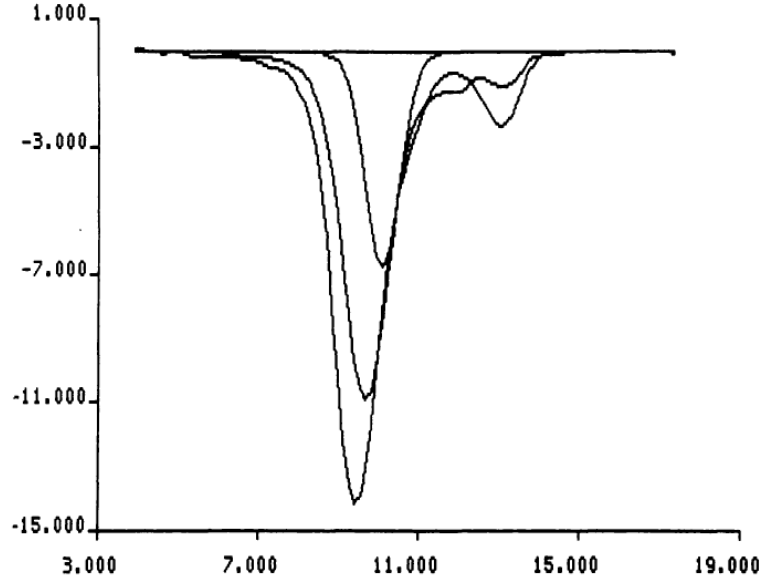

Fig. 1. Spectra of the 1667 (strongest) and 1665 lines observed for $13^h\ 18^m$ toward NGC 2024 (RA/DEC [1950.0] $05^h\ 39^m\ 14^s.3$ / −01° 55' 57"). The weakest line is the assumed gaussian component used for Zeeman analysis.

The abscissa scale in all figures is the same and is given in km s^{-1} relative to the LSR. The ordinate scale in °K antenna temperature is correct except that displacements of zero have been made in most figures.

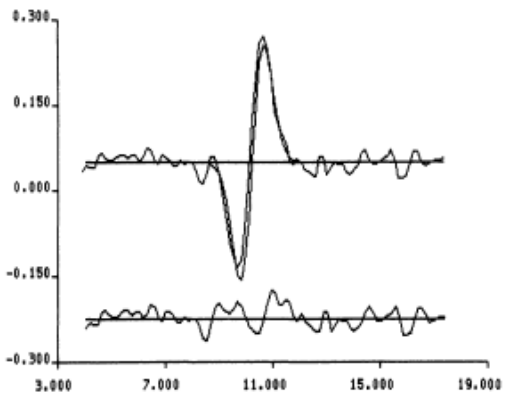

Fig. 4. Stokes V spectrum of the 1667 line together with a fit derived from the gaussian of figure 1. At the bottom the fitted minus the observed residuals are shown.

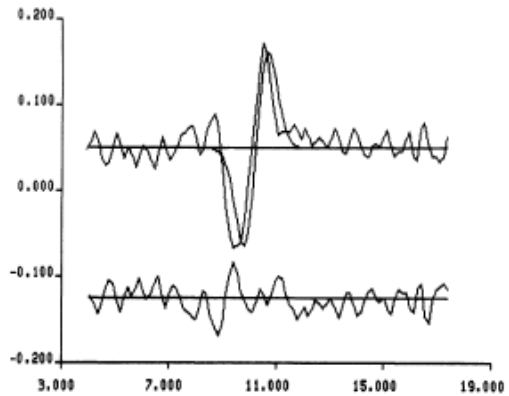

Fig. 5. Stokes V spectrum of the 1665 line together with a fit derived from the gaussian of figure 1. At the bottom the observed minus the fitted residuals are shown.

Faraday Rotation --- rotation of the plane of polarization when light passes through a magnetic field

Circularly polarized light → $\boldsymbol{E}$ field rotates → force on the charged particles to make circular motion → creating its own $\boldsymbol{B}$ field, either parallel or in opposite direction to the external field → phase difference → Change of position angle of the linear polarization

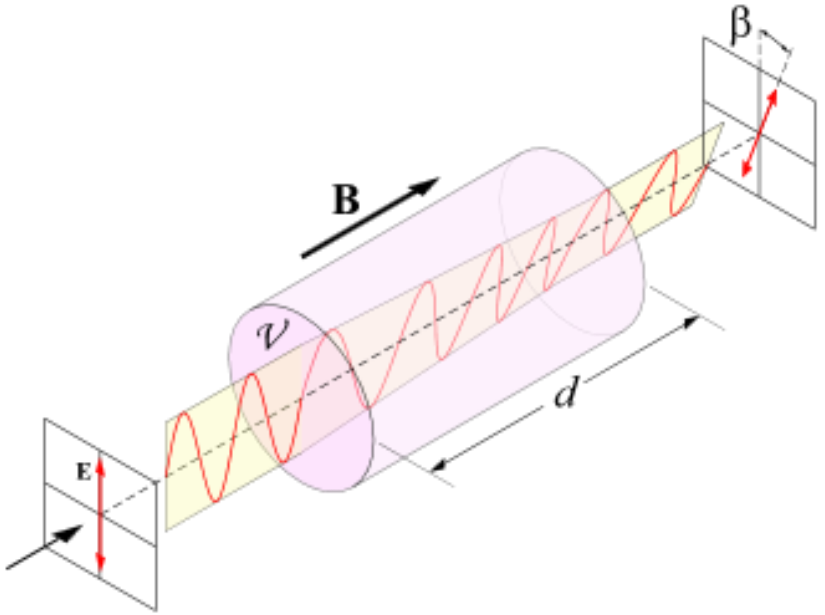

Faraday rotation angle $\beta = RM\ \lambda^2$ where the rotation measure (RM) is

$$\mathrm{RM} = \frac{e^3}{2\pi m^2 c^4} \int_0^d n_e(s) B_{\parallel}(s)\, \mathrm{d}s$$

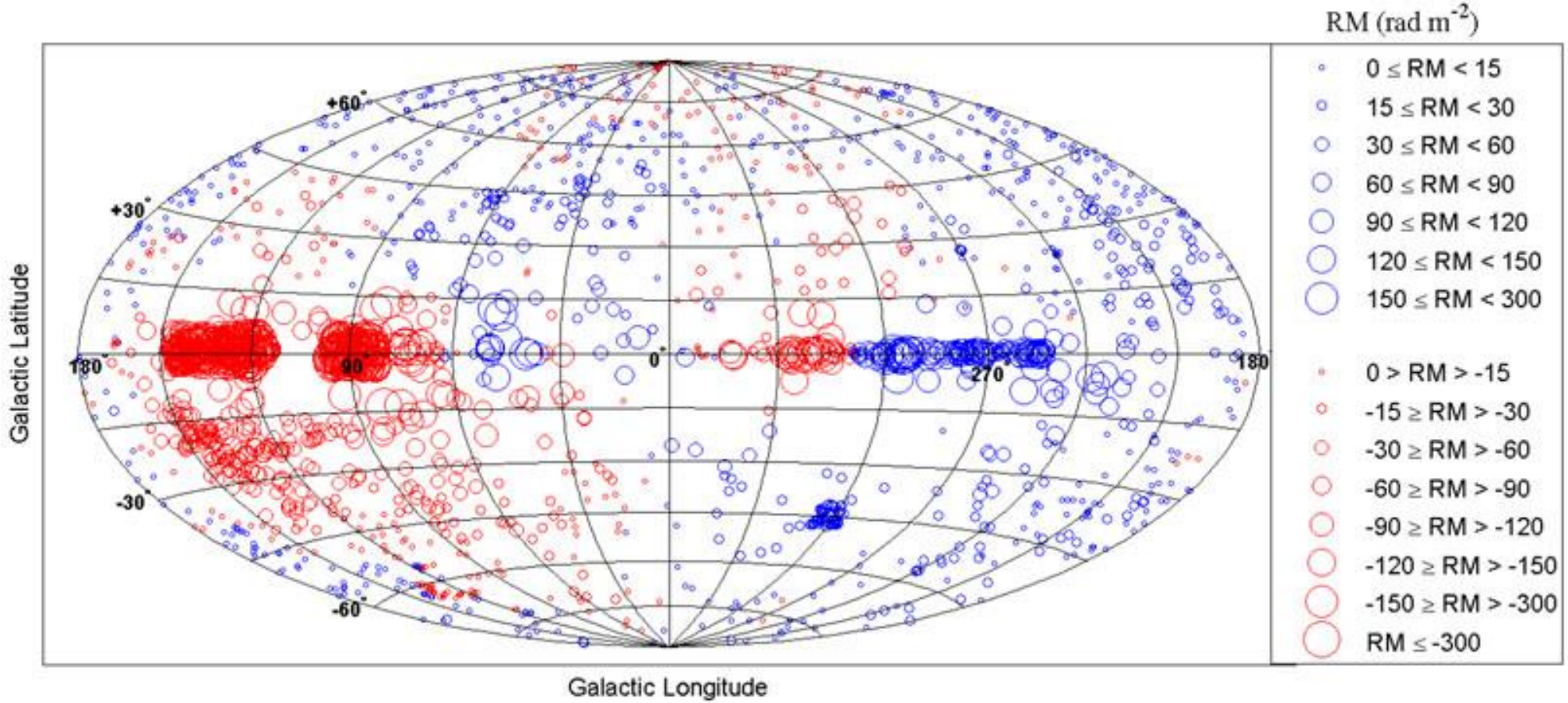

Figure 3. A smoothed representation of 2257 **Faraday rotation** measures in Galactic coordinates with the Galactic center at (0,0). (Kronberg & Newton-McGee, [3]). Blue and red circles represent positive and negative RM's respectively, and the circle size is proportional to RM strength.

http://ned.ipac.caltech.edu/level5/Sept10/Kronberg/Figures/figure3.jpg

Milky Way (and galaxies)

- Primordial (seed) weak field (origin unknown) could not last

$$\xrightarrow{\text{dynamo}}$$ a strong field

- Dynamo needs turbulence and differential rotation (alpha-Omega dynamo)
  - ✓ Spherical objects (stars/planets) → double torus near equator with a reversal
  - ✓ Flat objects (galactic disks) → single torus of spiral shape with no reversal

Rainer Beck (2007) Scholarpedia, 2, 2411

http://www.scholarpedia.org/article/Galactic_magnetic_fields#The_Origin_of_Galactic_Magnetic_Fields

For **magnetic support** to be important,

$$\frac{3}{5}\frac{GM^2}{R} = \frac{B^2}{8\pi}\left(\frac{4}{3}\pi R^3\right) = \frac{1}{6}B^2R^3$$

So, $M \propto BR^2$, and since $M \propto \rho R^3$, we get R $\propto \frac{B}{\rho}$

The magnetic Jeans mass becomes

$$M_{\text{Jeans}}^{B} \propto BR^2 \propto {}^{B^3}\!/_{\rho^2}$$

Numerically, $M_{\text{Jeans}}^{B} \approx 2.4 \times 10^4\ B_{\mu\text{G}}^{3}\ n_H^{-2}\ [M_\odot]$

and $B_{\text{crit}} = 0.1\ \frac{M}{M_\odot}\ (\frac{\text{pc}}{R})^2\ [\mu\text{G}]$

If the magnetic flux is conserved, $\boldsymbol{B} \propto \frac{1}{R^2}$

Because $M \propto R^3 \rho =$ constant, the **frozen-in** (i.e., flux conservation) condition would have led to $\boldsymbol{B} \propto R^{-2} \sim \rho^{2/3}$

If flux is conserved, $\boldsymbol{B}_0$ (ISM) $\sim 10^{-6}$ [G]

$$R_0 \approx 0.1 \text{ [pc]} \rightarrow R = R_\odot \text{ ➔ } \boldsymbol{B} \approx 10^7 \text{ [G]}$$

But what has been actually observed is

$$\boldsymbol{B} \propto \rho^{1/3} \text{ to } \rho^{1/2},$$

implying **magnetic flux loss**.

THE ASTROPHYSICAL JOURNAL, 301:339–345, 1986 February 1

INTERSTELLAR MAGNETIC FIELD STRENGTHS AND GAS DENSITIES: OBSERVATIONAL AND THEORETICAL PERSPECTIVES

T. H. TROLAND
Physics and Astronomy Department, University of Kentucky
AND
CARL HEILES
Astronomy Department, University of California, Berkeley
Received 1985 January 31, accepted 1985 July 16

ABSTRACT

We present an updated compilation of observational data concerning the relationship between the interstellar magnetic field strength and the gas density. Pulsar and Zeeman-effect data provide the only reliable information about the (B, n) relationship, and they now span nearly six orders of magnitude in gas density. Field strengths show no evidence of increase over the density range 0.1–$\sim$100 cm^{-3}. At higher densities, a modest increase in field strength is observed in some regions, in line with theoretical expectations for self-gravitating clouds. In two regions of the interstellar medium, the magnetic field is unusually high; however, these are not locales where self-gravitation is important. Despite the consistency between observations and theory, questions still exist about how the magnetic field strength remains constant for densities up to $\sim$100 cm^{-3}. Further Zeeman effect studies and a better theoretical understanding of the formation of interstellar clouds and complexes will be necessary to answer these questions.

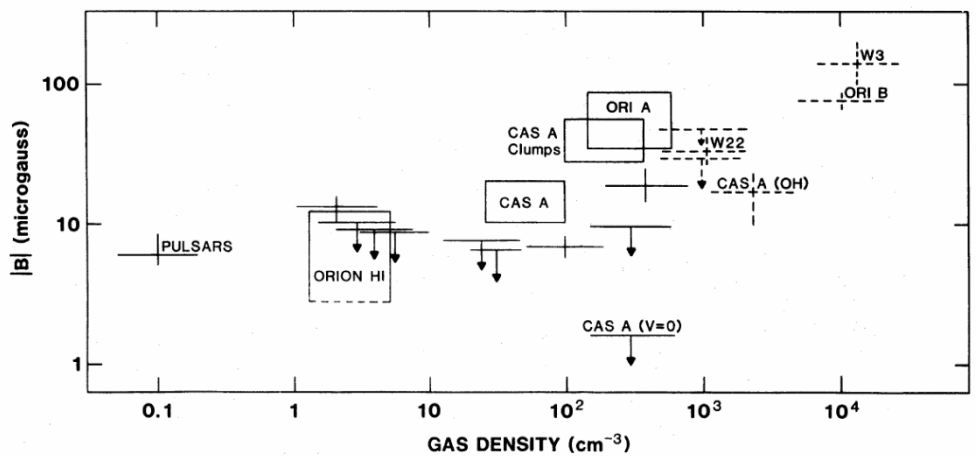

FIG. 1.—Observed magnetic field strengths as a function of estimated volume density. All results come from measurements of the H I (*solid lines*) and OH (*dashed lines*) Zeeman effect, except for the point labeled "pulsars." This point is derived from pulsar rotation and dispersion measures. Rectangular boxes represent ranges of field strengths encountered in Zeeman effect maps made either with a single-dish or with aperture synthesis instruments. See § II for further details.

A&A 484, 773-781 (2008)
DOI: 10.1051/0004-6361:200809447

A new probe of magnetic fields during high-mass star formation

Zeeman splitting of 6.7 GHz methanol masers*

W. H. T. Vlemmings

Argelander Institute for Astronomy, University of Bonn, Auf dem Hügel 71, 53121 Bonn, Germany

Received 24 January 2008 / Accepted 30 March 2008

Abstract

Context. The role of magnetic fields during high-mass star formation is a matter of fierce debate, yet only a few direct probes of magnetic field strengths are available.

Aims. The magnetic field is detected in a number of massive star-forming regions through polarization observations of 6.7 GHz methanol masers. Although these masers are the most abundant of the maser species occurring during high-mass star formation, most magnetic field measurements in the high-density gas currently come from OH and H_2O maser observations.

Methods. The 100-m Effelsberg telescope was used to measure the Zeeman splitting of 6.7 GHz methanol masers for the first time. The observations were performed on a sample of 24 bright northern maser sources.

Results. Significant Zeeman splitting is detected in 17 of the sources with an average magnitude of 0.56 m s^{-1}. Using the current best estimate of the 6.7 GHz methanol maser Zeeman splitting coefficient and a geometrical correction, this corresponds to an absolute magnetic field strength of 23 mG in the methanol maser region.

Conclusions. The magnetic field is dynamically important in the dense maser regions. No clear relation is found with the available OH maser magnetic field measurements. The general sense of direction of the magnetic field is consistent with other Galactic magnetic field measurements, although a few of the masers display a change of direction between different maser features. Due to the abundance of methanol masers, measuring their Zeeman splitting provides the opportunity to construct a comprehensive sample of magnetic fields in high-mass star-forming regions.

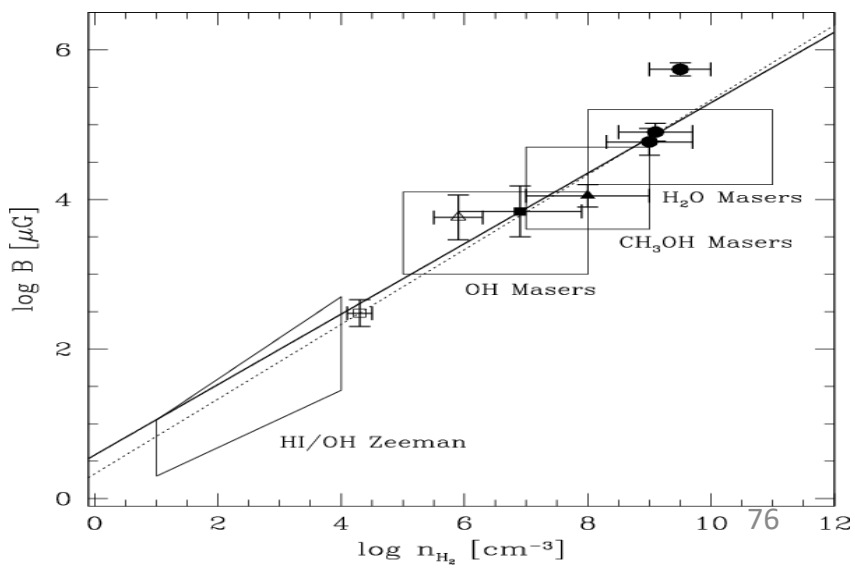

$\vec{B}$ confines the motion of charged particles.

Molecular clouds → mostly neutral with only a tiny fraction of particles ionized by cosmic rays or by natural radioactivity

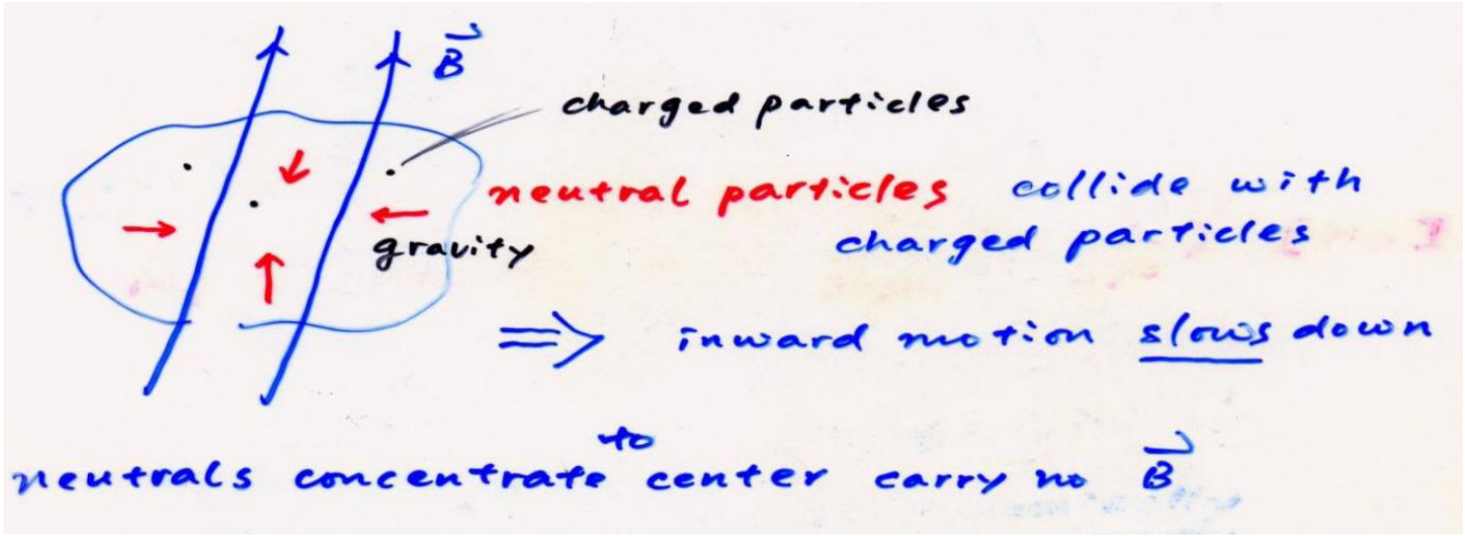

= decoupling of neutral particles from plasma in the initial stage of star formation

Leading to 1. charged particles escaped from magnetic poles;

2. leakage of $\vec{B}$

(**ambipolar diffusion=plasma drift**)

If $\mathcal{M}_{\rm cloud} > \mathcal{M}_{\rm crit}$ → supercritical → Cloud will collapse dynamically

→ Massive star formation

If $\mathcal{M}_{\rm cloud} < \mathcal{M}_{\rm crit}$ → subcritical → Cloud collapses, if ever, quasi-statically

→ Low-mass star formation

Clouds tend to condense with $\mathcal{M} \sim 10^4 M_\odot$, but the observed stellar mass ranges $0.05 \leq \mathcal{M}/M_\odot \leq 100$

Why is there a lower mass limit and an upper mass limit for stars?

Cloud collapse → (local) density increase → (local) $M_{\rm J}$ decrease
→ easier to satisfy $M > M_{\rm J}$, i.e., cloud becomes more unstable
→ **fragmentation**

Formation of a cluster of stars ~~

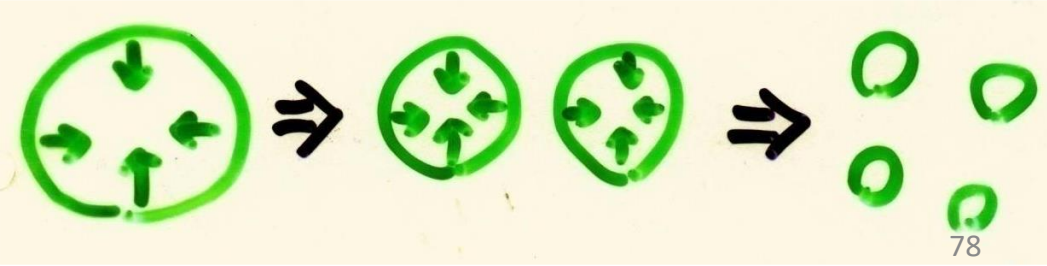

Recall Jeans mass $M_J \approx 1.2 \times 10^5 \left(\frac{T}{100\ K}\right)^{3/2} \left(\frac{\rho_0}{10^{-24}\ \mathrm{g\ cm^{-3}}}\right)^{-1/2} \frac{1}{\mu^{3/2}}\ [M_\odot]$

$$\propto T^{3/2} / \rho^{1/2}$$

A small/decreasing M_J favors cloud collapse.

If during collapse, local $M_J \downarrow$ → subregions become unstable and continue to collapse to ever smaller (**fragmentation**).

Since during collapse ρ always ↑, the behavior of M_J depends on T.

If gravitational energy is radiated away, i.e., $\tau_{\mathrm{cooling}} \ll \tau_{\mathrm{ff}}$ and collapse is **isothermal**, $T =$ const, so $M_J \propto \rho^{-1/2}$ ➔ collapse continues

However, once the isothermal condition is no longer valid, e.g., when the cloud becomes optically thick, the collapse is **adiabatical**.

$$T \propto P^{2/5} \propto \rho^{2/3}$$

So $M_J \propto \frac{\rho}{\rho^{1/2}} = \rho^{1/2}$, i.e., grows with time (ever more difficult to collapse), so the collapse halts

For a monatomic idea gas, the adabatic index

$$\gamma \equiv c_p/c_v = \frac{f+2}{f} = {}^{5/2}\!/_{3/2} = 5/3$$

$$\mathrm{P}V^{\gamma} = \text{const};\ \mathrm{T}V^{\gamma-1} = \text{const};$$

Exercise

1. What is the temperature and density of the universe after recombination?
2. What is the corresponding Jeans mass to form protogalaxies at this epoch?

- Likely all stars form in a clustered environment.
- Star formation is cluster formation.
- Molecular clouds are short-lived, and so are infant star clusters.
- (Initial) Molecular clouds are clumpy and filamentary; so are the youngest star clusters.
- (Internal) Mutual gravitational interaction among members virializes the cluster into spherical shape, with more massive stars more concentrating toward the center (*mass segregation*). Lowest-mass members are vulnerable to ejection out from the system (*stellar evaporation*).
- (External) Eventually Galactic perturbations (tidal forces, differential rotation) distort and rip apart the star clusters.

Star clusters are good laboratories to study stellar evolution, because member stars in a star cluster

- are (almost) of the same age;
- are (almost) at the same distance;
- evolve in the same Galactic environments;
- have the same chemical composition;
- are dynamical bound.

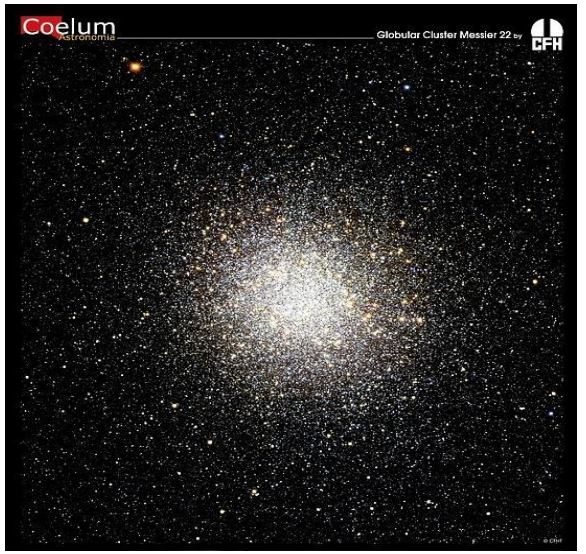

Two distinct classes:

- ✓**globular clusters** (100+ in the MW)
- ✓**open clusters** (a few 10^3 known in the MW)

How do these two classes differ in terms of shape, size, spatial distribution, number of member stars, and stellar population?

Open Clusters

10^2 to 10^3 member stars; ~10 pc across; loosely bound;
open shape; young population I;
located mainly in spiral arms;
>1000 open clusters known in the MW

Globular Clusters

10^5 to 10^6 member stars; up to 100 pc across; tightly bound; centrally concentrated;
spherical shape; old population II;
located in the Galactic halo;
200 globular clusters known in the MW

Stars in M80 are mostly old, metal poor members of Population II.

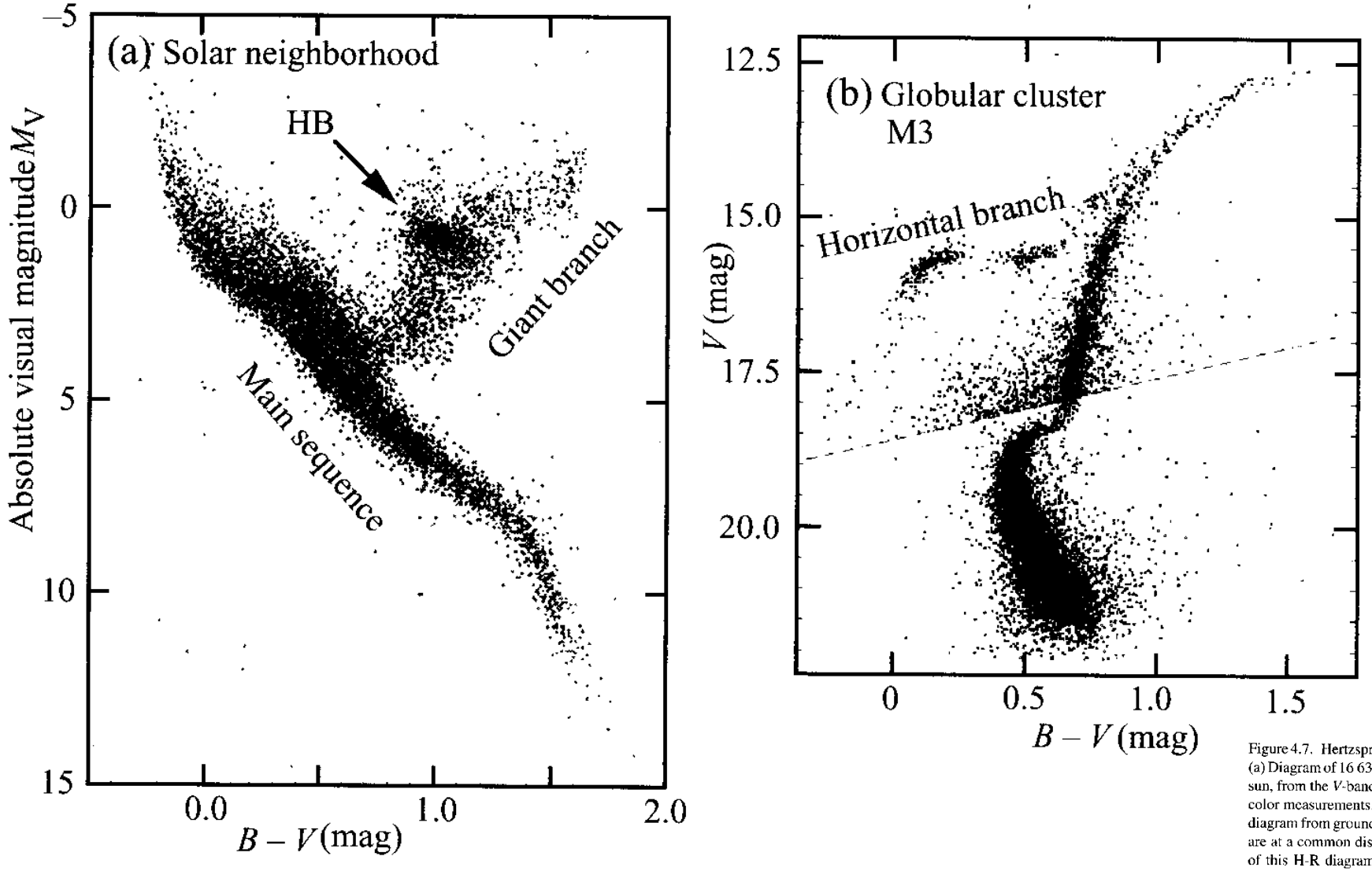

Figure 4.7. Hertzsprung–Russell color-magnitude diagrams for two very different samples of stars. (a) Diagram of 16 631 stars of various ages and various distances that are within about 330 LY of the sun, from the V-band and parallax distance measures by the Hipparcos satellite and ground-based color measurements. Horizontal-branch (HB) stars overlie the giant branch. (b) Color-magnitude diagram from ground-based studies of ~12 200 stars in globular cluster M3. The stars in the cluster are at a common distance of ~32 000 LY, and thus apparent magnitudes suffice for the ordinate of this H-R diagram. The stars are mostly of the common age of ~12 Gyr. The data come in two distinct samples. A deep photographic sample yields most of the stars in the diagram both above and below the diagonal line. Short exposures with a charge-coupled device (CCD) camera provide fluxes for the rarer brighter stars plotted only above the dashed line representing B = 18.6. The scatter just above the diagonal line is mostly due to increased uncertainty at the fainter end of the CCD sample. The distance modulus of M3 is 14.93. Thus, $M_V = 0$ in (a) corresponds to $V = 14.93$ in (b). Note the absence of bright main-sequence stars in M3 and also the well-defined horizontal branch. [(a) ESA SP-1200, Hipparcos catalog (1997) in J. Kovalevsky, *ARAA* **36**, 121 (1998); (b) F. Ferraro *et al.*, *A&A* **320**, 757 (1997); photographic data from R. Buonanno *et al.*, *A&A* **290**, 69 (1994)]

Bradt “Astrophysics Processes”

Globular Clusters in M31

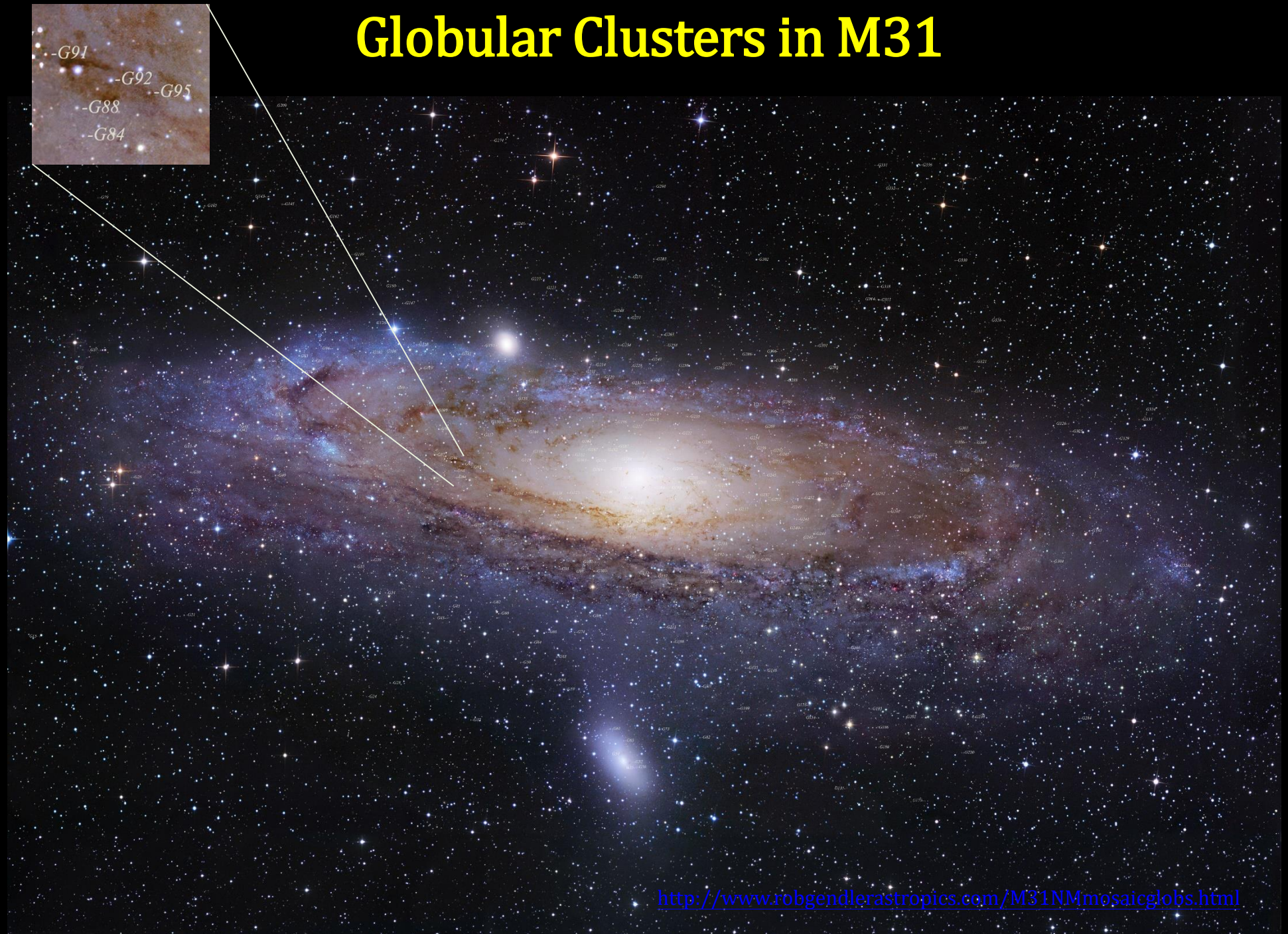

http://www.robgendlerastropics.com/M31NMmosaicglobs.html

Equation of motion for a spherical surface at r is

$$\frac{d^2r}{dt^2} = -\frac{GM}{r^2}$$

with initial condition $r(0) = r_0, \frac{dr}{dt}(0) = 0, M = 4\pi {r_0}^3 \rho_0/3.$

Multiplying both sides by dr/dt, and since $\frac{d}{dt}(\frac{dr}{dt})^2 = 2\frac{dr}{dt}\frac{d^2r}{dt^2}$,

$$\frac{d}{dt}(\frac{dr}{dt})^2 = -\frac{2GM}{r^2}\frac{dr}{dt}$$

Integrating both sides, we get

$$\left(\frac{dr}{dt}\right)^2 = 2GM\left(\frac{1}{r} - \frac{1}{r_0}\right)$$

Substituting m, we get

$$\frac{dr}{dt} = -\left[\frac{8\pi G\rho_0 {r_0}^2}{3}\left(\frac{r_0}{r} - 1\right)\right]^{\frac{1}{2}}$$

Define a new variable θ, so that $r(t) = r_0 \cos^2\theta$, ($\theta = 0$ at $t = 0$) then

$$\frac{d\theta}{dt}\cos^2\theta = \frac{1}{2}\left(\frac{8\pi G\rho_0}{3}\right)^{1/2}$$

Integrating this, we obtain $\theta + \frac{1}{2}\sin 2\theta = \left(\frac{8\pi G\rho_0}{3}\right)^{1/2} t$

The free-fall time is when $\theta = {}^{\pi}/_{2}$, $\boxed{t_{\mathrm{ff}} = \left(\frac{3\pi}{32\, G\rho_0}\right)^{\frac{1}{2}}} = \frac{3.4\times 10^7}{\sqrt{n_0}}$ [yr]

Bodenheimer p.34

… the time when density becomes ∞ for each δm.

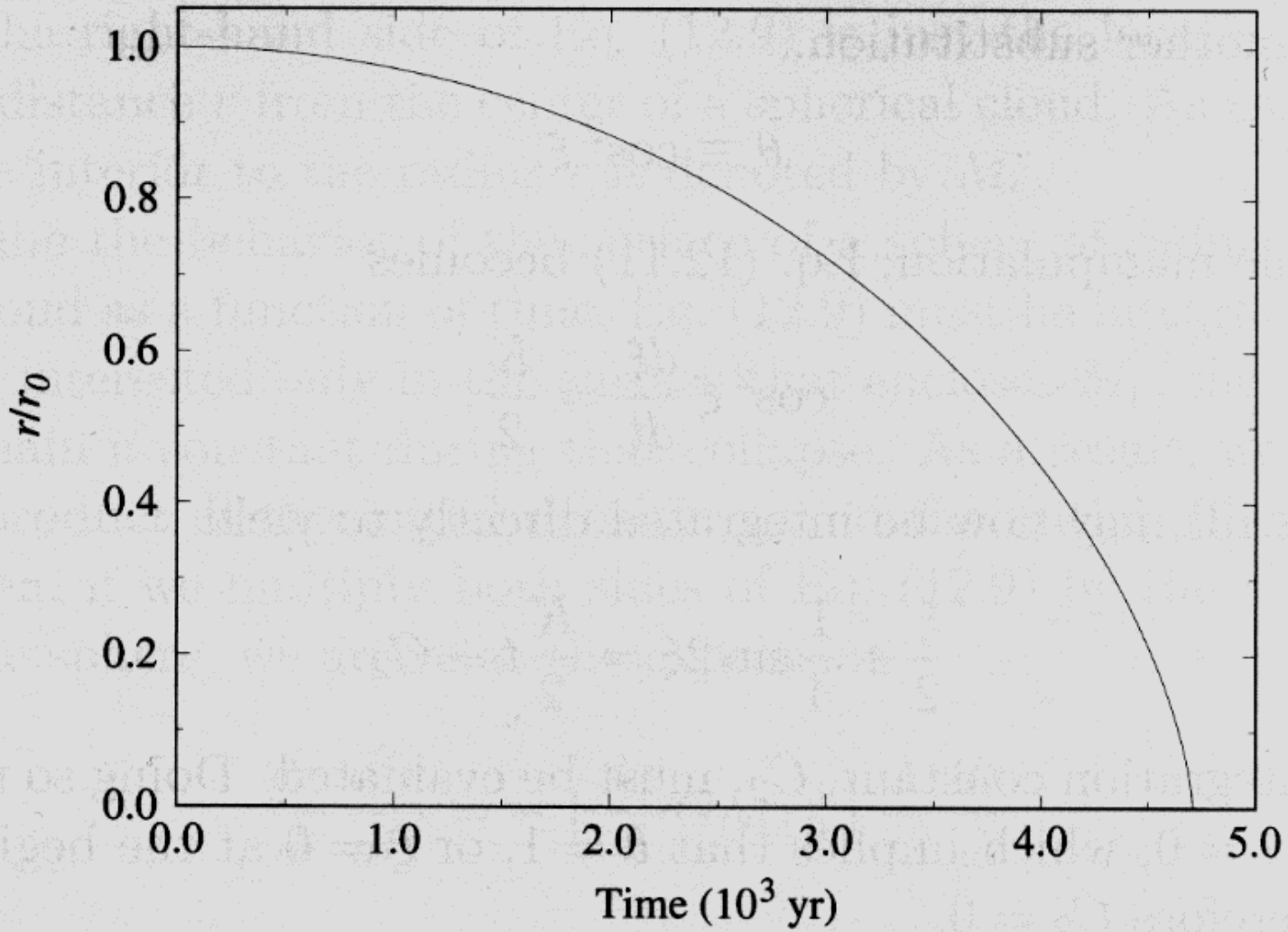

Figure 12.5 The ratio of the radius relative to its initial value as a function of time for the homologous collapse of a molecular cloud. The collapse is assumed to be isothermal, beginning with a density of $\rho_0 = 2 \times 10^{-16}$ g cm^{-3}.

Carroll & Ostlie

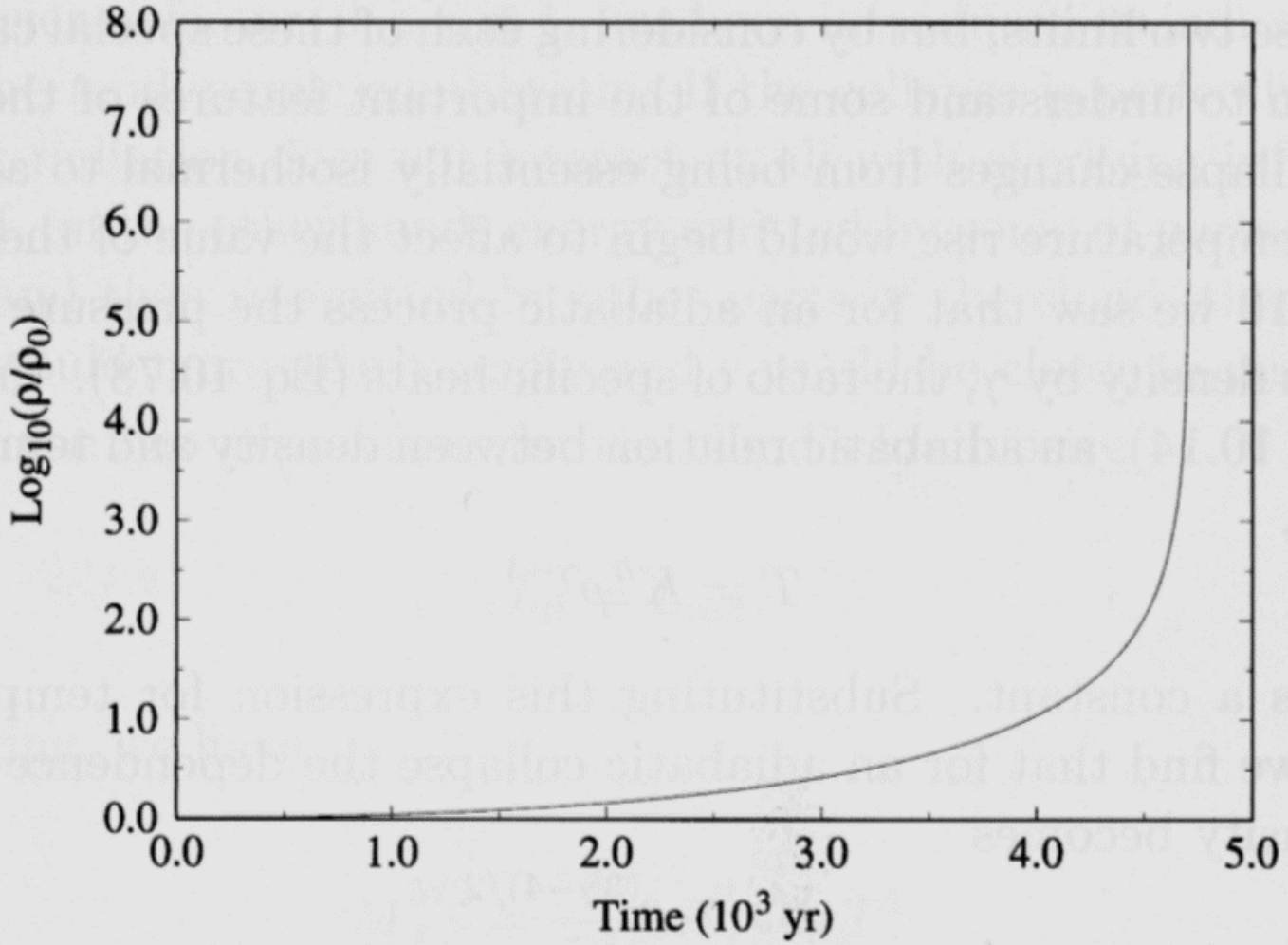

Figure 12.6 The ratio of the cloud's density relative to its initial value as a function of time for the isothermal, homologous collapse of a molecular cloud with an initial density of $\rho_0 = 2 \times 10^{-16}$ g cm^{-3}.

Carroll & Ostlie

$$\tau_{\rm ff} \sim 66120/\sqrt{\rho}_{\rm MKS} \sim 35/\sqrt{\rho}_{\rm cgs}[{\rm min}]$$

Note that $t_{\rm ff} \propto \frac{1}{\sqrt{G\rho_0}}$ has no dependence on r_0.

If ρ_0 is uniform, all m collapse to the center at the same time

→ **homologous collapse**

If ρ_0 is somewhat centrally condensed, as observed,

e.g., $\rho_0 \propto r^{-1}$ to r^{-2}, inner region (small r), $t_{\rm ff} \downarrow\downarrow$

→ **inside-out collapse**

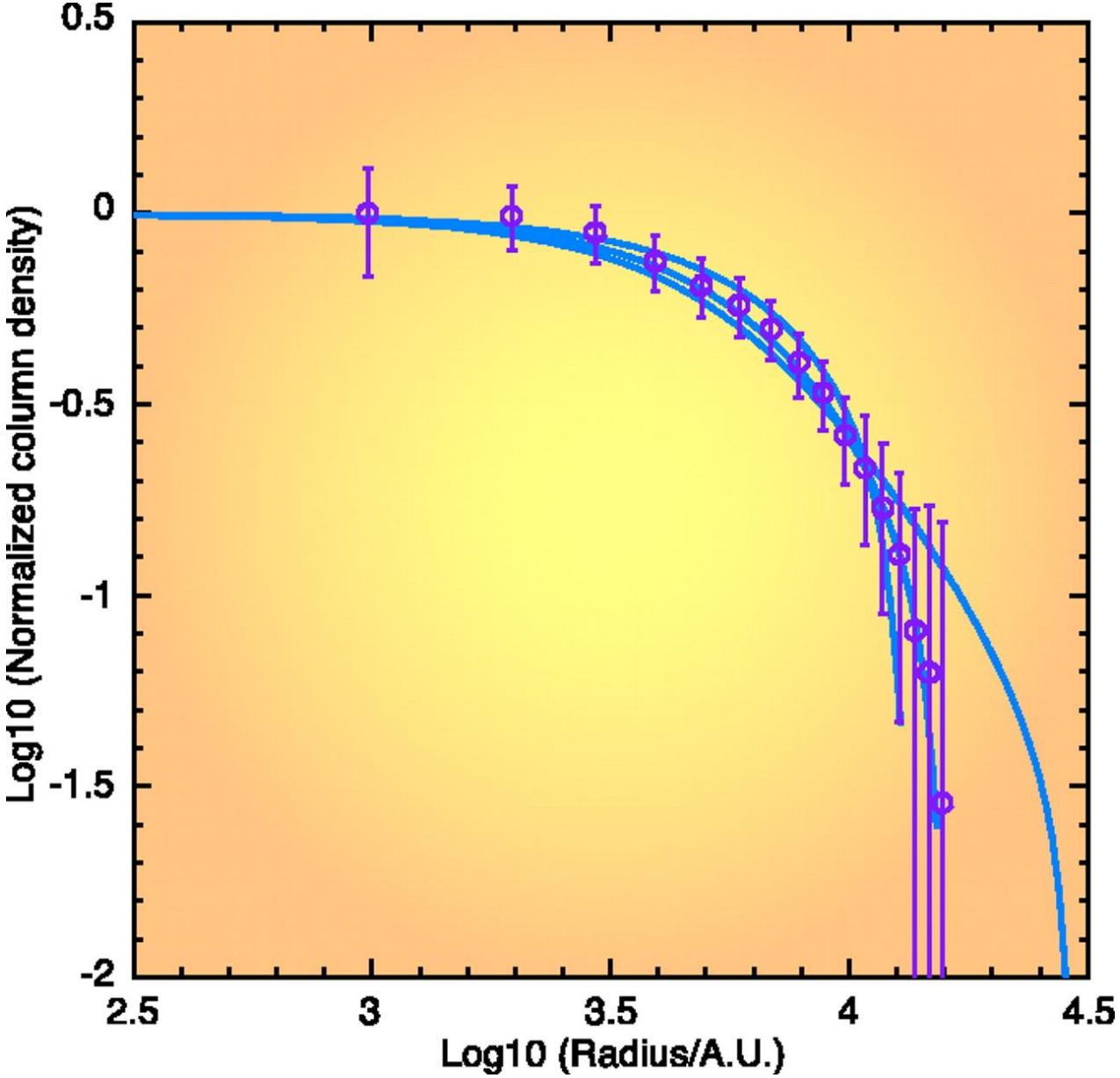

The typical radial density profile of a prestellar core

From the inner region,

$\rho =$constant $\rightarrow \rho \propto r^{-1}$,

steeping toward the edge

$\rho \propto r^{-2} \rightarrow \rho \propto r^{-5}$

Ward-Thomson (2002)

Free-fall Collapse

$$\frac{d^2r}{dt^2} = -\frac{GM}{r^2}$$

Dimensional analysis gives

$$\frac{R}{t^2} \sim \frac{GM}{R^2} \Longrightarrow t_{\rm ff} \sim \frac{1}{\sqrt{\rm G\rho}}$$

In reality, as $r \downarrow \longrightarrow \rho \uparrow$

Collapse proceeds in an inside-out fashion. A protostellar core is formed, followed by material "raining down" → **accretion**

Gravitational energy → kinetic energy → heat

$$L_{\rm acc} \sim GM_* \dot{M}/R_*$$

Recall the relation between a circular motion and a simple harmonic motion.

Acceleration to the center
Time scale = ¼ period

<u>Applications</u>:
- Gas in a collapsing cloud
- Stars in a globular cluster
- Galaxies in a galaxy cluster

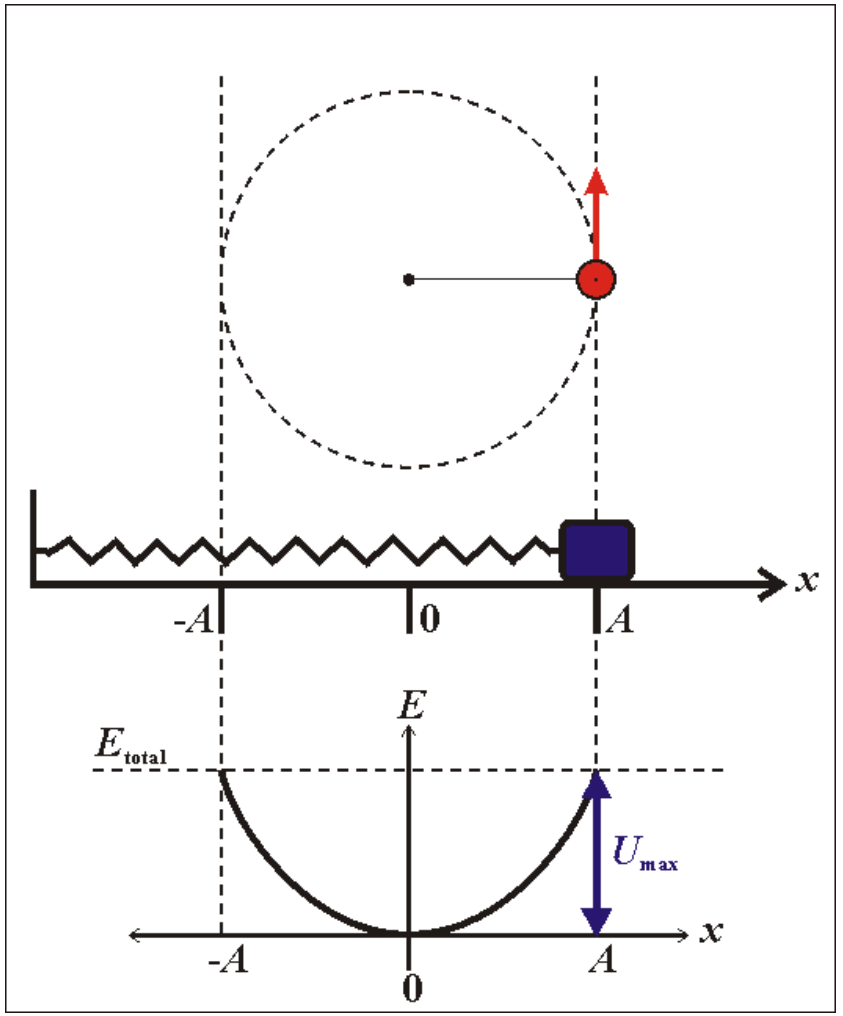

http://prism.texarkanacollege.edu/physicsbook/shm-ucm.gif

Exercise

1. For the sun, i.e., mass $\mathcal{M} = 1\,\mathcal{M}_{\odot}$, luminosity $\mathcal{L} = 1\,\mathcal{L}_{\odot}$, and radius $\mathcal{R} = 1\,\mathcal{R}_{\odot}$, compute the free-fall time scale τ_{ff} and the Kelvin-Helmholtz time scale $\tau_{\text{KH}} \approx {}^{G\mathcal{M}^2}/_{RL}$. Which time scale is longer?
2. Note that both time scales have different dependence on the size scale. At what size, do the two time scales equal?

Ann. Rev. Astron. Astrophys. 1987. 25: 23–81

STAR FORMATION IN MOLECULAR CLOUDS: OBSERVATION AND THEORY

Frank H. Shu, Fred C. Adams, and Susana Lizano

Astronomy Department, University of California, Berkeley, California 94720

Cores form within molecular clouds.

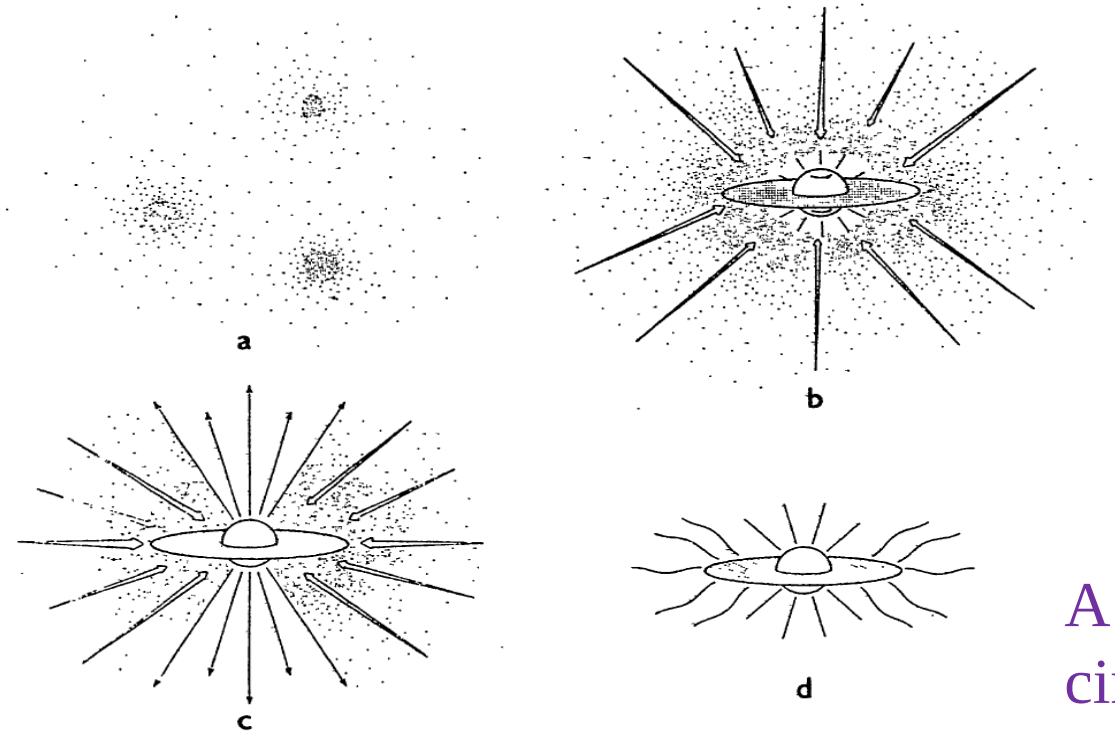

A core collapse inside-out and form a protostar with a toroid.

A stellar wind with a bipolar flow forms.

A star is form with a circumstellar disk.

Figure 7 The four stages of star formation. (*a*) Cores form within molecular clouds as magnetic and turbulent support is lost through ambipolar diffusion. (*b*) A protostar with a surrounding nebular disk forms at the center of a cloud core collapsing from inside-out. (*c*) A stellar wind breaks out along the rotational axis of the system, creating a bipolar flow. (*d*) The infall terminates, revealing a newly formed star with a circumstellar disk.

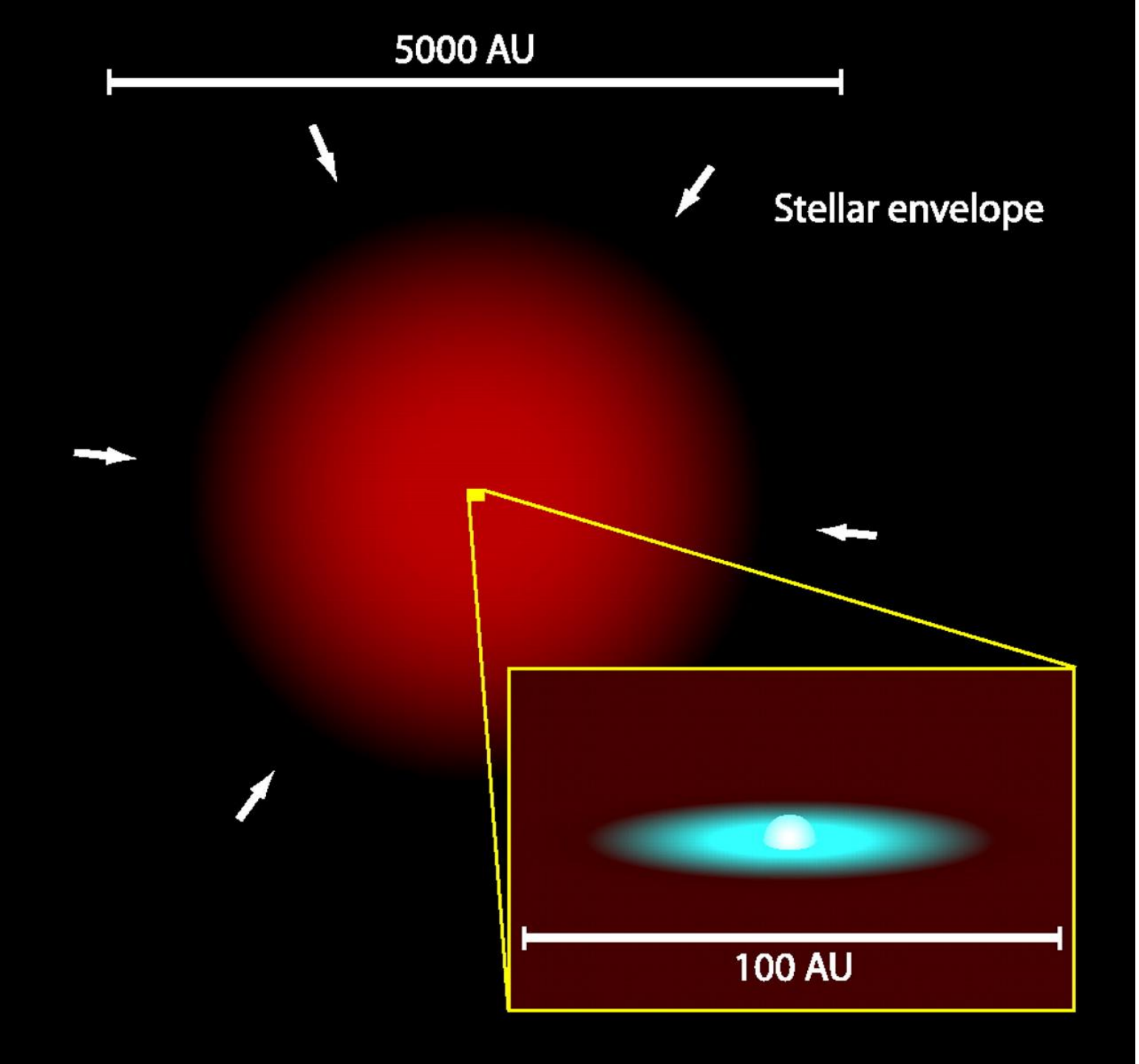

Central condensed protostar,
$r \sim$ a few $R_\odot$

Circumstellar disk,
$r \sim 100$ au

Surrounding envelope,
$r \sim 5000$ au

Matter accretes from the envelope via the disk onto the protostar

Ward-Thomson (2002)

Evolution from a circumstellar toroid (geometrically thick) to a disk (geometrically thin but optically thick) ; the opening angle of the outflows widens

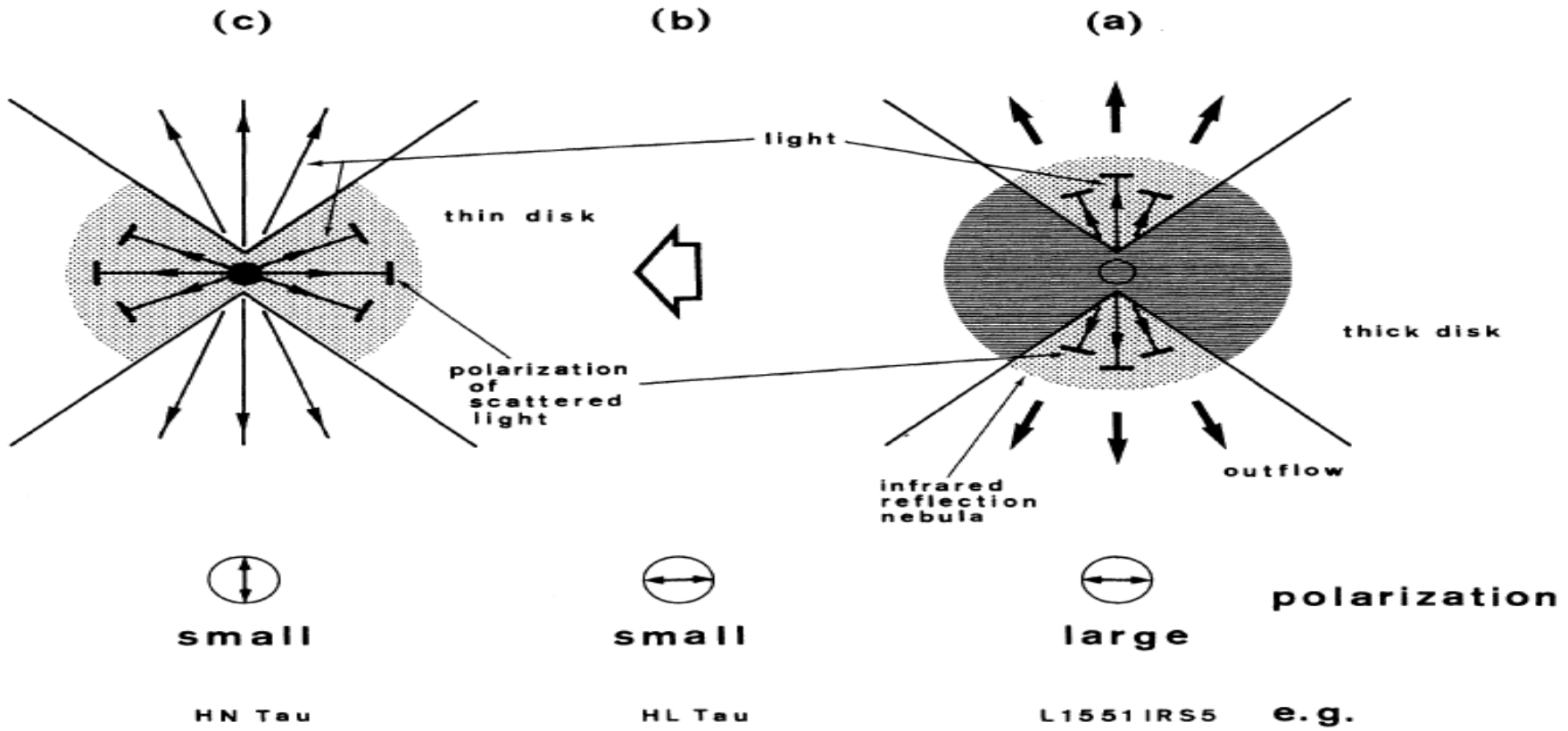

FIG. 10. Model of infrared polarization of (a) young stellar objects with mass outflows, (b) T Tauri stars with extreme mass-outflow phenomena, and (c) T Tauri stars without extreme mass outflow.

1980ApJ...239L..17S

OBSERVATIONS OF CO IN L1551: EVIDENCE FOR STELLAR WIND DRIVEN SHOCKS

RONALD L. SNELL
Astronomy Department and Electrical Engineering Research Laboratory, University of Texas at Austin; and
Five College Radio Astronomy Observatory, University of Massachusetts at Amherst

ROBERT B. LOREN
Electrical Engineering Research Laboratory and McDonald Observatory, University of Texas at Austin

RICHARD L. PLAMBECK
Radio Astronomy Laboratory, University of California at Berkeley

ABSTRACT

CO observations reveal the presence of a remarkable, double-lobed structure in the molecular cloud L1551. The two lobes extend for ~0.5 pc in opposite directions from an infrared source buried within the cloud; one lobe is associated with the Herbig-Haro objects HH28, HH29, and HH102. We suggest that the CO emission in the double-lobed structure arises from a dense shell of material which has been swept up by a strong stellar wind from the infrared source. This wind has a velocity of ~200 km s^{-1}, and evidently is channeled into two oppositely directed streams. The CO observations indicate that the shell has a velocity of ~15 km s^{-1}, a mass of 0.3 $M_\odot$, and a kinetic temperature of 8–35 K. Its age is roughly 3×10^4 years. A stellar mass-loss rate of $\sim 8 \times 10^{-7}$ $M_\odot$ yr^{-1} would be sufficient to create such a shell.

Data cube (sky position and frequency)

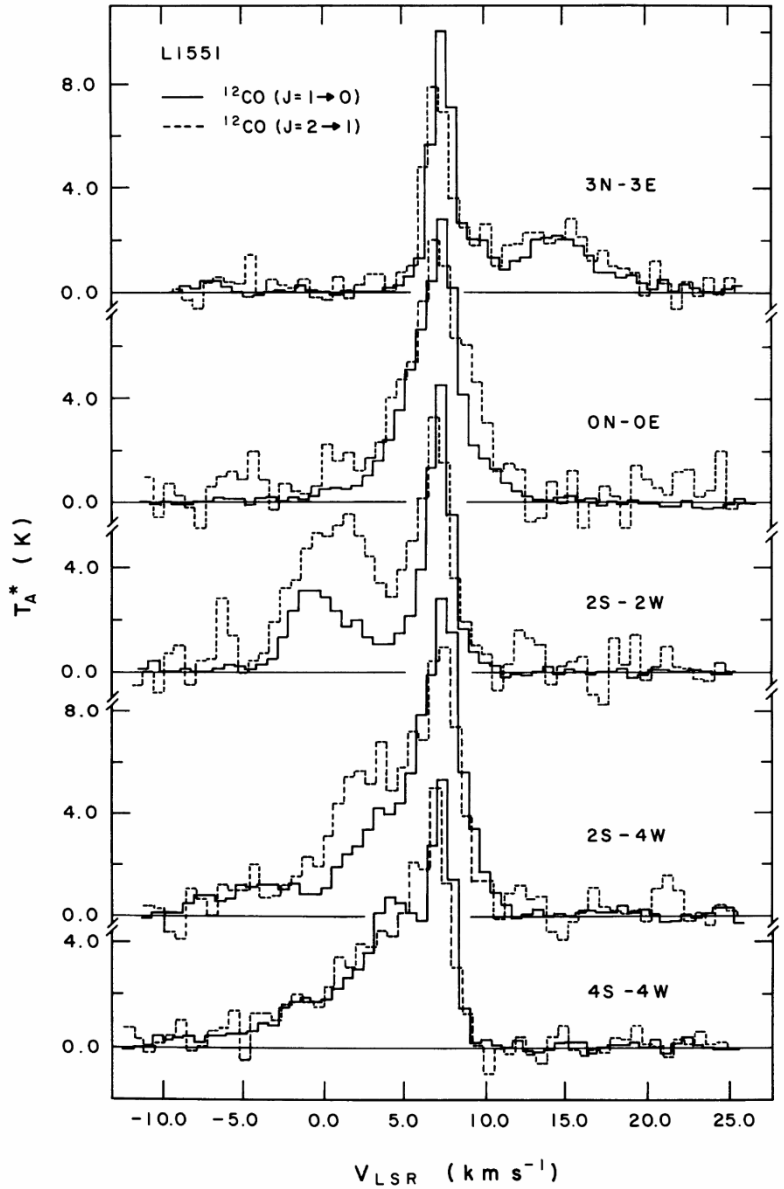

FIG. 1.—Spectra of the $J = 1$–0 (*solid*) and $J = 2$–1 (*dashed*) lines of ^{12}CO taken toward five selected positions in L1551. Offsets are measured in arcmin relative to the position of IRS-5 at $\alpha(1950) = 04^h28^m40^s$, $\delta(1950) = 18°01'52''$. The $J = 1$–0 spectra were taken at NRAO with a 1.′1 beam; the $J = 2$–1 spectra were taken at the MWO with a 1.′2 beam. The ratio of the 2–1 and 1–0 antenna temperatures in the broad velocity features can be used to infer the kinetic temperature of the gas responsible for these features.

What is V_{LSR}?

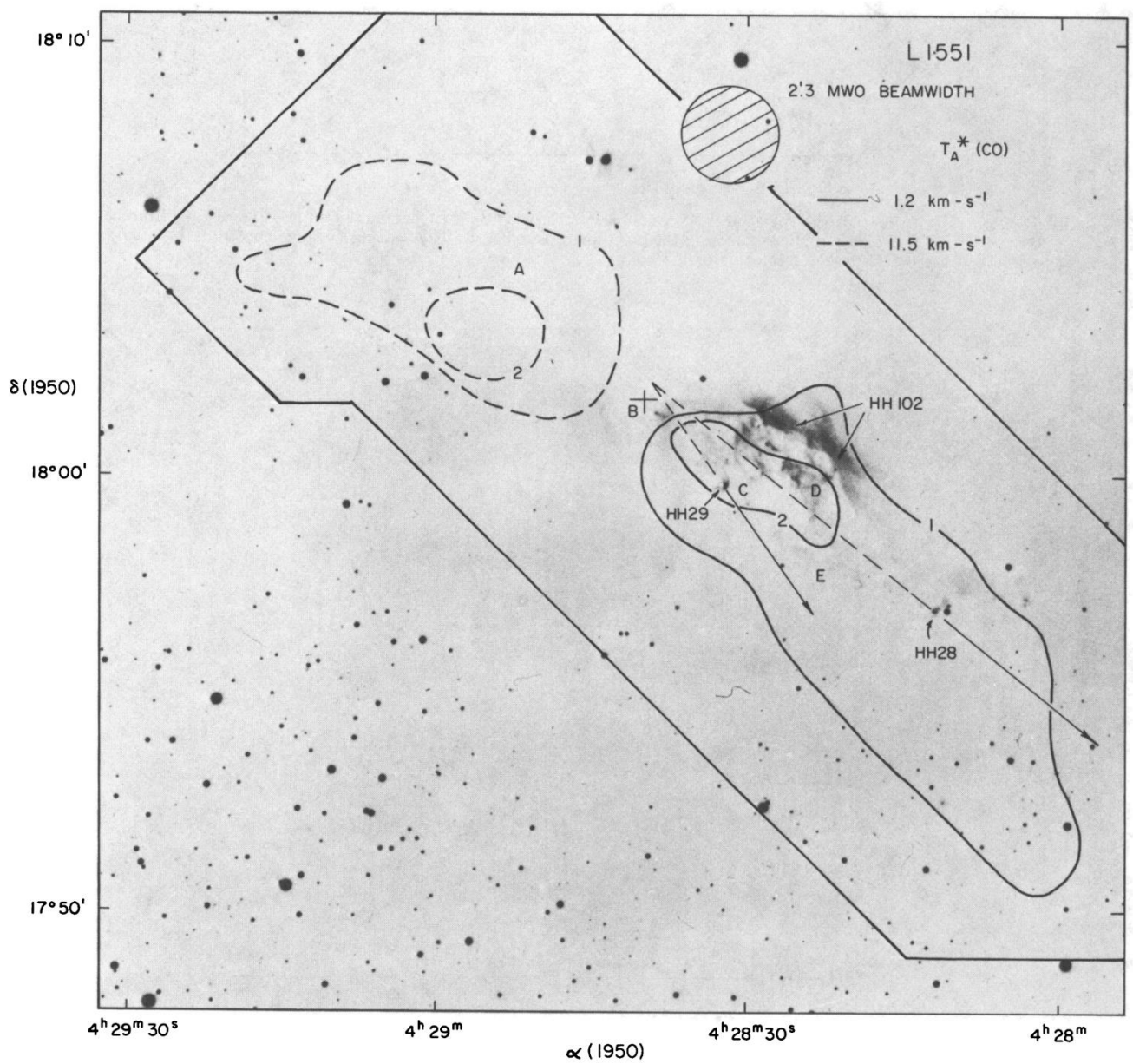

FIG. 2.—Contour map of the $J = 1$–0 ^{12}CO antenna temperatures in the broad velocity components, superposed on an optical photo of the region taken by Strom with the 4 m telescope at KPNO. The map is based on CO spectra taken at 115 positions within the enclosed border with 1′–2′ spacings. A cross indicates the position of IRS-5; letters A–E indicate the positions of the five spectra in Fig. 1 from top to bottom. Also shown are the directions of the proper motions of the two compact Herbig-Haro objects, HH28 and HH29; tracing their motion backward suggests a common origin at the infrared source.

Snell et al. (1980)

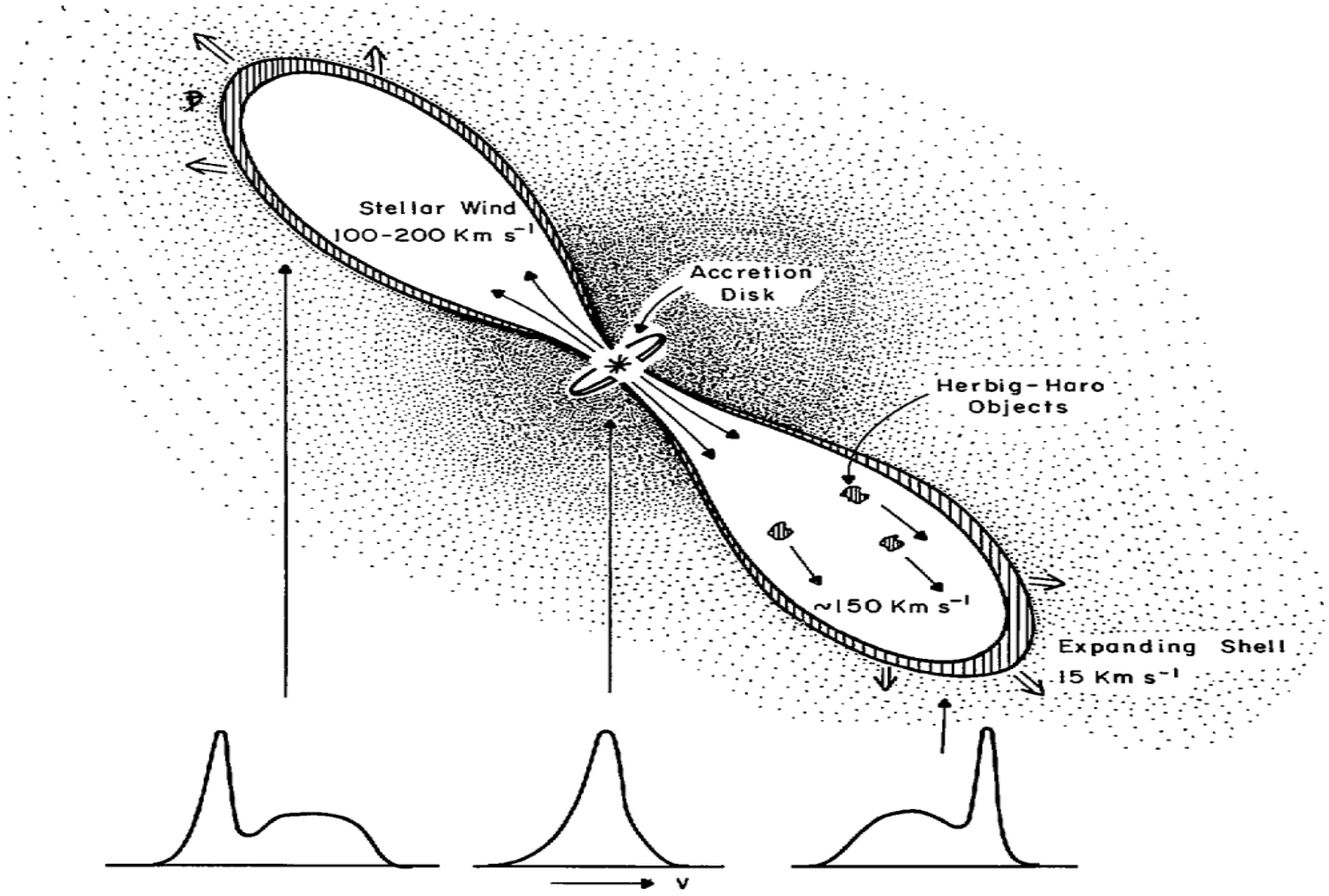

FIG. 5.—A schematic picture of the stellar wind driven shock model for L1551, indicating the CO line profiles which would be expected at different positions across the source. The Herbig-Haro objects are not necessarily located inside the shell; because of their high velocities, they may have been ejected through the shell and into the surrounding medium.

Snell et al. (1980)

Herbig-Haro (HH) Objects

-- (shock) excited nebulosity

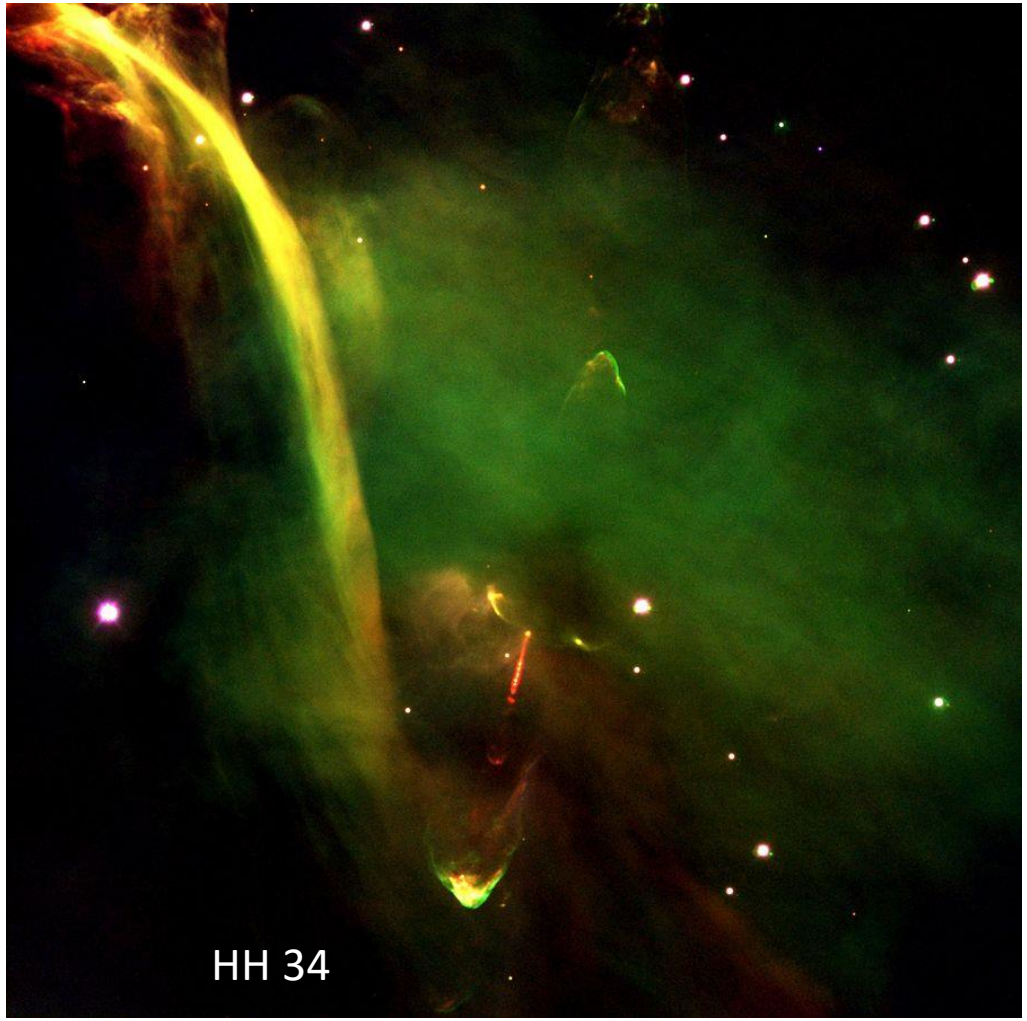

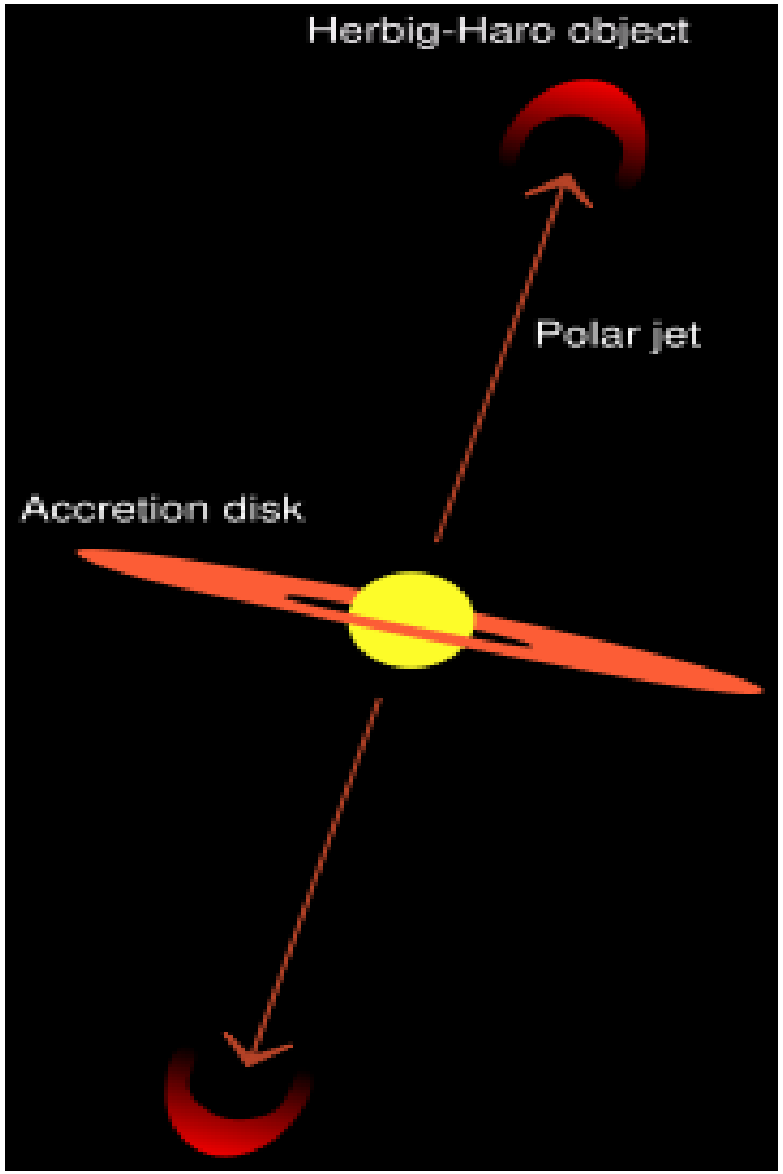

Ann. Rev. Astron. Astrophys. 1983. 21 : 209–37

HERBIG-HARO OBJECTS

Richard D. Schwartz

Department of Physics, University of Missouri, St. Louis, Missouri 63121

1. INTRODUCTION

The peculiar, semistellar emission nebulae called Herbig-Haro (HH) objects were discovered independently by Herbig (72, 73) and Haro (63, 64) in the course of Hα-emission star surveys of a dark-cloud region immediately south of the Orion Nebula. The prototype objects HH 1, 2, and 3, located near NGC 1999, each exhibit structure with tightly grouped knot-like condensations (see Figure 1). The spectra of HH objects are usually dominated by hydrogen Balmer emission lines and low-excitation emission lines of [O I], [S II], [N I], [Fe II], with moderate strength [O II] and [N II] lines, and relatively weak [O III] emission. Their locations in or near dark clouds in regions of star formation led to early speculation that the objects are associated with processes of star formation (2). Indeed, their properties and apparent lack of coincidence with visible young stars (e.g. T Tauri stars) led to the suggestion that the HH objects are themselves the sites of prestellar activity (75, 76). This notion still persists in some popular astronomy texts, although investigations over the past ten years have established that the HH objects are most likely the by-products of star formation rather than incipient stars.

Schwartz 1983

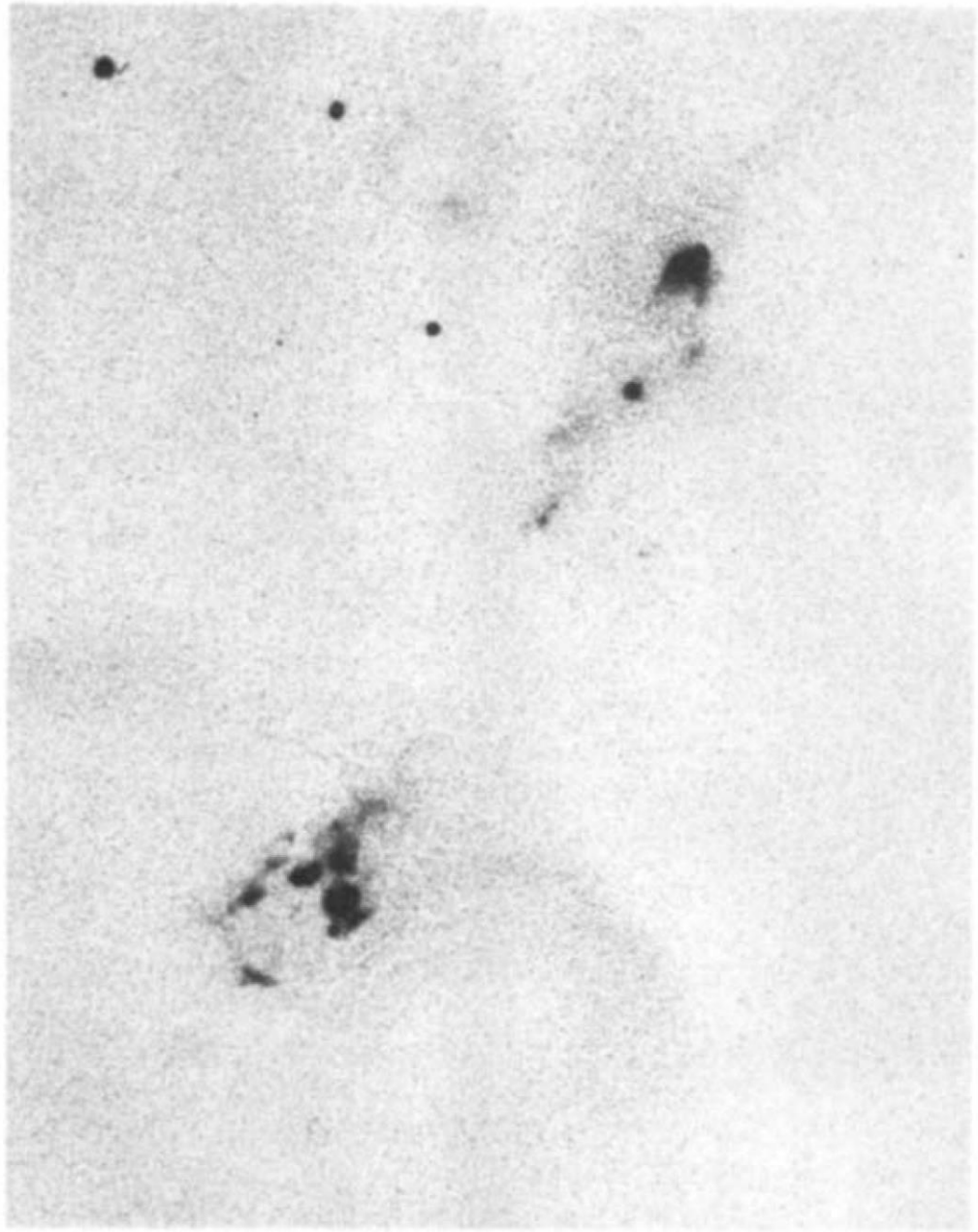

Figure 1 The prototype HH objects: HH 1 and 2. See Figure 2 for identifications and scale [from Herbig & Jones (80) and kindly supplied by the authors].

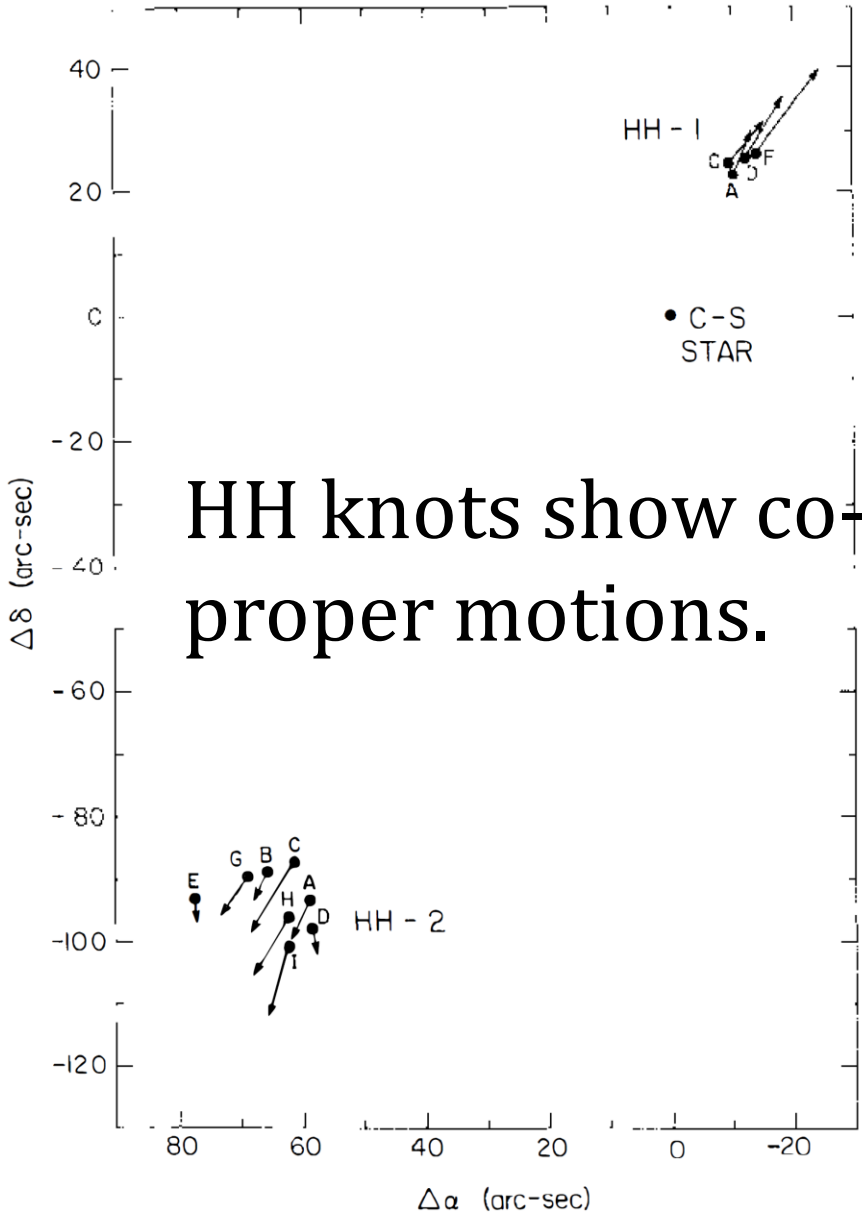

HH knots show co-moving proper motions.

Figure 2 The proper motion vectors indicating 100-year motions for the individual knots in HH 1 and 2. The C-S star is a 17th mag T Tauri star that has evidently ejected the HH objects [from Herbig & Jones (80)].

Schwartz 1983

HH objects have emission-line spectra, with little continua.

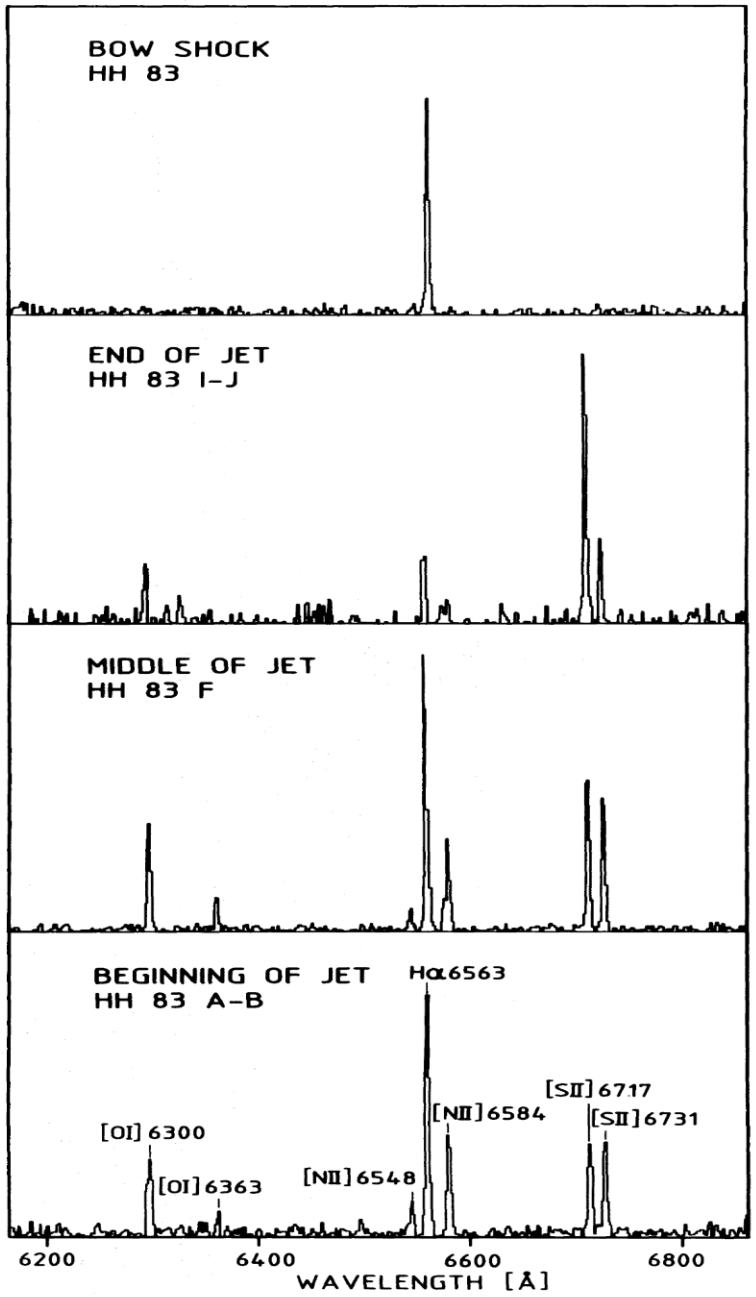

Fig. 5. Spectra of knots A-B, F, I-J in the HH 83 jet and of the bow shock in the wavelength range approx. 6200 Å to 6800 Å. Note the increasing [S II] 6717/Hα ratio as one moves out along the jet, as well as the changing sulphur line ratio, indicating decreasing electron density. The bow shock is pure Hα emission

Reipurth (1989)

Annu. Rev. Astron. Astrophys. 1996. 34:111–54

BIPOLAR MOLECULAR OUTFLOWS FROM YOUNG STARS AND PROTOSTARS

Rafael Bachiller

Observatorio Astronómico Nacional (IGN), Campus Universitario, Apartado 1143, E–28800 Alcalá de Henares (Madrid), Spain

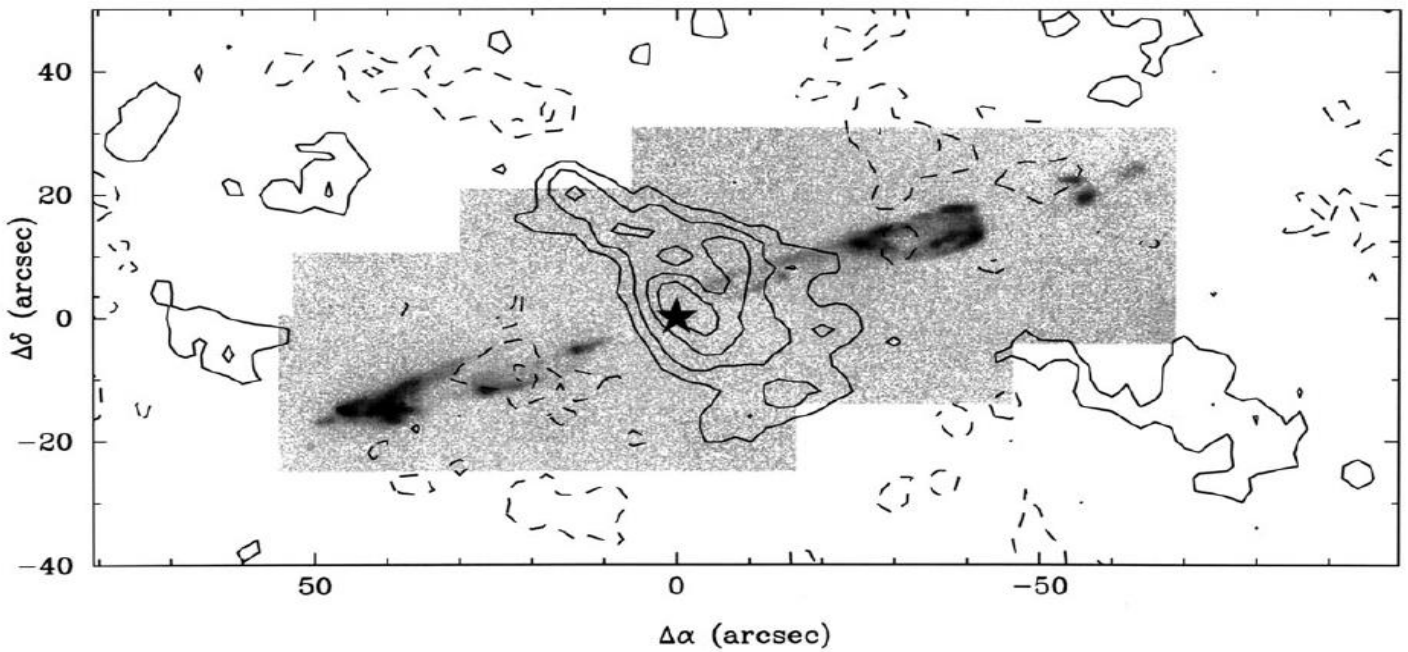

Figure 4 Superposition of a gray-scaled image of the HH 211 jet taken in the H_2 $v = 1–0$ S(1) line at 2.122 μm (from McCaughrean et al 1994) with a NH_3 (1,1) image obtained with the VLA at its D configuration (6″ angular resolution) (R Bachiller & M Tafalla 1995, unpublished data). The star marks the position of the jet source HH 211-mm (see also Table 1).

Molecular Hydrogen Objects (MHOs) 1000+ now known

Infrared image of molecular bow shocks (MHO 27) associated with bipolar outflows in Orion. Credit: UKIRT/Joint Astronomy Centre

SED

Spectral Energy Distribution

Optical depth

$\tau \sim 1$ at 100 μm

~ 0.01 at 1 mm

$\tau > 100$ at 1 μm

Obs. at mm → total dust mass

⇒ $A_V \gtrsim 300$!

i.e. Star should be invisible

But obsed $A_V \sim 3$

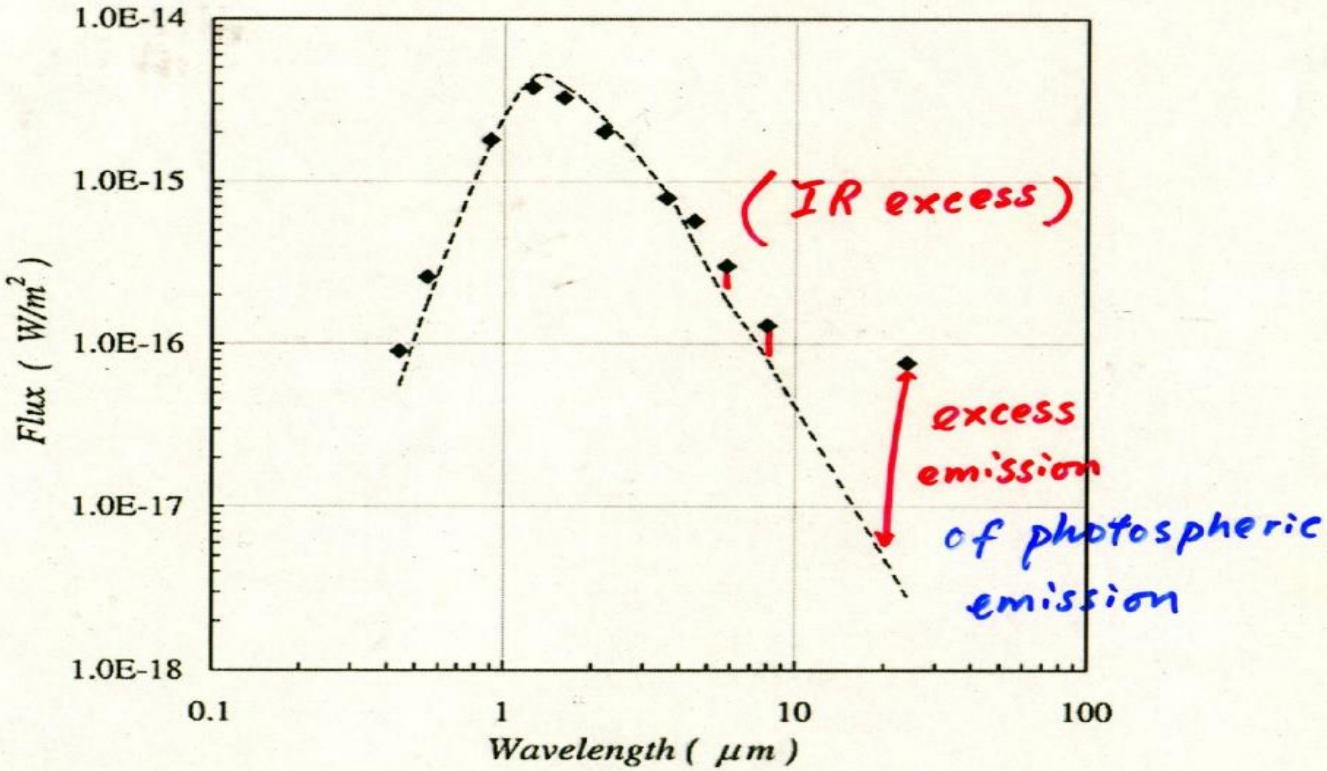

SED for 2MASS 08093547-4913033, with that of an M5 star (Young et al. 2004, ApJS, 154, 428)

⇒ clear line-of-sight ⇒ disk or thin shell

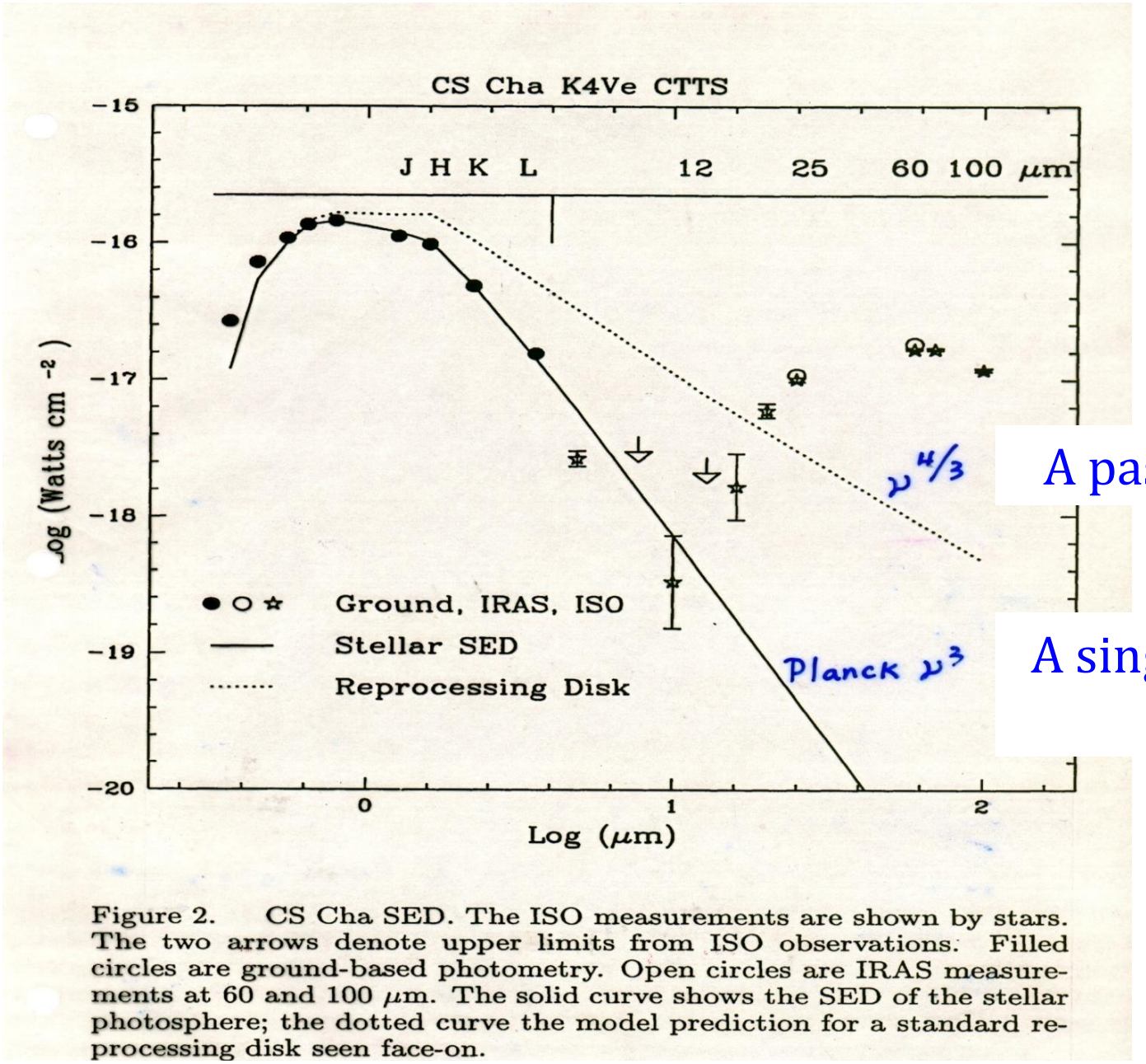

Figure 2. CS Cha SED. The ISO measurements are shown by stars. The two arrows denote upper limits from ISO observations. Filled circles are ground-based photometry. Open circles are IRAS measurements at 60 and 100 μm. The solid curve shows the SED of the stellar photosphere; the dotted curve the model prediction for a standard reprocessing disk seen face-on.

A passive disk

A single-temperature blackbody

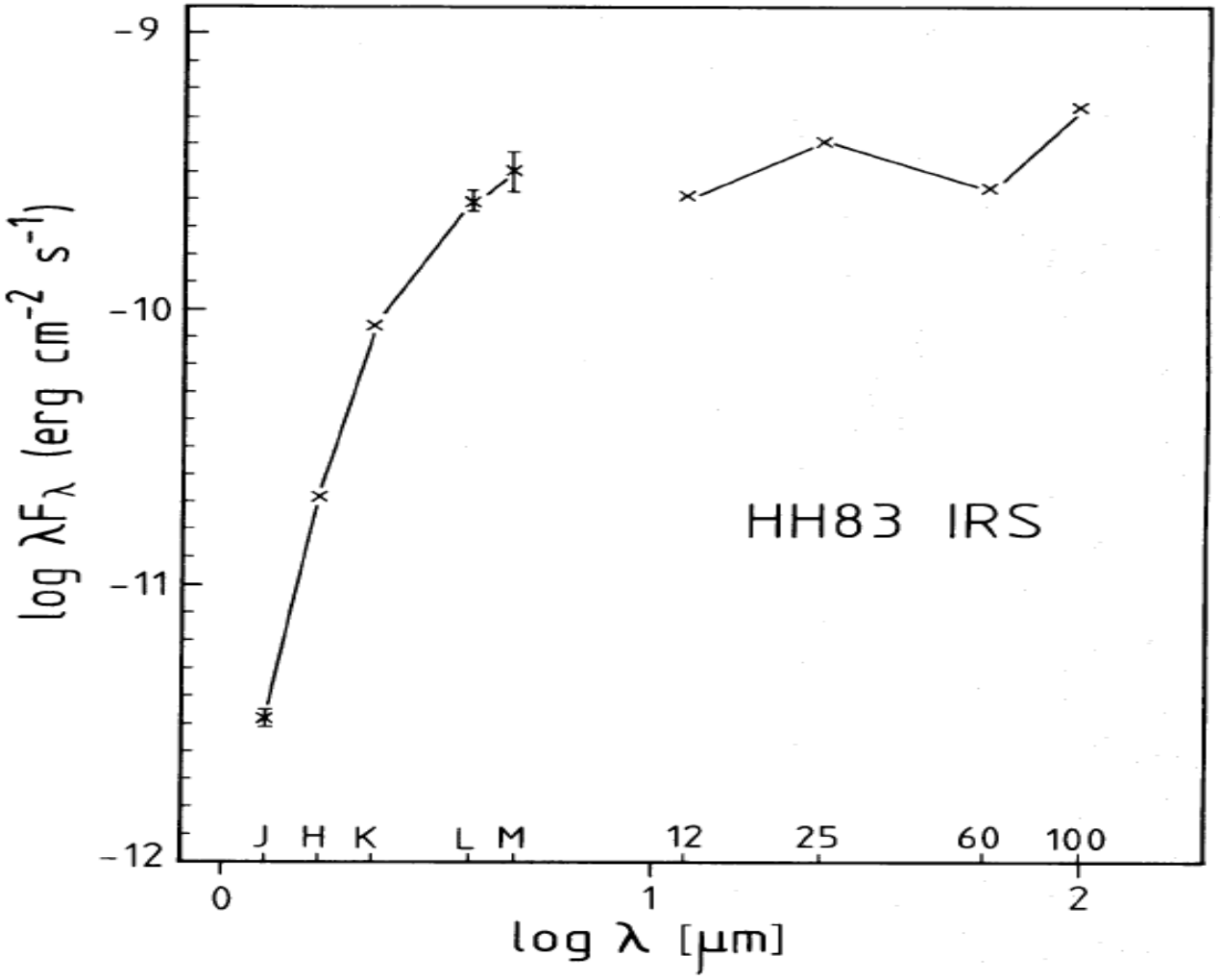

Fig. 6. The energy distribution of the infrared source of HH 83 based on near- and far-infrared photometry. Error bars are shown for the near-infrared data points where the errors are larger than the extent of the crosses. No error bars are given for the far-infrared IRAS data

The exciting source of an HH object = a protostar

A flat FIR SED

very prominent IR excess; lots of dust; a very young age

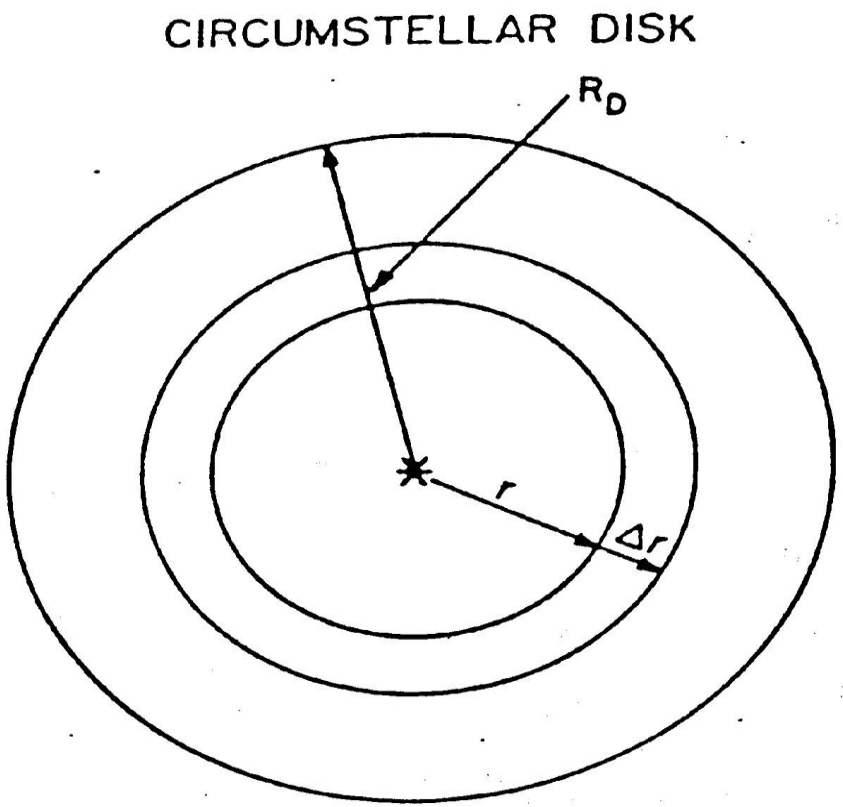
CIRCUMSTELLAR DISK
R_D
r
Δr

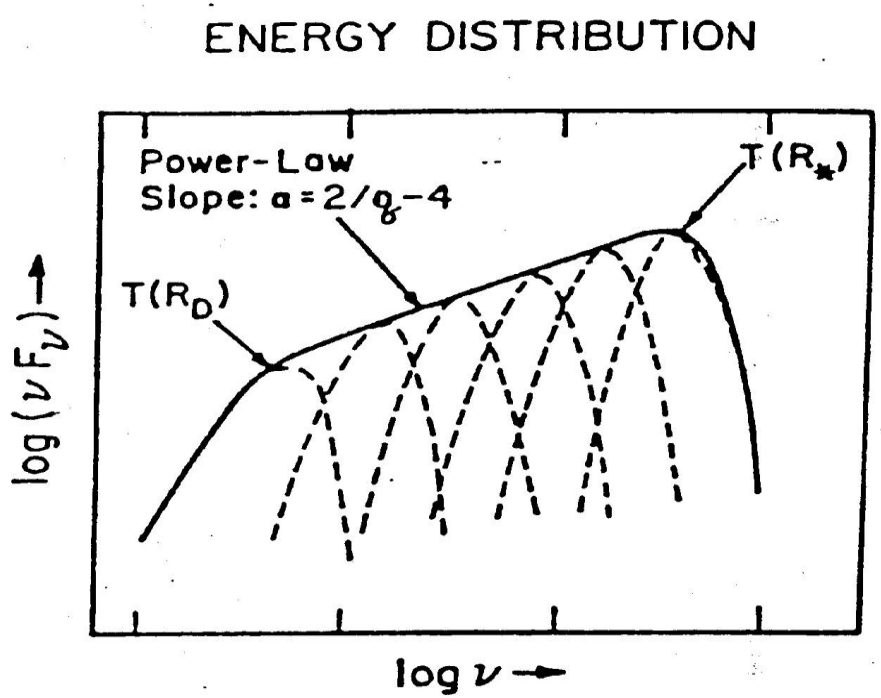
ENERGY DISTRIBUTION
Power-Law
Slope: a = 2/q − 4
T(R*)
T(R_D)
log (νF_ν)
log ν

Water and carbon dioxide in solid form → cold materials near the protostar

Silicate feature → thick dusty cocoon

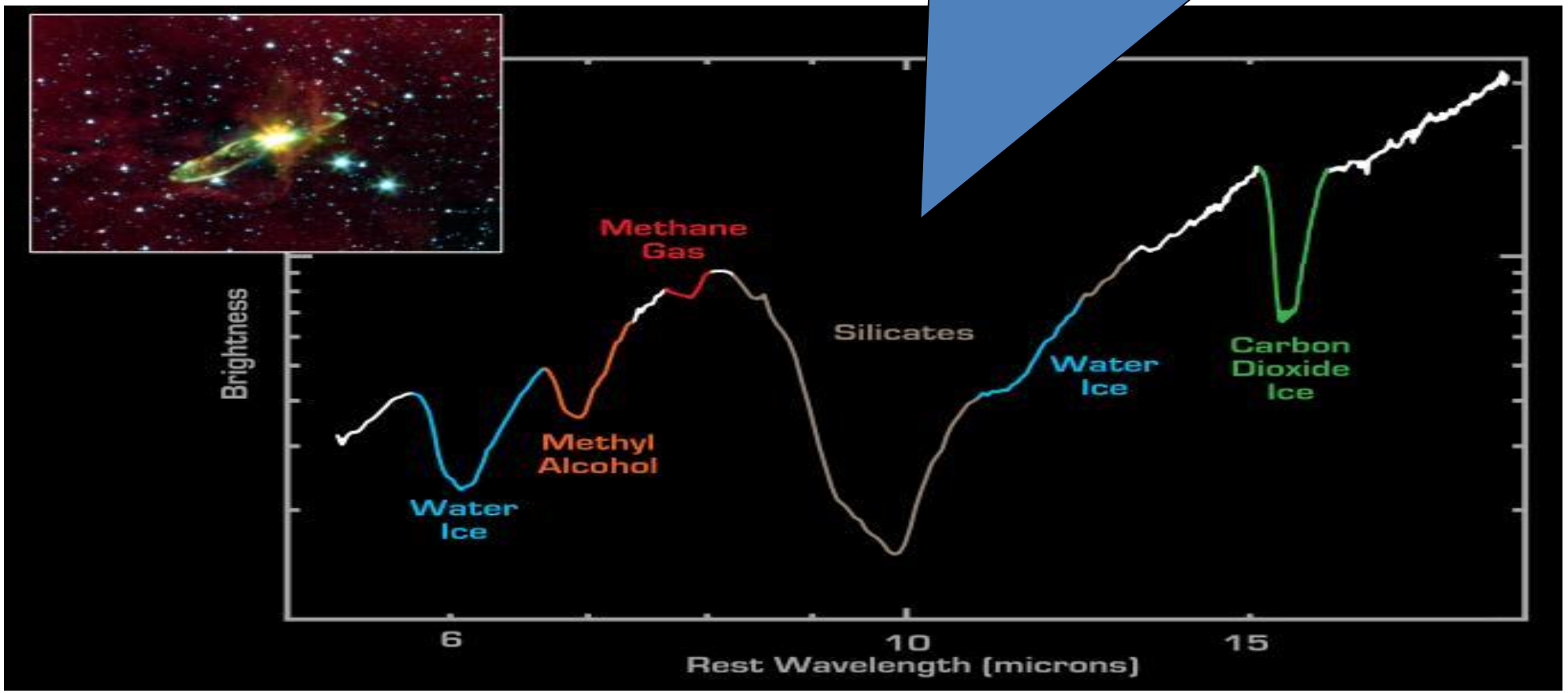

Spitzer IRS

Pre-main-Sequence (PMS) Stars

- Massive stars have no PMS phase.

  A 15 $\mathcal{M}_\odot$ protostar reaches the MS in 6×10^4 yr

  1 $\mathcal{M}_\odot$ in 5×10^7 yr

- Intermediate-mass → **Herbig Ae/Be stars**
- Low-mass (sun-like) → **T Tauri stars**
  - ✓ Classical T Tauri stars (CTTSs): EW(Hα) ≥ 10 Å
  - ✓ Weak-lined ('naked') T Tauri stars (WTTSs)

Observational characteristics of T Tauri stars

TTSs: pre-main-sequence sun-like stars

- Seen in regions of obscuration
- Spectra types later than F
- Emission-line spectra
- IR excess and UV excess
- Often as X ray sources
- Brightness variability (x rays to infrared)
- In T associations (and OB associations)

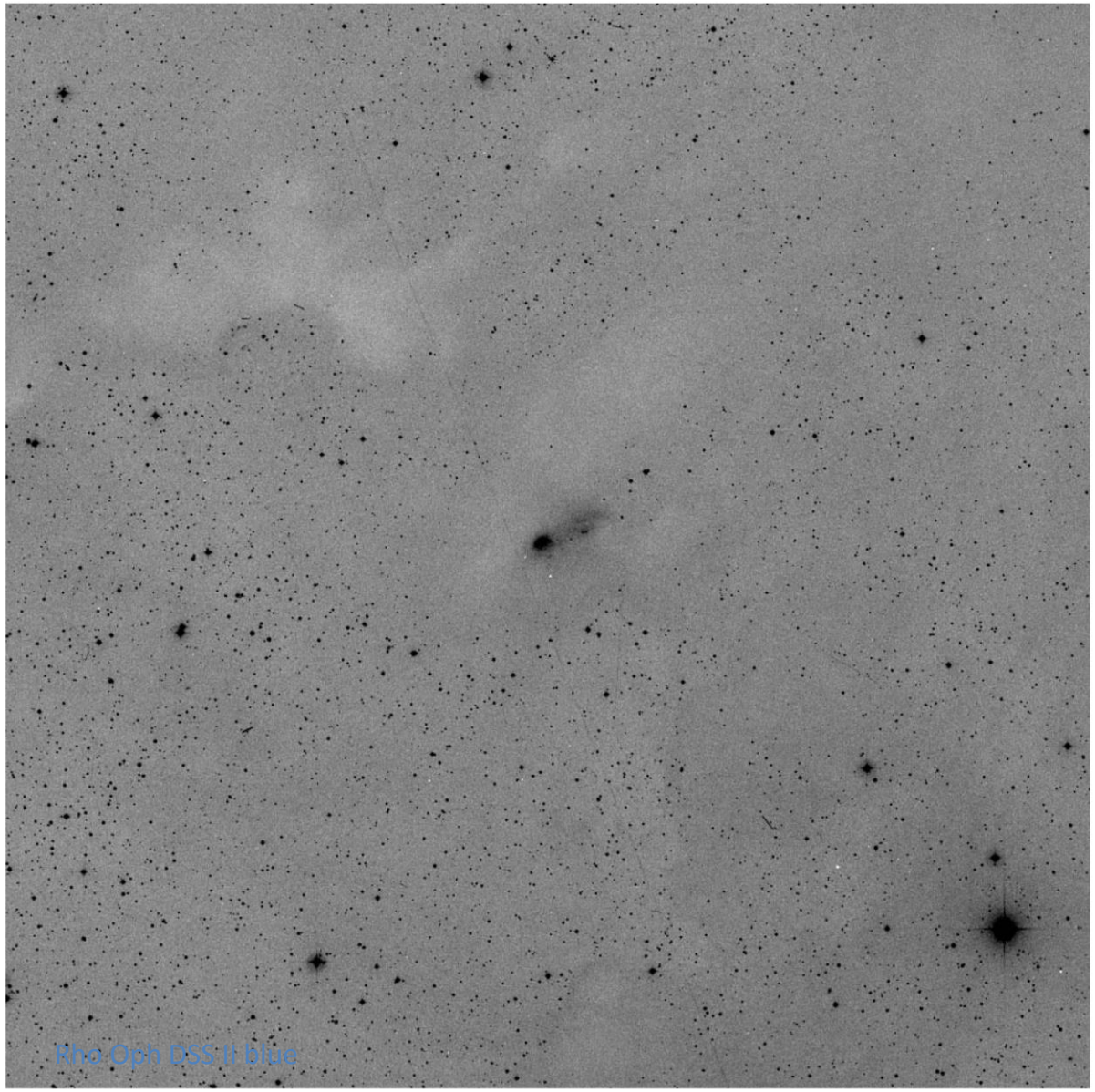

CTTSs characterized by strong emission lines in the spectra

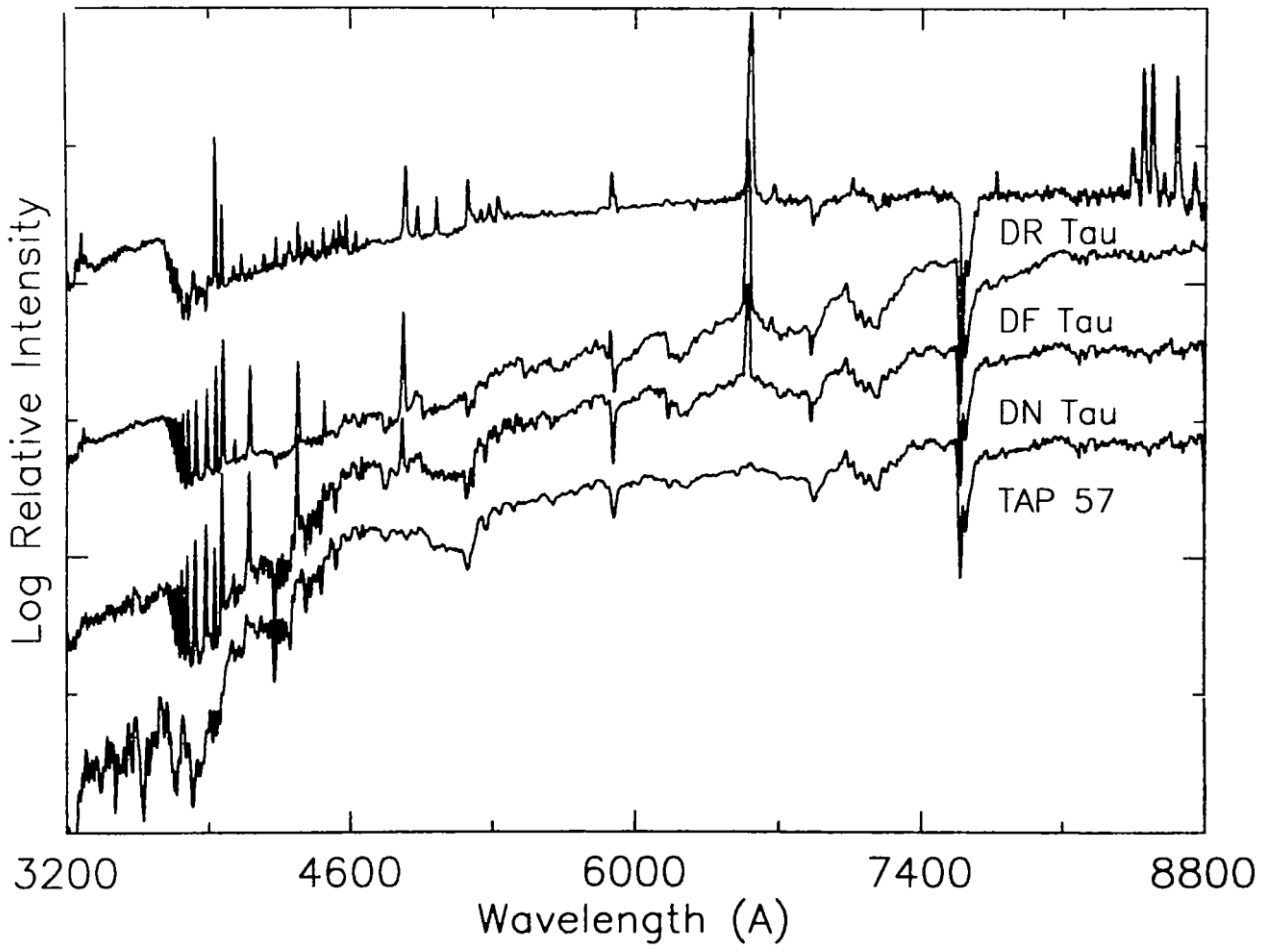

Figure 2 Medium-resolution spectrograms covering the spectral range 3200–8800 Å of four late-K or early-M T Tauri stars, shown in order of increasing emission levels. The relative intensity is displayed in wavelength units.

Bertout 1989 ARAA

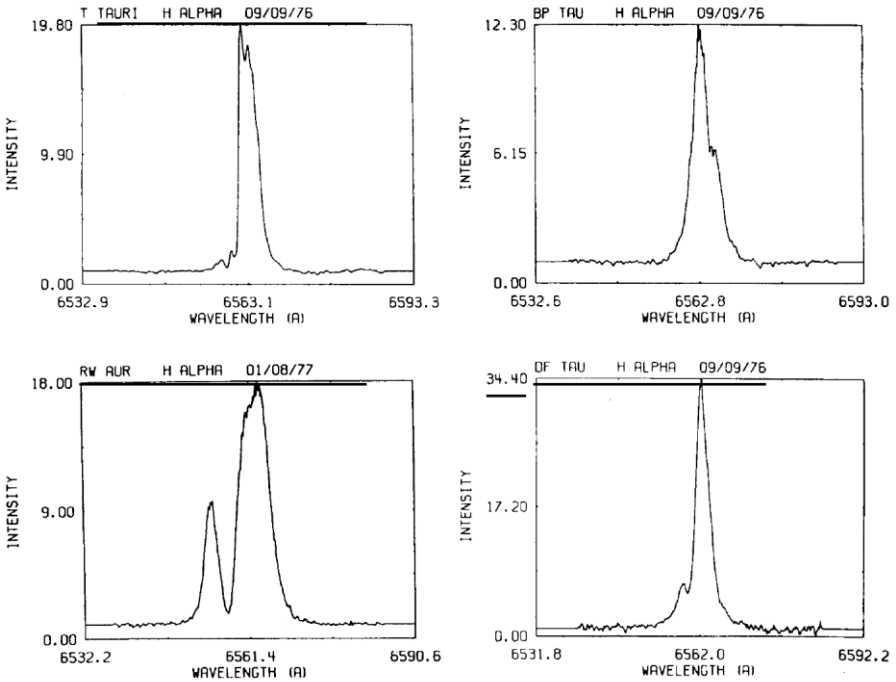

Fig. 4. Hα emission line profiles in 4 T Tau stars [10].

Cohen 1984

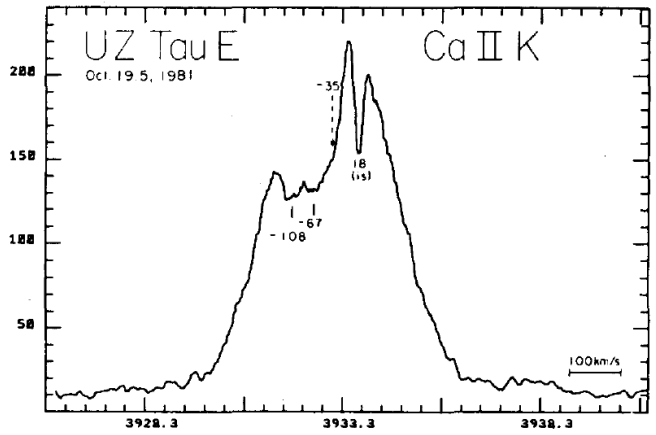

P Cygni profile → A spectral profile showing an expanding envelope

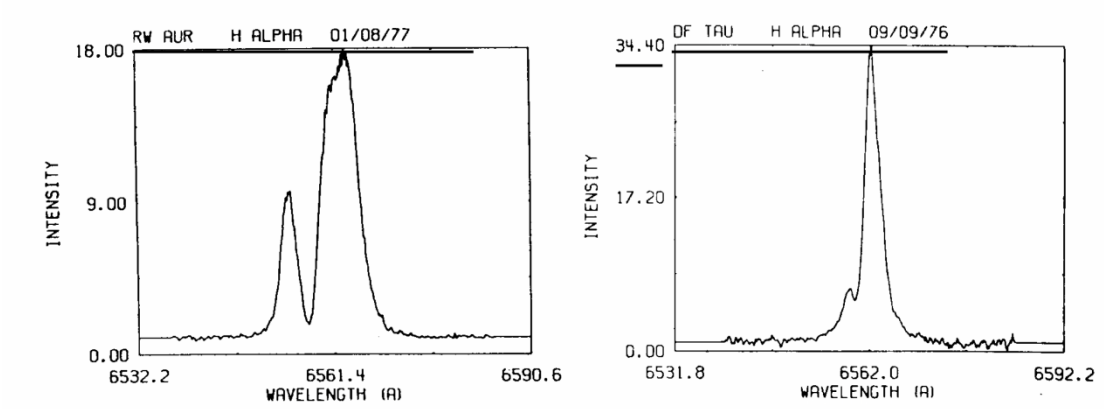

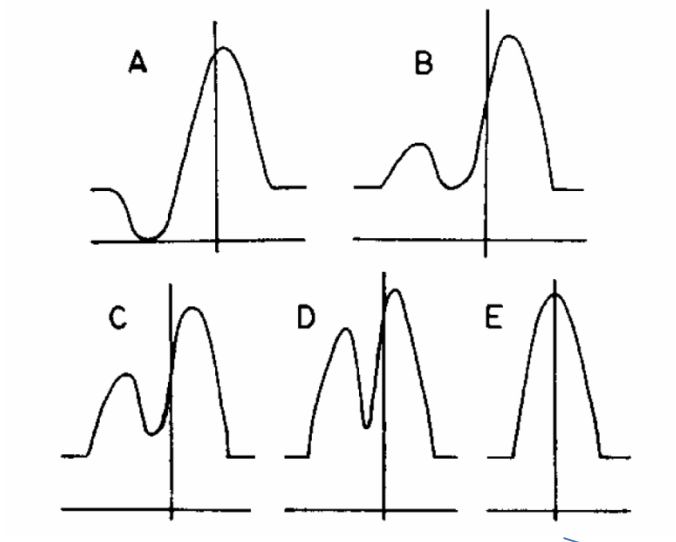

Stellar velocity

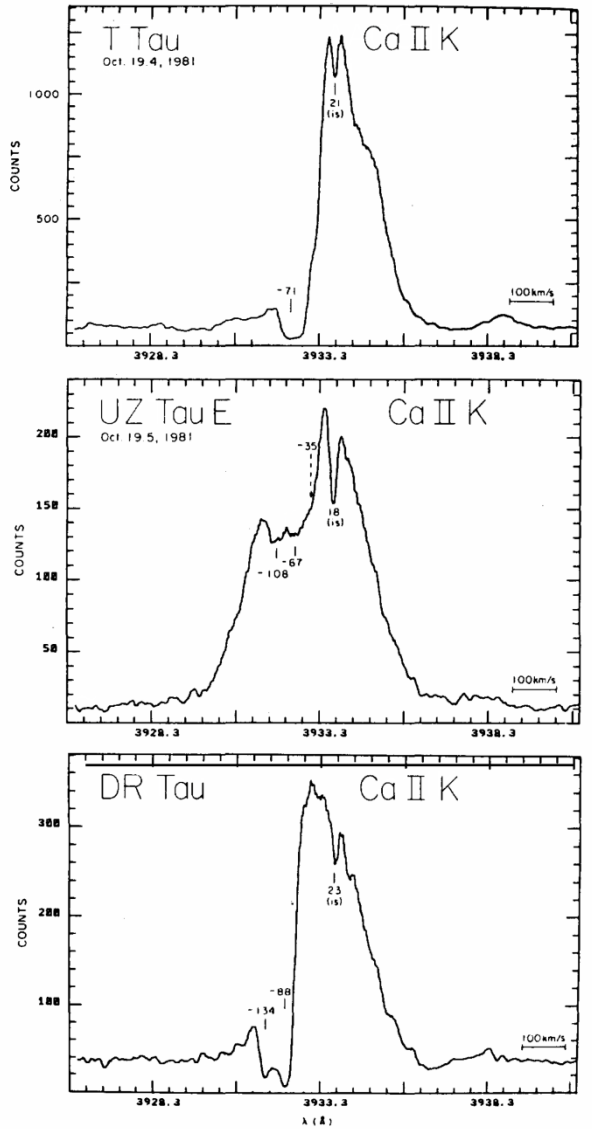

Cohen (1984)

CTTSs characterized by infrared excess in the SEDs

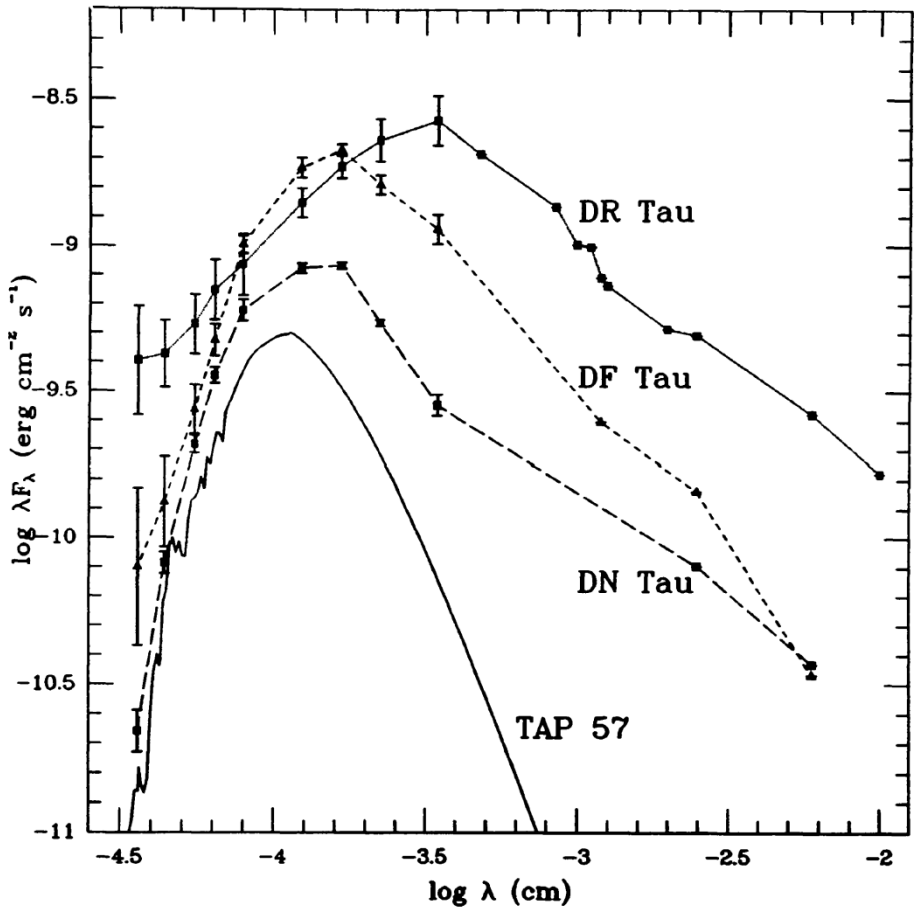

Figure 3 Observed spectral energy distributions from 3600 Å to 100 μm of the stars whose spectra are shown in Figure 2. The energy distribution of the K7V WTTS TAP 57, shown as a solid line, has been displaced downward by 0.3 dex. The filled symbols are simultaneous (for DN Tau and DF Tau) or averaged (for DR Tau) photometric data (cf. Bertout et al. 1988) supplemented by *IRAS* data (Rucinski 1985). When available, observed variability is indicated by error bars. When compared with WTTSs such as TAP 57, CTTSs display prominent ultraviolet and infrared excesses. Excess continuum flux and optical emission-line activity are often correlated.

… and also <u>UV excess</u>
→ spectral "veiling"

Bertout (1989)

T Tauri stars are PMS objects, contracting toward the **zero-age main sequence (ZAMS).**

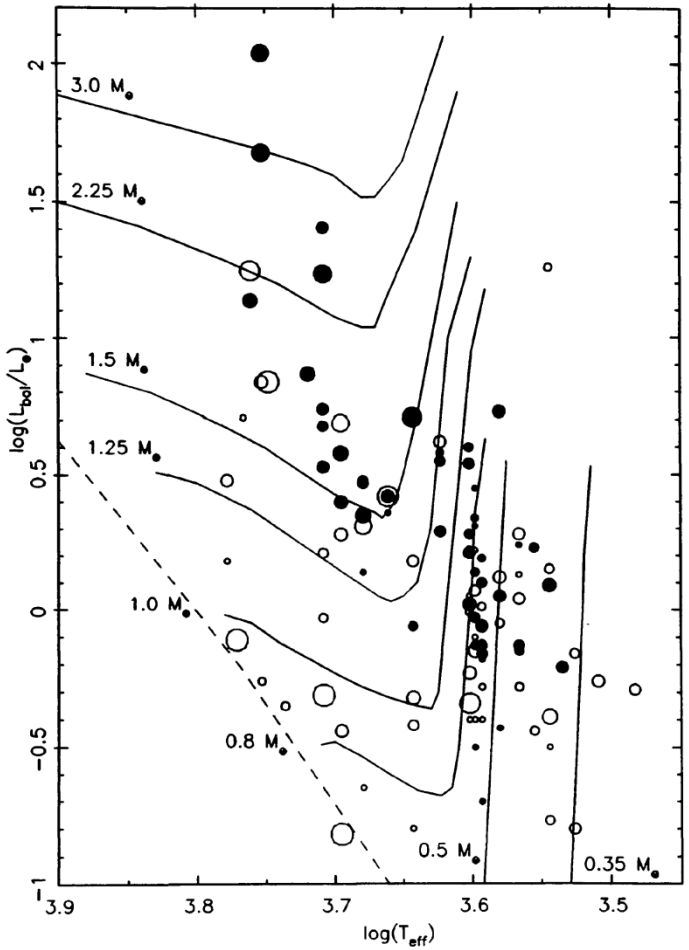

Figure 4 Position in the Hertzsprung-Russell diagram of all CTTSs and WTTSs with known $v \sin i$. WTTSs are represented by open circles, and CTTSs by dark circles. In both cases, the circle area is proportional to the stellar $v \sin i$. Approximate pre-main-sequence quasi-static evolutionary tracks for various masses are also plotted together with the zero-age main sequence (dashed line).

Classical T Tauri stars (CTTSs)

vs

Weak-lined T Tauri stars (WTTSs)

Bertout (1989)

Spectral index useful to classify a young stellar object (YSO)

$$\alpha = \frac{d \log (\lambda F_\lambda)}{d \log (\lambda)}$$

Where λ=wavelength, between 2.2 and 20 μm; F_λ=flux density

Class 0 sources --- undetectable at $\lambda < 20$ μm

Class I sources --- $\alpha > 0.3$

Flat spectrum sources --- $0.3 > \alpha > -0.3$

Class II sources --- $0.3 > \alpha > -1.6$

Class III sources --- $\alpha < -1.6$

➔ Evolutionary sequence in decreasing amounts of circumstellar material (disk clearing)

Annu. Rev. Astron. Astrophys. 1996. 34:111–54

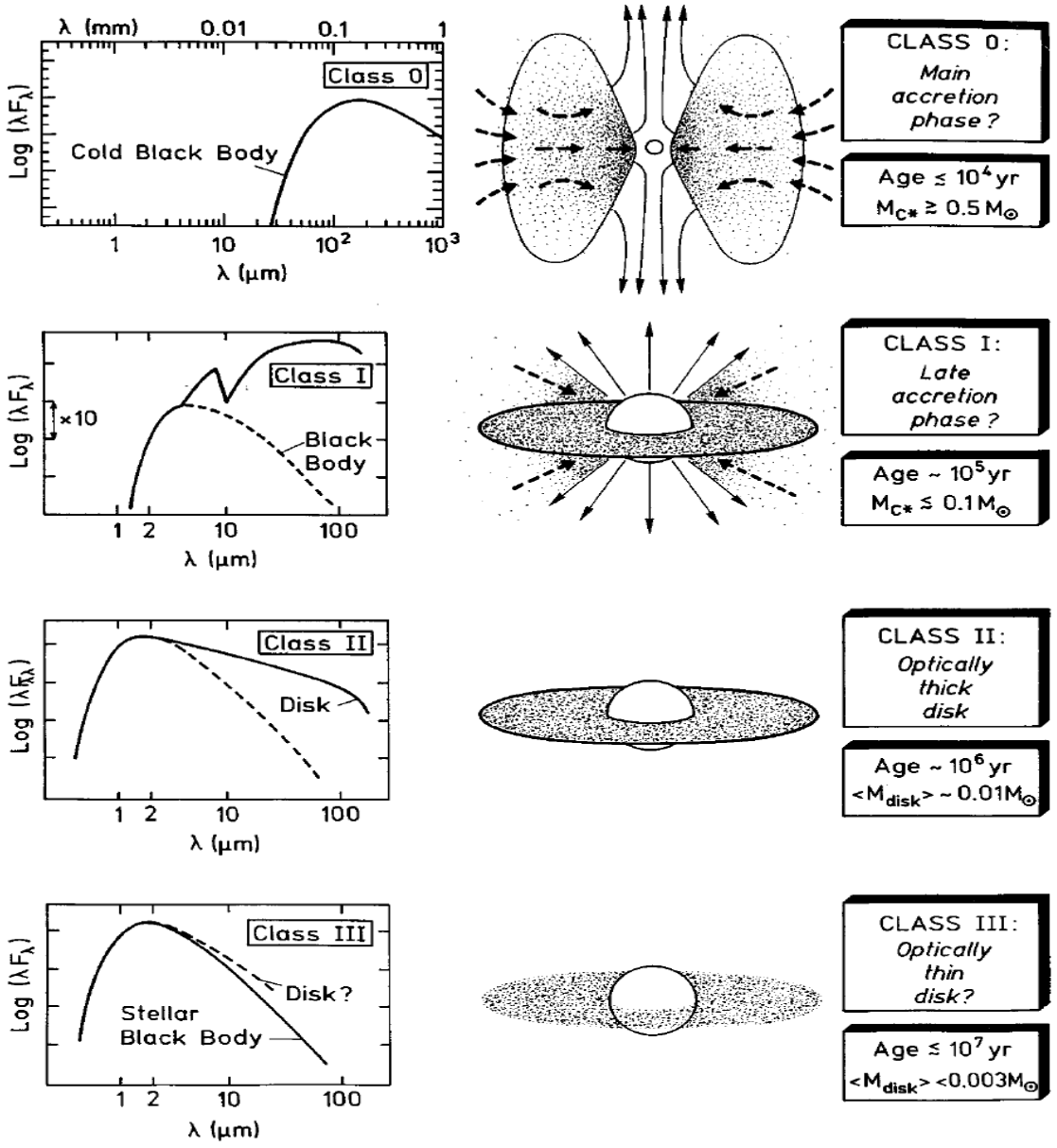

Figure 11 Evolutionary sequence of the spectral energy distributions for low-mass YSOs as proposed by André (1994). The four classes 0, I, II, and III correspond to successive stages of evolution.

Class 0
Submilimeter cores

Class I
Protostars

Class II
Classical T Tauri stars

Class III
Weak-lined T Tauri stars

Rafael Bachiller

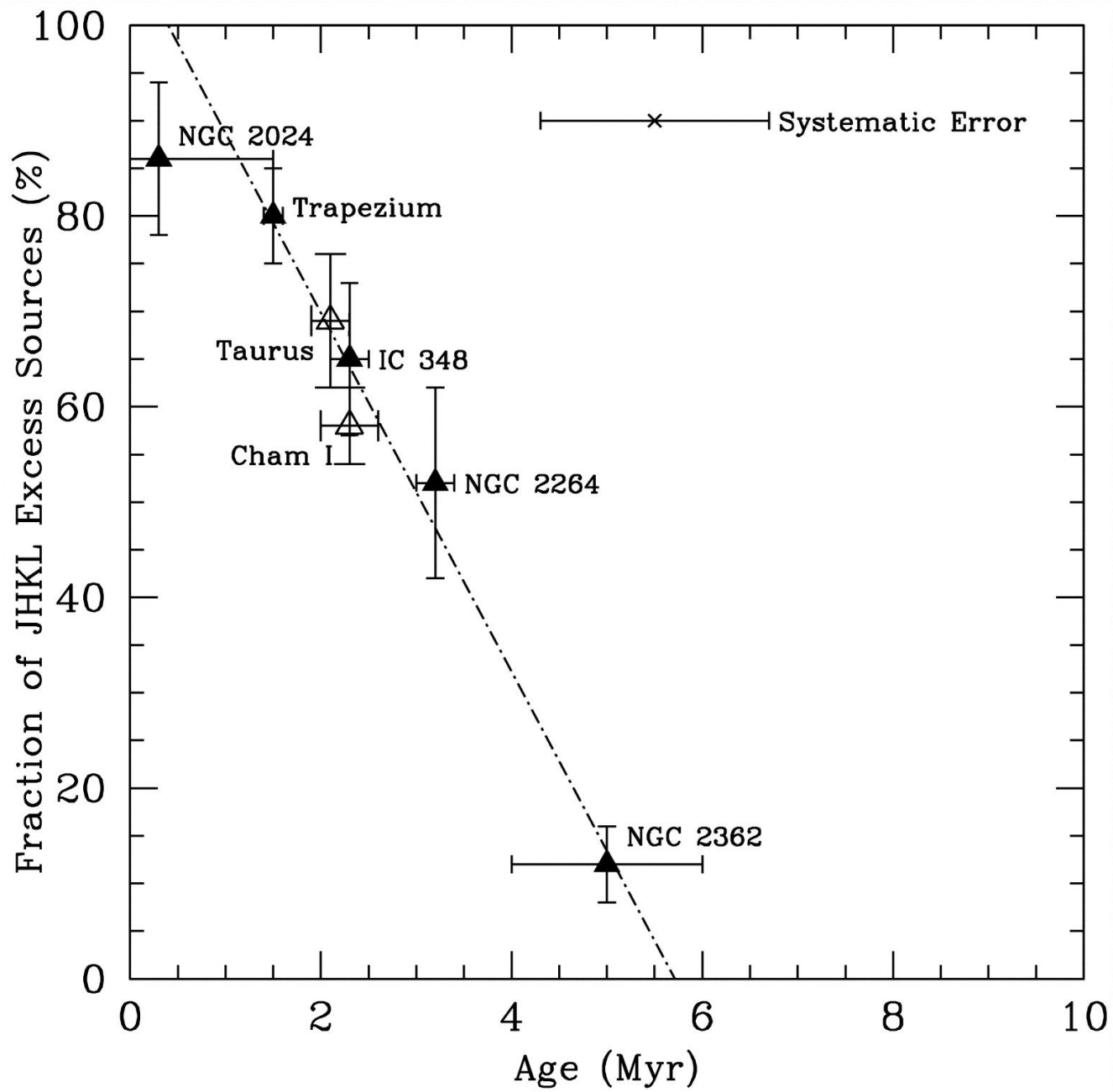

One half of stars lose disks within 3 Myr.

Disks are disposed in ~6 Myr; in competition with planet formation

(or planet formation largely completed by this time?)

Haisch+ 2001

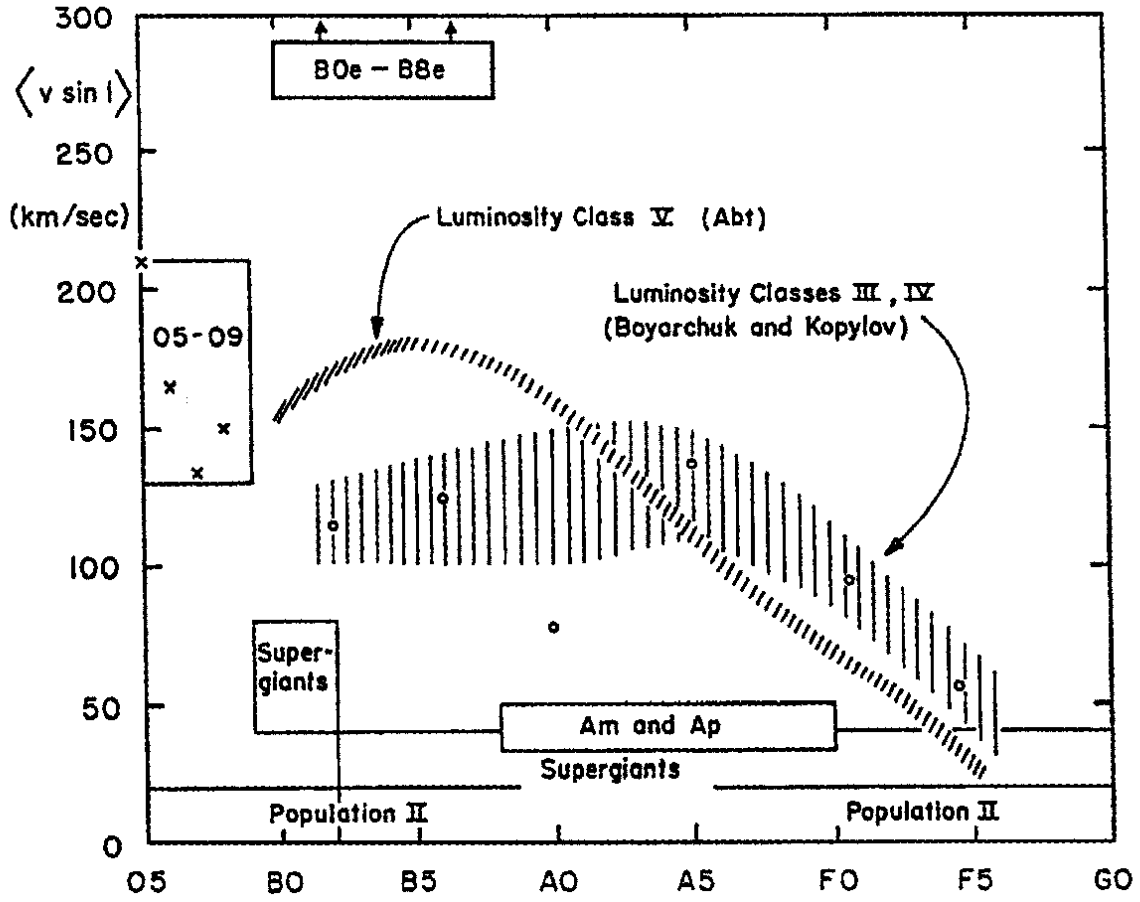

Fig. 3. Projected equatorial velocities, averaged over all possible inclinations, as a function of spectral type. On the main sequence (luminosity class V), early-type stars have rotational velocities that reach and even exceed 200 km/s; these velocities drop to a few km/s for late-type stars, such as the Sun (type G2) (Slettebak [20]; courtesy Gordon & Breach)

- Early-type stars are fast rotators
- Stars later than ~F5 rotate very slowly
- Disk/planet formation?

Young Stellar Variability

(Herbst et al. 1994)

- Rotational modulation of cool spots
- Accretion and rotation of hot spots
- Variable obscuration by circumstellar dust (**UXors**)

Eruptive YSO Variability

- **FUors** brighten up to 6 mag in a few months; followed by a slow decline in years to decades.
- **EXors** brighten up to 5 mag in a few months; followed by a fading on about the same time scale.

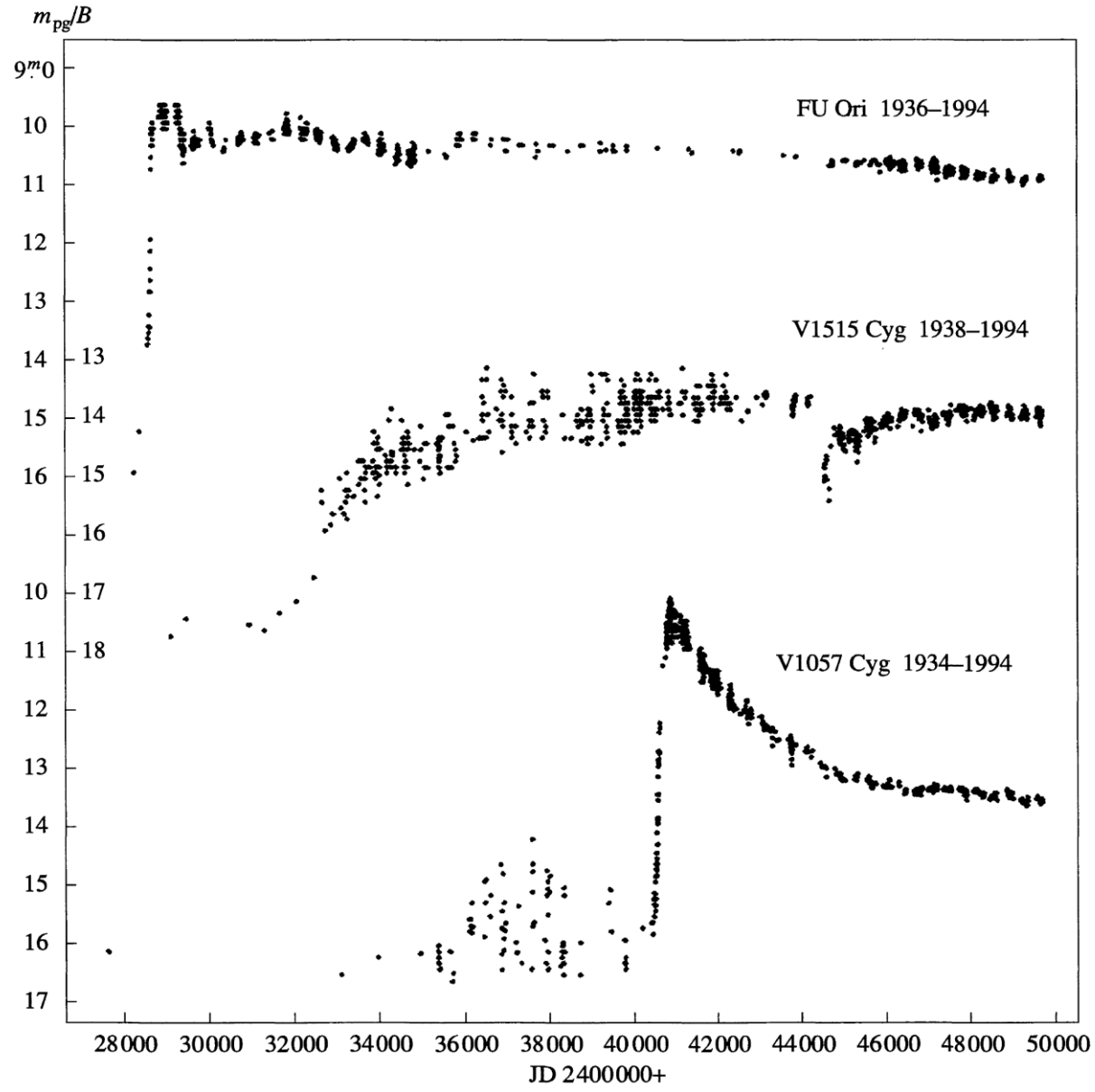

Fig. 4. Overall m_{pg}/B light curves of FU Ori, V1515 Cyg, and V1057 Cyg from the mid-1930s until 1994.

Ibragimov 1997

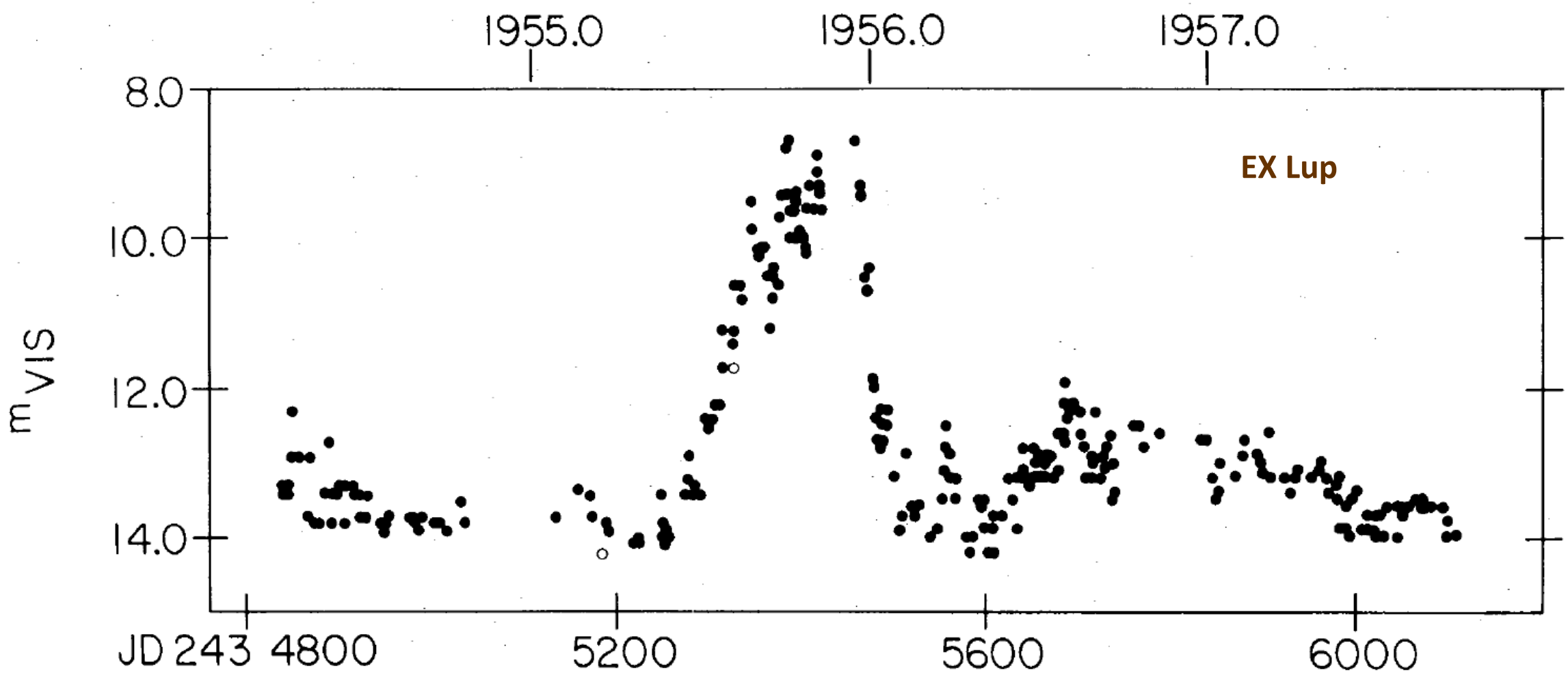
1955.0
1956.0
1957.0
8.0
10.0
12.0
14.0
m_{VIS}
EX Lup
JD 243 4800
5200
5600
6000

Herbig 1977

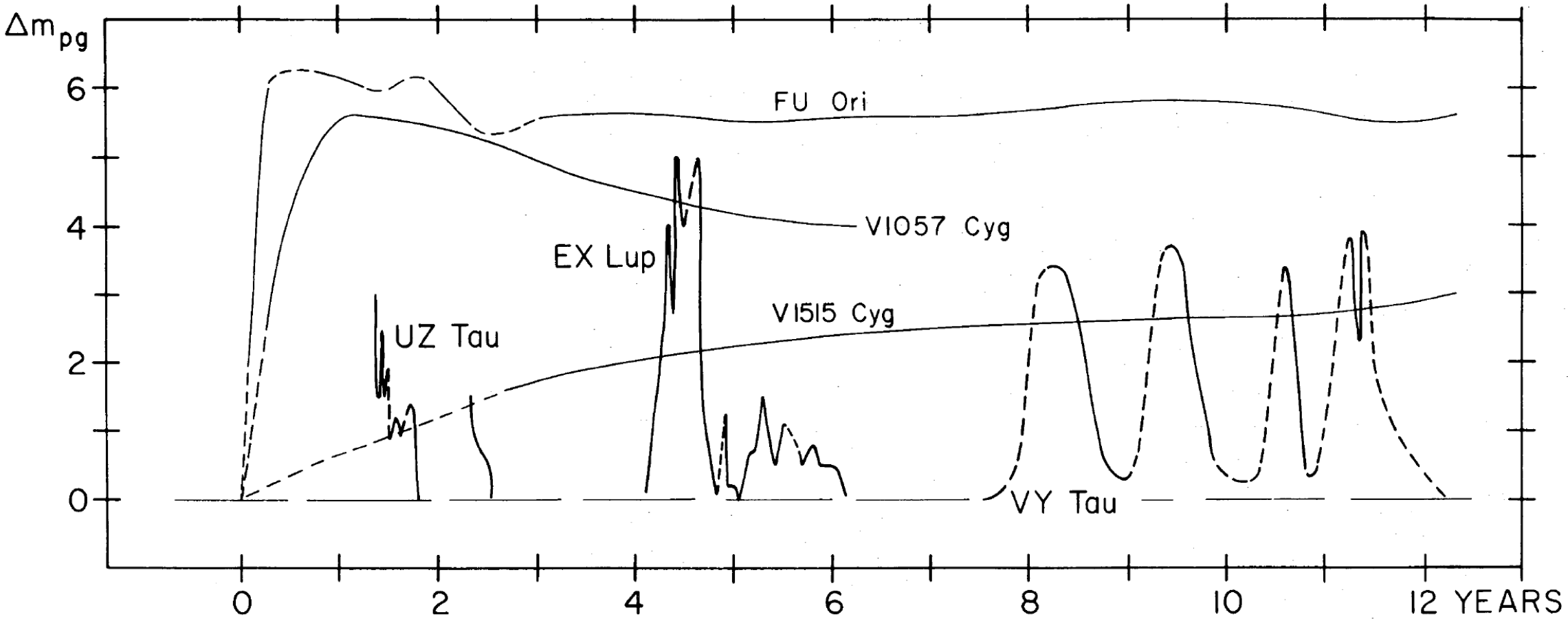
Δm pg
6
4
2
0
FU Ori
V1057 Cyg
EX Lup
V1515 Cyg
UZ Tau
VY Tau
0
2
4
6
8
10
12 YEARS

Herbig 1977

Annu. Rev. Astron. Astrophys. 1996. 34:207–40

THE FU ORIONIS PHENOMENON[1]

Lee Hartmann and Scott J. Kenyon

Harvard-Smithsonian Center for Astrophysics, 60 Garden Street, Cambridge, Massachusetts 01238

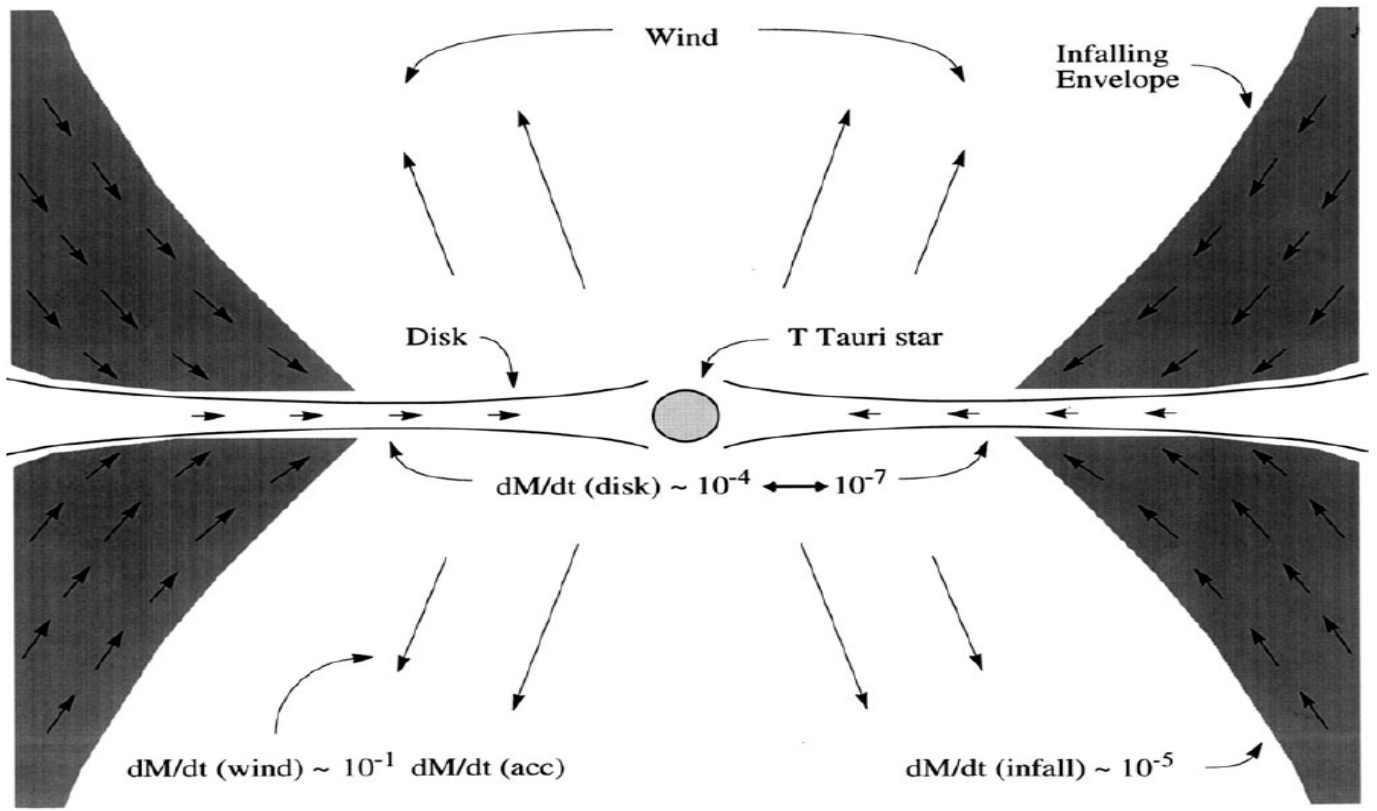

Figure 1 Schematic picture of FU Ori objects. FU Ori outbursts are caused by disk accretion increasing from $\sim 10^{-7}\ M_\odot\ \mathrm{yr}^{-1}$ to $\sim 10^{-4}\ M_\odot\ \mathrm{yr}^{-1}$, adding $\sim 10^{-2}\ M_\odot$ to the central T Tauri star during the event. Mass is fed into the disk by the remanant collapsing protostellar envelope with an infall rate $\lesssim 10^{-5}\ M_\odot\ \mathrm{yr}^{-1}$; the disk ejects roughly 10% of the accreted material in a high-velocity wind.

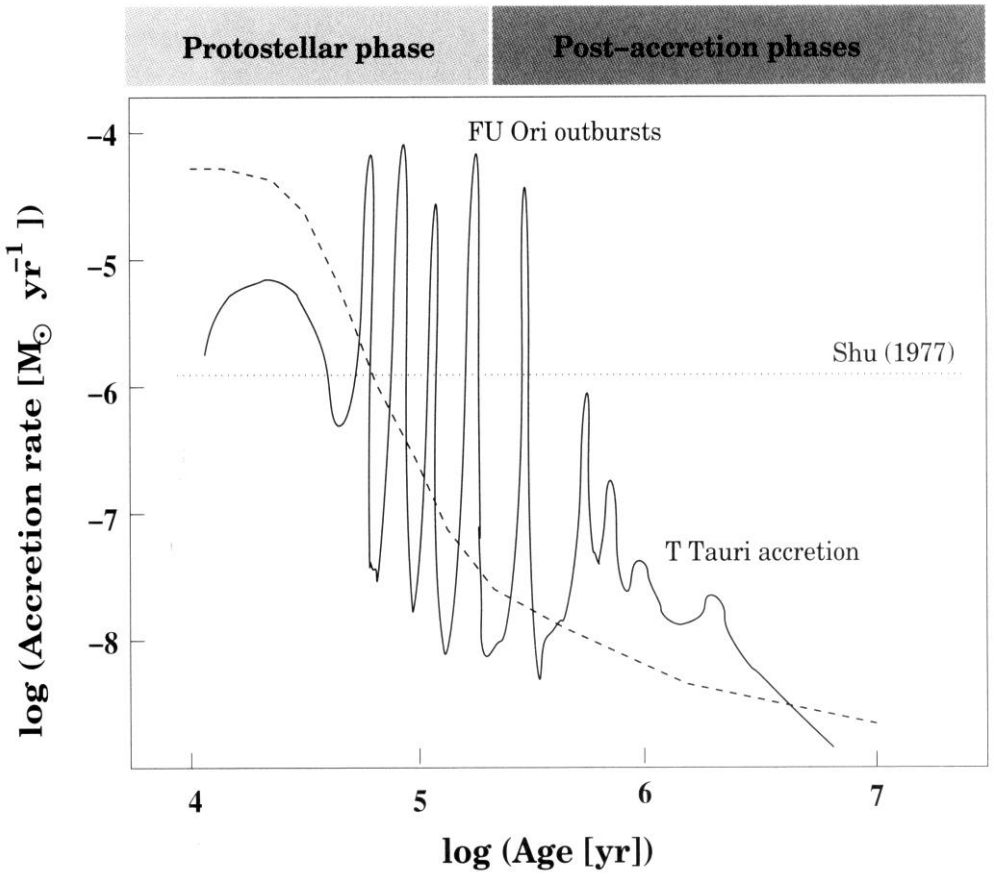

Fig. 6.1. The diagram schematically shows the time development of the accretion rates as they appear in various calculations and in relation to observed phenomena. The dotted straight line resembles the result from standard star formation [777], which does not depend on time and is based on infinitely large radius and mass and thus appears as a flat line throughout the entire time interval. The hatched curve represents an approximation to the results of the many more realistic calculations. The thick line was adapted from Hartmann [344] and shows additional features such as outbursts of FU Ori type protostars and T Tauri disk accretion. All rates apply for typical low-mass ($\sim M_{\odot}$) stars only.

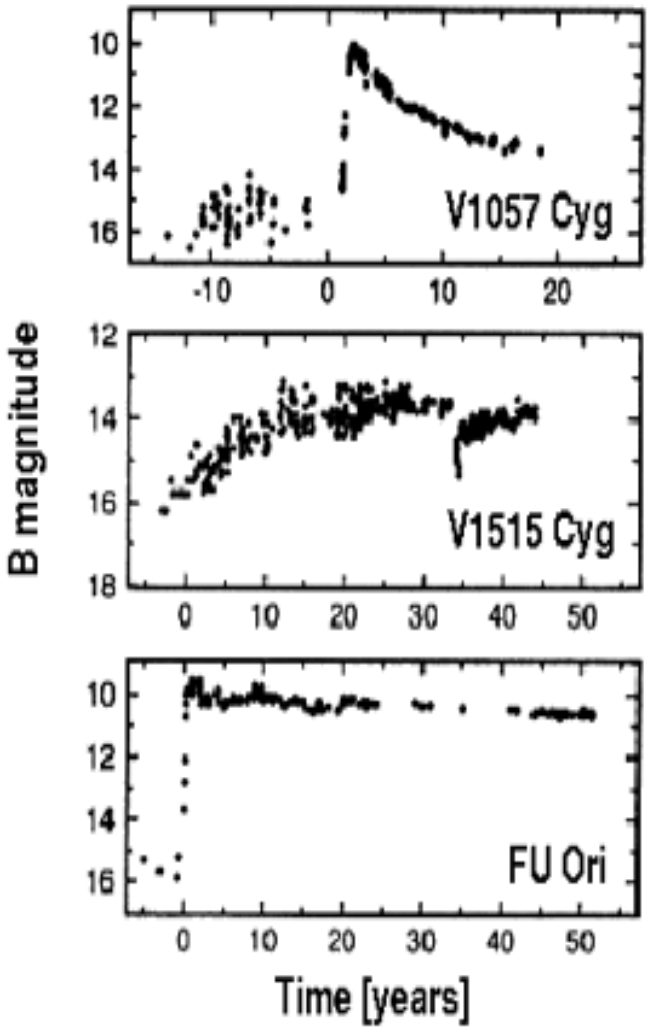

Inside-out collapse (Shu 1977) isothermal sound speed → constant accretion rate

Accretion Disks

- Found in YSOs, supermassive BHs in AGB, binaries, Saturnian rings
- Turbulent viscosity important
  - generating heat
  - transporting angular momentum outwards
  - transporting matter inwards

Fact: The sun has > 99% of the total mass in the solar system, but accounts for ~3% of the total angular momentum (rotation), whereas Jupiter's orbital angular moment accounts for 60%.

Fact: Outer planets rotate fast (thus are flattened in shape.)

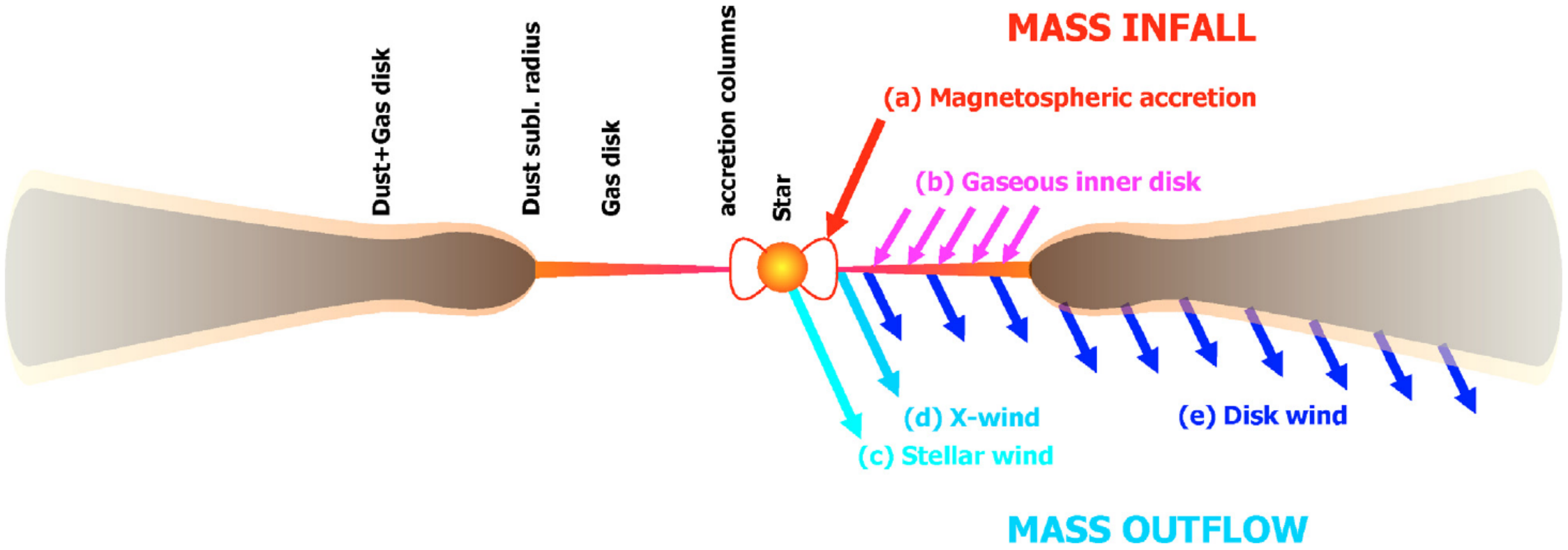

Fig. 1. Illustration of the regions which have been proposed as the origin of the permitted hydrogen recombination line emission observed towards HAeBe stars (this sketch is not to scale; read Sect. 1 for details about the individual mechanisms).

Kraus+08

The X-wind Model

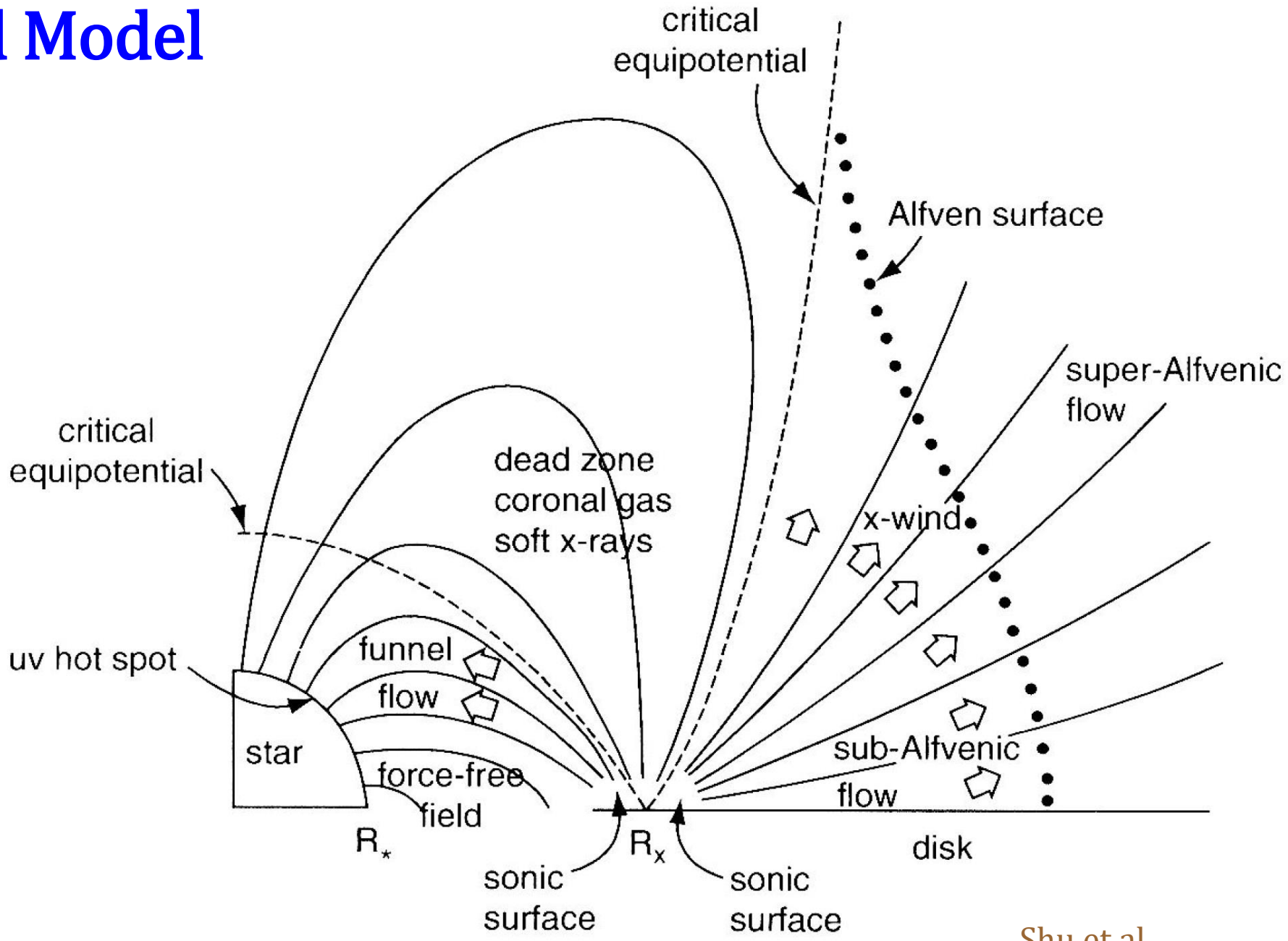

Shu et al.

Annu. Rev. Astron. Astrophys. 1996. 34:111–54

critical equipotential: gravitational force = centrifugal force

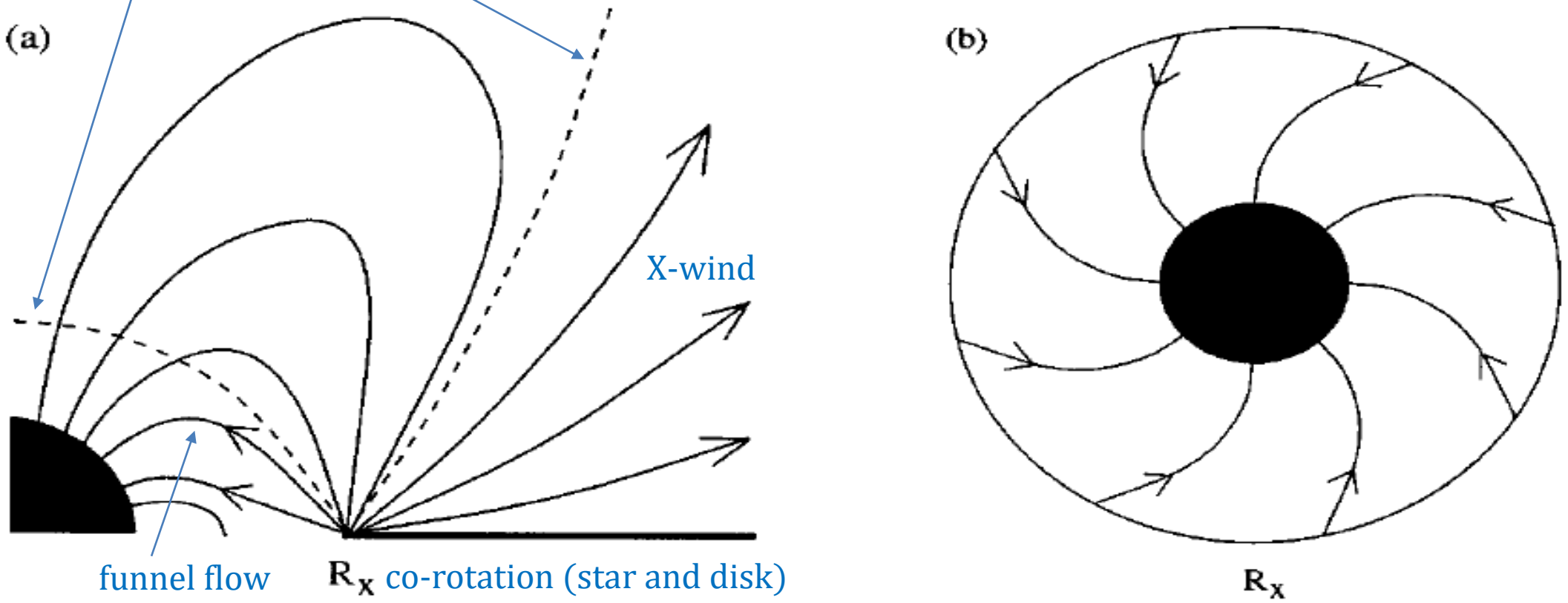

Figure 13 Schematic views of the (*a*) meridional plane and (*b*) equatorial plane of the configuration modeled by Shu et al (1994a,b) for the origin of bipolar outflows. The circumstellar disk is truncated at a distance R_X from the star. Both energetic outflows and funnel flows emerge from the disk truncation region. Gas accreting from the disk onto the star in a funnel flow drags the stellar field into a trailing spiral pattern. (From Najita 1995.)

Rafael Bachiller

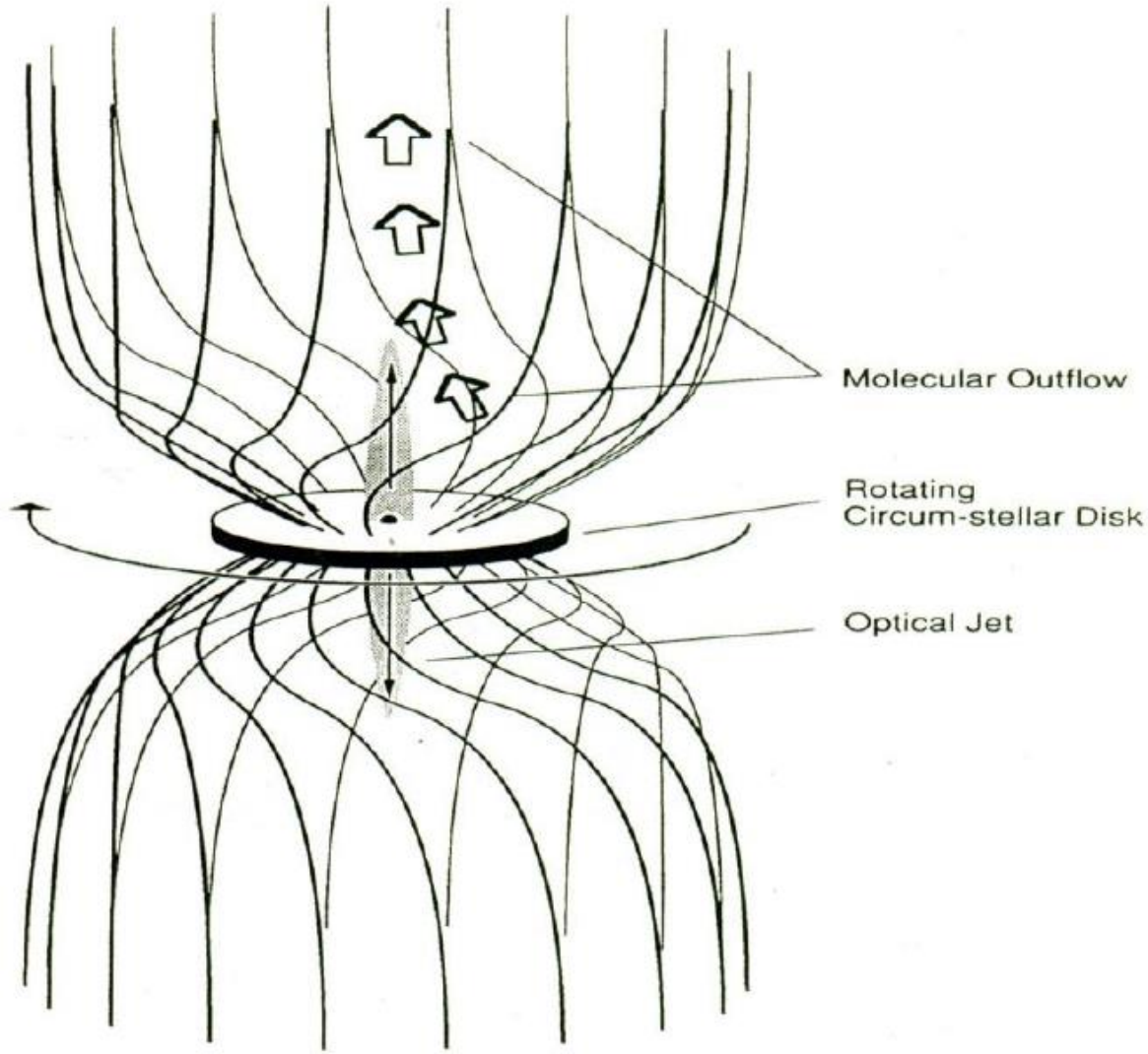

Figure 6. A schematic drawing of the magnetohydrodynamical model.

Exercise

1. Compare the angular momenta of the Sun, Jupiter, and Earth.
2. What is the specific angular momentum of the Earth versus Jupiter?
3. How round (or flat) is the shape of the Earth, of Jupiter, and of the Sun?

http://www.zipcon.net/~swhite/docs/astronomy/Angular_Momentum.html

http://www.astro.ncu.edu.tw/~wchen/wp_chen/essay/sizes.pdf

Main-Sequence Lifetime of the Sun

Energy Gained in a PP Chain

- 4H → 1 He + neutrinos + energy
- Mass of 4 H = 6.693×10^{-27} kg
- − Mass of 1 He = 6.645×10^{-27} kg

Mass deficit → 0.048×10^{-27} kg = 0.7%

$$M_\odot \approx 2 \times 10^{33}\ [\mathrm{g}]$$
$$L_\odot \approx 4 \times 10^{33}\ [\mathrm{ergs/s}]$$

Fusion efficiency

Nuclear physics — **Stellar physics**

$$\tau_\odot^{\mathrm{MS}} \approx M_\odot \frac{(0.007)(0.1)\,c^2}{L_\odot} = 3.15 \times 10^{17}[\mathrm{s}] = 10^{10}\ [\mathrm{yr}]$$

$$\text{Given } L_{\mathrm{MS}}/L_\odot \approx \left(M/M_\odot\right)^4 \rightarrow \tau^{\mathrm{MS}} \approx 10^{10}\left(M_\odot/M\right)^3\ [\mathrm{yr}]$$